International Scientific-Technical and Production Journal

The Paton WELDING JOURNAL

September 2005 # 9

English translation of the monthly «Avtomaticheskaya Svarka» (Automatic Welding) journal published in Russian since 1948

Founders: *E.O. Paton Electric Welding Institute of the NAS of Ukraine*
International Association «Welding»

Publisher: *International Association «Welding»*

Editor-in-Chief B.E.Paton

Editorial board:

Yu.S.Borisov, V.F.Grabin, Yu.Ya.Gretskii, A.Ya.Ishchenko, B.V.Khitrovskaya, V.F.Khorunov, I.V.Krivtsun, S.I.Kuchuk-Yatsenko, Yu.N.Lankin, V.K.Lebedev, V.N.Lipodaev, L.M.Lobanov, V.I.Makhnenko, A.A.Mazur, V.F.Moshkin, O.K.Nazarenko, I.K.Pokhodnya, I.A.Ryabtsev, Yu.A.Sterenbogen, N.M.Voropai, K.A.Yushchenko, A.T.Zelnichenko

International editorial council:

N.P.Alyoshin (Russia), B.Braithwaite (UK), C.Boucher (France), Guan Qiao (China), U.Diltey (Germany), P.Seyffarth (Germany), A.S.Zubchenko (Russia), T.Eagar (USA), K.Inoue (Japan), N.I.Nikiforov (Russia), B.E.Paton (Ukraine), Ya.Pilarczyk (Poland), D. von Hofe (Germany), Zhang Yanmin (China), V.K.Sheleg (Belarus)

Promotion group:

V.N.Lipodaev, V.I.Lokteva, A.T.Zelnichenko (exec. director)

Translators:
A.V.Gorskaya, I.N.Kutianova, T.K.Vasilenko

Editor
N.A.Dmitrieva

Electron galley:
I.S.Batasheva, T.Yu.Snegiryova

Address:
E.O. Paton Electric Welding Institute,
International Association «Welding»,
11, Bozhenko str., 03680, Kyiv, Ukraine
Tel.: (38044) 287 67 57
Fax: (38044) 528 04 86
E-mail: journal@paton.kiev.ua
http://www.nas.gov.ua/pwj

State Registration Certificate
KV 4790 of 09.01.2001

Subscriptions:
$324, 12 issues per year,
postage and packaging included.
Back issues available.

All rights reserved.
This publication and each of the articles contained herein are protected by copyright. Permission to reproduce material contained in this journal must be obtained in writing from the Publisher.
Copies of individual articles may be obtained from the Publisher.

CONTENTS

© PWI, International Association «Welding», 2005

Науково-технічна
бібліотека
ІЕЗ ім.
Инв. №

INHERITANCE OF STRUCTURE-ORIENTED STATE OF METALLIC MATERIALS BY WELDED JOINTS

K.A. YUSHCHENKO[1], O.P. KARASEVSKAYA[2], S.S. KOTENKO[1], E.P. POLISHCHUK[1], V.S. SAVCHENKO[1] and B.A. ZADERY[1]

[1]E.O. Paton Electric Welding Institute, NASU, Kiev, Ukraine
[2]G.V. Kurdyumov Institute of Metal Physics, NASU, Kiev, Ukraine

Peculiarities of fusion welding of textured and oriented-solidification polycrystalline and single-crystal molybdenum, tungsten and nickel alloys are considered. X-ray examination methods were used to generate data on inheriting the structural and crystallographic orientation in different zones of a welded joint. It was found that in solidification of the weld pool the epitaxial growth of crystalline grains of the weld metal from the substrate (surface of melted grains of the fusion zone) might result in the weld metal reproducing the crystallographic orientation of structural elements of the initial material. As proved, the welded joint may retain the crystallographic orientation and structural state close to those of the base metal.

Keywords: *molybdenum, tungsten, nickel alloy, polycrystal, single crystal, texture, welded joint, X-ray method, crystallographic and structural orientation*

Structure-oriented metallic materials find an increasingly wide application in modern engineering. Conventional approaches to production of welded joints in such alloys by fusion welding are no longer adequate in terms of maintaining the required level of physical-mechanical characteristics of the initial material. In this case the main task is to provide a welded joint with the structural state as close as possible to that of the initial material. Given that in one-pass welding of relatively thin materials the scheme of solidification of the weld pool is of a two-dimensional character, and that the melted grains of the fusion zone act as solidification centres, in case of maintaining the epitaxial growth of crystalline grains of the weld pool the weld metal may inherit crystallographic orientation of those grains from the melted surface of which the solidification process begins.

This study considers the mechanisms of formation of the structural state of welded joints made by electron beam (EBW) and helium-arc tungsten-electrode welding of textured polycrystalline molybdenum alloys, as well as nickel alloys produced by the oriented solidification method, single crystals of tungsten and nickel alloys.

Irrespective of chemical composition, initial structural state or phase composition, it seems expedient to subdivide the materials studied into two groups. The first group includes polycrystalline materials, as well as textured polycrystalline alloys, while the second group includes single crystals, as well as alloys produced by the oriented solidification method. In a polycrystalline alloy, the sufficiently equiaxed grains have a chaotic distribution of crystallographic orientations (Figure 1, *a*). Such a material is almost isotropic, and its ductility is lower and yield stress is higher than the average values of these parameters for individual grains [1]. Based on the isotropic nature of a polycrystalline alloy, it can be assumed that the level of physical-mechanical properties of its welded joints does not depend upon the welding direction. If the polycrystalline material is subjected to a directed plastic deformation (e.g. rolling), this will result in the formation of a certain structural state in it, and this state can be defined as a structural and crystallographic texture (Figure 1, *b*). In this case the structural texture implies a different elongation of grain along directions differently oriented with respect to rolling, whereas the crystallographic texture implies formation of primarily crystallographic planes and orientations in the plane of plate. Molybdenum alloys deformed by rolling, considered in this study, had the following components of the crystallographic texture: (001) [110], {111} <112> and <110>. The density of defects in textured molybdenum alloys deformed by rolling was 10^{10} cm^{-2}. Material produced by the oriented solidification method (Figure 1, *c*) contains several coarse crystalline grains with a preferentially crystallographic orientation, separated by the high-angle boundaries. This material has the intermediate structural state between a preferentially oriented polycrystal and single crystal. In the initial state, no clearly defined sub-structure was detected in the single crystal of a heat-resistant nickel alloy (Figure 1, *d*), and the density of dislocations of its crystallographic lattice was not in excess of 10^6 cm^{-2}.

X-ray diffractometry was used as the main method for evaluation of inheritance of the initial material structural state by the weld metal. X-ray examinations were conducted by three methods [2, 3]. The method of constructing pole figures was employed to determine crystallographic orientation of different zones of a welded joint. To examine individual regions of a single crystal that do not correspond to the main orientation of the initial material, the presence of the high-angle boundaries was detected from existence of random reflexes. The volume of the crystal marked out by these boundaries from the base single crystal

© K.A. YUSHCHENKO, O.P. KARASEVSKAYA, S.S. KOTENKO, E.P. POLISHCHUK, V.S. SAVCHENKO and B.A. ZADERY, 2005

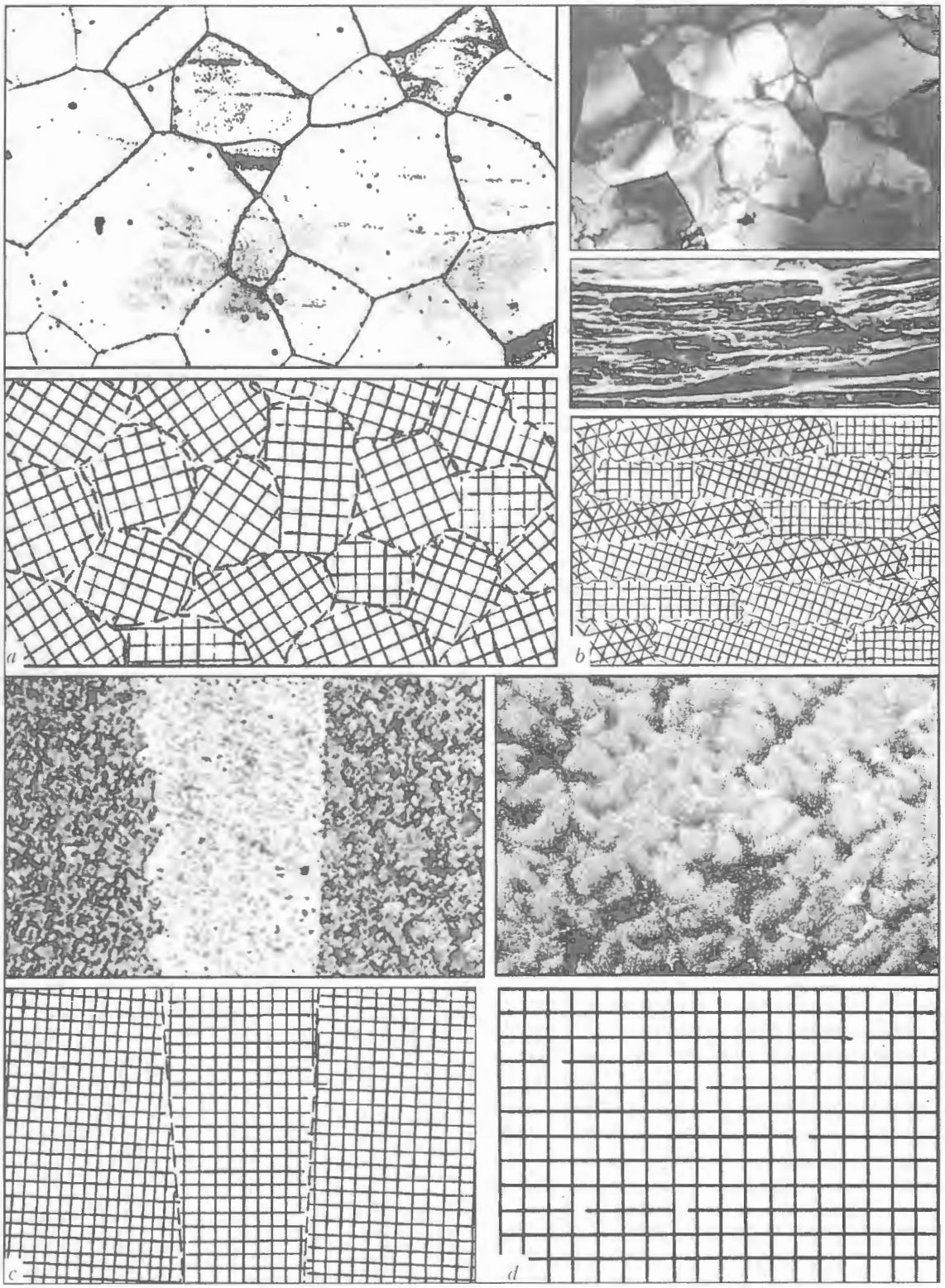

Figure 1. Microstructure and schematic drawing of structure of the materials studied: *a* — polycrystalline molybdenum (×200); *b* — textured molybdenum alloy (×19,000; ×500); *c* — nickel alloy produced by the oriented solidification method; *d* — nickel alloy single crystal (×1000)

was estimated from an integral value of intensity under the random reflections. The shape and width of the Debye lines, i.e. the distribution of the intensity of reflections along diffraction vector $I_{q\parallel}$, were studied by the θ–2θ method. The intensity of scattered X-ray radiation about the reciprocal lattice nodes in the azimuthal plane, i.e. plane normal to diffraction vector $I_{q\perp}$, was examined by the method of four-circle X-ray diffractometry [4–6]. This method allows analysis of $I_{q\perp}$ in any direction of the azimuthal plane, and is similar to the method of rocking curves or ω-scanning in marking out of the distribution of $I_{q\perp}$ in one of the azimuthal directions.

The Paton WELDING JOURNAL

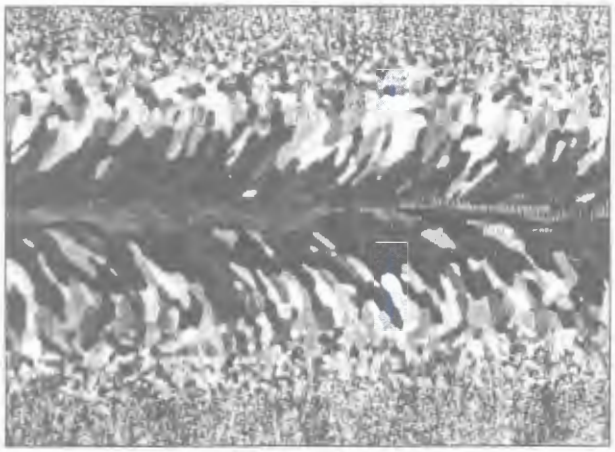

Figure 2. Macrostructure of arc welded joint in polycrystalline molybdenum

As the initial material of a welded joint in polycrystalline molybdenum, produced by TIG welding at a speed of 20 m/h (Figure 2) had a chaotic distribution of crystallographic orientations of individual grains, no pronounced preferential orientation was detected in the HAZ and weld metals. It should be noted, however, that growth of some grains of the weld metal from the surface of melted grains of the fusion zone was suppressed by the neighbouring grains that solidified at a higher speed. In addition, it was noticed that the welds produced at higher welding speeds (v_w > 70 m/h) retained the structural state of the initial material to a larger degree.

Structure of the welded joint in low molybdenum alloy TsM-10 (0.007 % Al and 0.002 % B), made at a speed of 70 m/h, is shown in Figure 3. Molybdenum alloy deformed by rolling contained in the initial state the following crystallographic texture components: (001) [110] and {111} <112> and <110>. Under the effect of the welding thermal cycle, component (001) [110] of the HAZ metal is transformed into (001) [130], while components {111} <112> and <110> undergo no changes. Solidifying grains of the weld metal retain orientation of melted grains of the fusion zone, from the surface of which they started growing.

The principles of inheritance of the initial material crystallographic orientations persist in welding of textured molybdenum alloys of a higher alloying level (MI-5 with 4.5 % Re, and TsM-12 with 0.12 % Hf and 0.1 % Zr). The character of crystallographic reorientation of grains in different regions of the HAZ metal during the welding process is given in the Table.

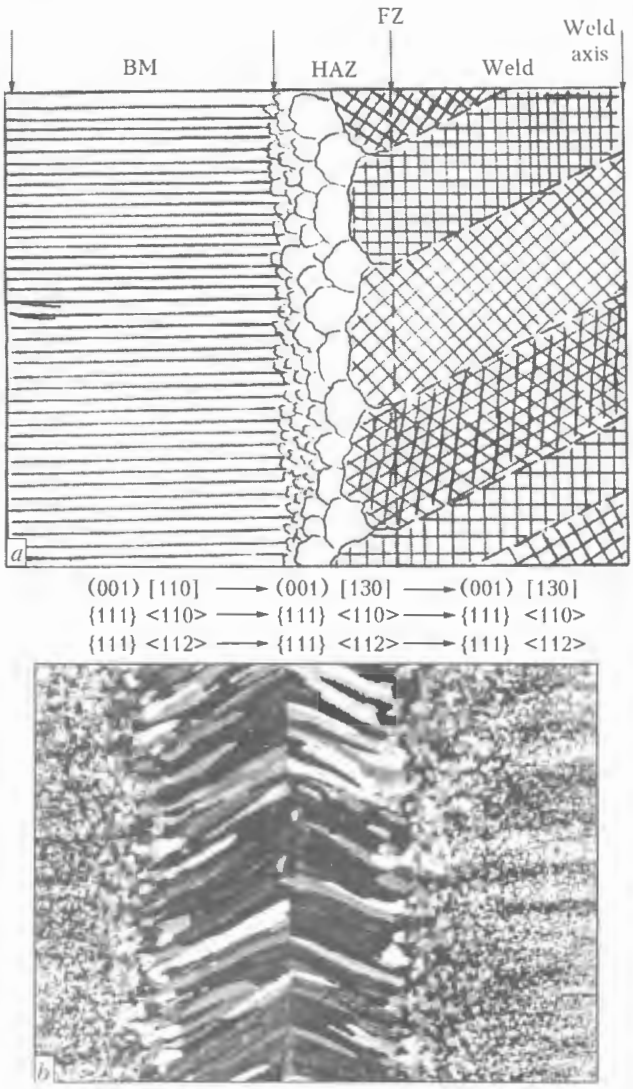

Figure 3. Schematic of solidification (*a*) and macrostructure of joint in textured molybdenum alloy TsM-10 (*b*)

As follows from these data, the main texture component (111) [112] and [110] in the HAZ metal of doped molybdenum alloys undergoes no substantial changes. At the same time, a weak component of the deformation texture, i.e. (001) [110], degenerates in heating to temperatures above the alloy re-crystallisation temperature. Therefore, in alloys MI-5 and TsM-12, grains with crystallographic orientation (111) [112] and [110] grow into the fusion zone. Further solidification of the weld metal from the surface of melted grains of the fusion zone is accompanied by inheritance of

Character of changes in texture components of the HAZ metal heated to different temperatures, K

Alloy	*Texture components*	*1300*	*1500*	*1700*	*1900*	*2100*	*2300*
MI-5	(001) [110]	(001) [110]	(001) [110]	–	–	–	–
	(111) [112]	(111) [112]	(111) [110]	(111) [112]	(111) [112] (111) [110]	(111) [112]	(111) [112]
TsM-12	(001) [110]	(001) [110]	(001) [110]	(001) [110]	(001) [110]	–	–
	(111) [112]	(112) [110]	(112) [110]	(112) [110]	(111) [110]	(111) [112]	(111) [112] (111) [110]

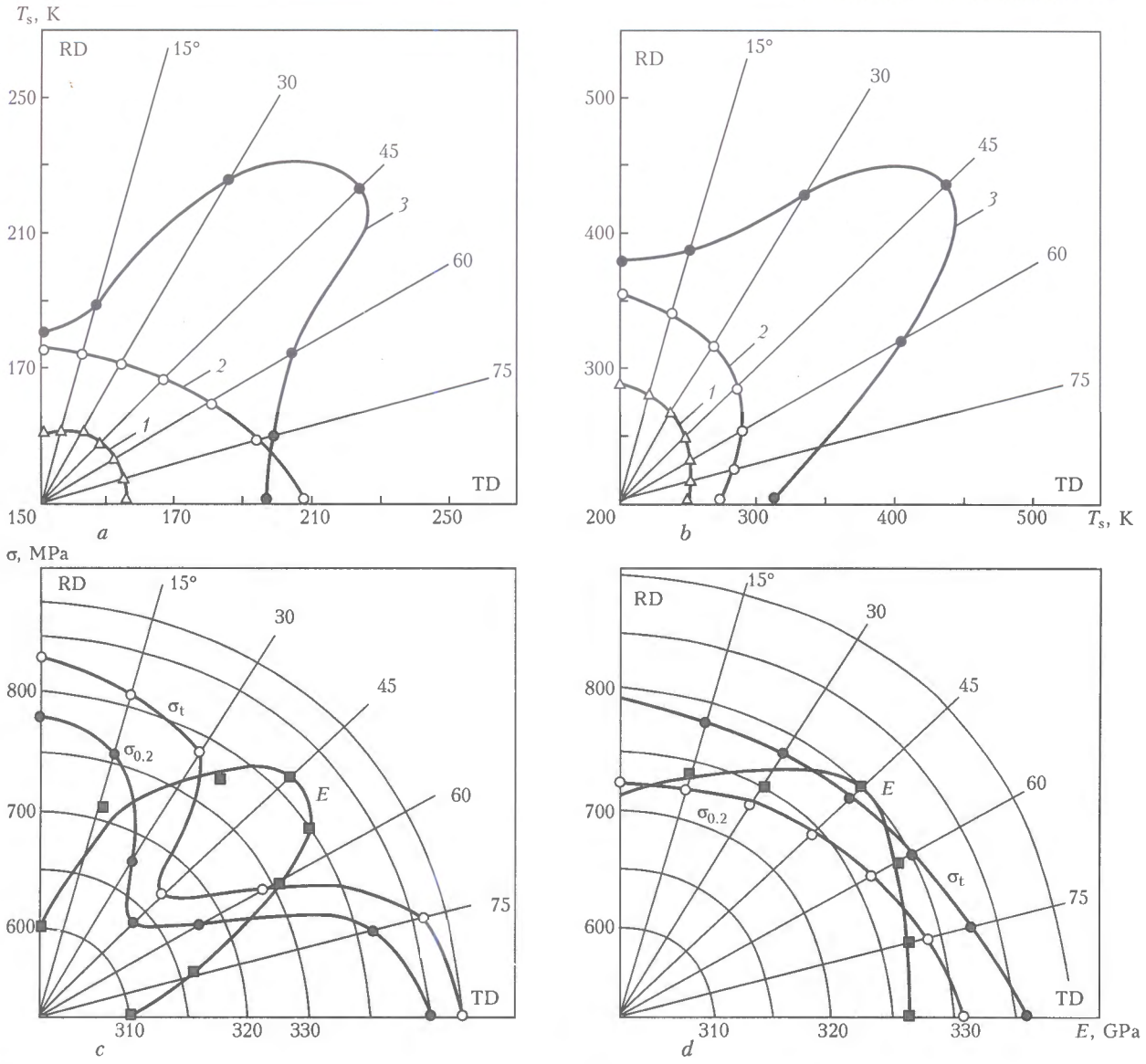

Figure 4. Dependence of cold shortness temperature (*a*, *b*) and strength characteristics (*c*, *d*) of base metal (*a*, *c*, *d*) and welded joint (*b*) upon the angle of cutting of specimens and welding direction: *a*, *b* — alloys MI-5 (*1*), TsM-10 (*2*), TsM-12 (*3*); *c*, *d* — alloys TsM-10 and TsM-12, respectively (RD — rolling direction; TD — transverse direction)

the initial orientations by crystalline grains of the weld metal. The direction of formation of these crystalline grains is turned, according to the shape of cooling isotherms, to 20–30° from normal to the weld axis. Directions [112] or [110] are normal to the front of the isotherms, while the nearest direction of easy growth <100> makes a comparatively high angle (35 or 45°, respectively) to the direction of growth of crystalline grains, and is out of the plate plane. Under these conditions, the weld metal crystalline grains inherit the crystallographic texture of melted grains of the fusion zone, i.e. they grow along direction [112] or [110] [7, 8].

Inheritance of base metal crystallographic texture by the weld metal during welding results in interrelation between physical-mechanical characteristics of the initial material and those of a welded joint made in it. As follows from the dependence shown in Figure 4, in a case where low-temperature ductility of textured molybdenum alloys results mainly from the type of the crystallographic texture and metal of the welded joint inherits crystallographic orientation of the initial material, direction which the minimal cold shortness temperature of the base metal corresponds to will correspond to the similar direction in the welded joint. Therefore, the minimal cold shortness temperature for welded joints made in textured molybdenum alloys corresponds to the case where the welding direction makes an angle of 90° to the rolling direction in the initial material.

The initial tungsten single crystal 1 mm thick, where plane (111) coincided with its surface, was EB welded in such a way that the welding direction coincided with direction [110]. The initial single crystal is characterised by a homogeneous distribution of dislocations, insignificant amount of low-angle boundaries, and disorientation of the sub-structure elements in an irradiated surface of about 1 mm^2 by less than 10–20 mrad (Figure 5, *a*, *b*). Examinations of welded joints made in tungsten and molybdenum single crys-

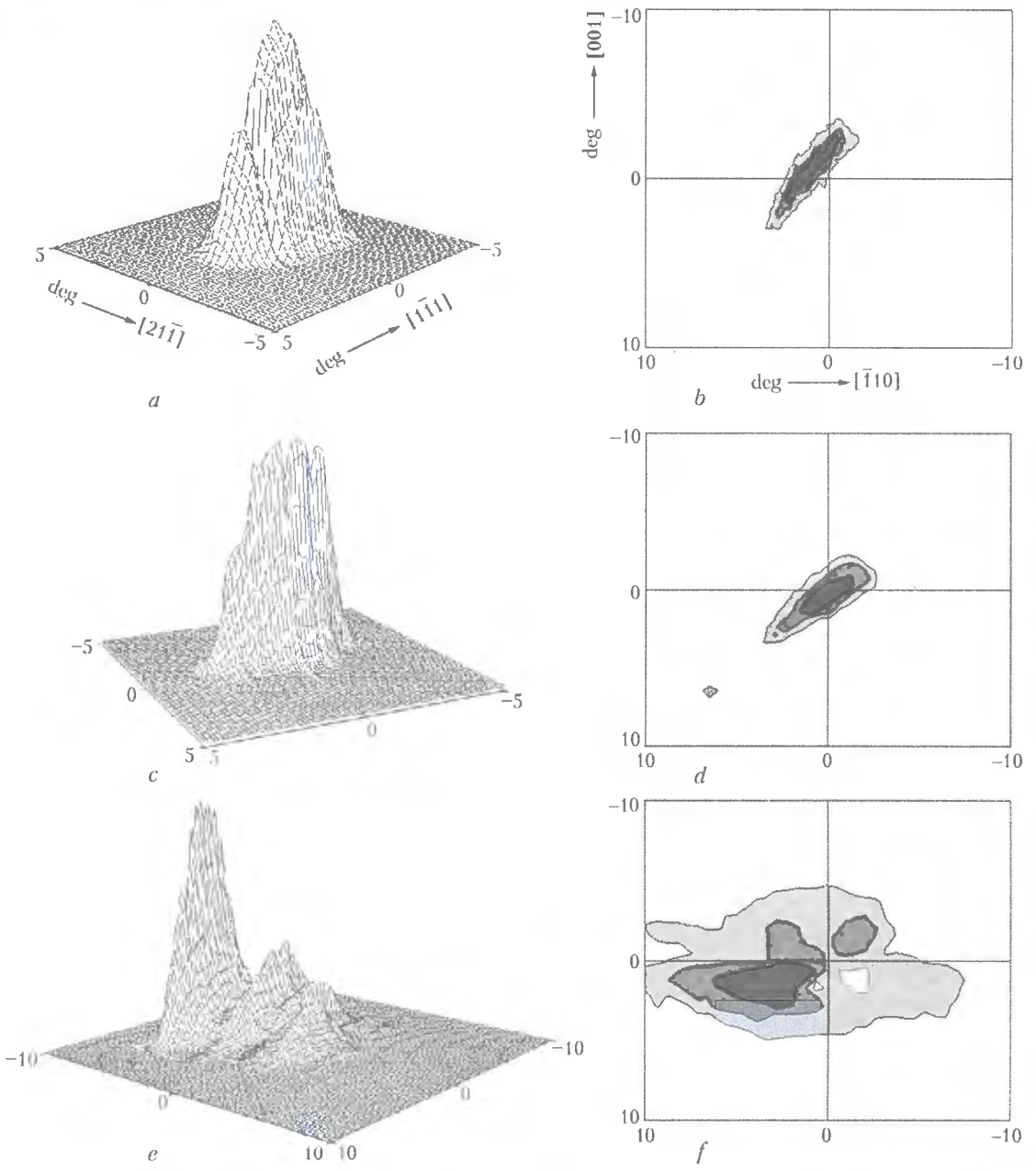

Figure 5. Spatial distribution of intensity I (*a*, *c*, *e*) and iso-intensive lines (*b*, *d*, *f*) of scattered X-ray radiation in azimuthal plane $I_{q\perp}$ for different zones of welded joint in tungsten single crystals: *a*, *b* — base metal; *c*, *d* — fusion zone; *e*, *f* — central part of the weld (fusion surface (111), welding direction [110], reflex (222), v_w = 100 m/h)

tals revealed the following structural peculiarities of the weld metal. Under certain welding conditions it is possible to provide a welded joint with a single-crystal state on the tungsten and molybdenum single crystals. At welding speeds of 10–100 m/h, independently of the welding method (EBW or helium-arc welding), or orientation of the fusion surface and welding direction during solidification of the weld pool, the mechanism of inheritance of crystallographic orientation of the initial metal by the weld metal is obvious (Figure 5). X-ray patterns of individual zones of the welded joint reveal deviations of orientation from the initial one to an angle of 35–175 mrad. As the disorientation angle depends primarily upon the accuracy of alignment of the weld edges, which in our case was 50 mrad, and allowing for the instrumental error, it seems impossible to establish an exact numerical dependence of changes in the crystallographic orientation of the weld metal upon the welding conditions. At the same time, it is possible to trace the main trends in inheritance of crystallographic orientation by metal of the welded joint depending upon the welding conditions and parameters. In welding of single crystals with plane (111) and at a welding direction coinciding with direction <112>, a good inheritance of single-crystal structure is seen for low speeds (v_w = 10 m/h). In this case, where disorientation of the sub-structure base metal elements was at a level of 20–30 mrad, deviation of the orientation of individual regions of the HAZ and weld metal at the central part of the weld made an angle of 30–50 mrad. Decreasing the welding speed to 3 m/h

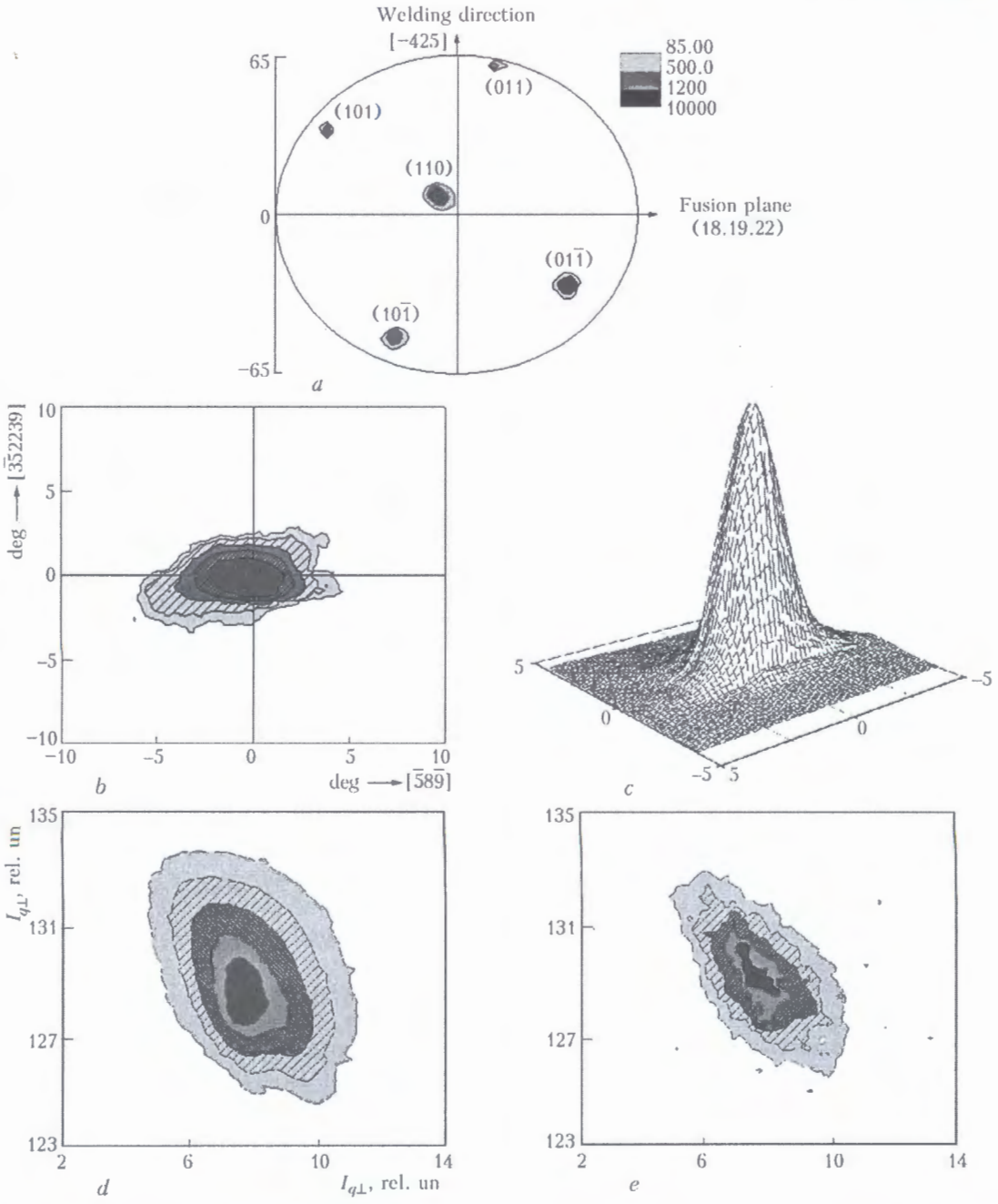

Figure 6. Pole figure {220} (*a*), spatial distribution of intensity I (*c*) and iso-intensity lines $I_{q\perp}$ (*b*, *d*, *e*) of scattered X-ray radiation in initial nickel alloy; *b*, *c* — reflex (331); *d* — (220); *e* — (110)

causes improvement in perfection of single-crystal structure of the welded joint, and decreases the density of the crystalline lattice defects. Disorientation of the sub-structure elements at the centre of the weld made on single crystal (001) [110] at a speed of 10 m/h amounts to 110–140 mrad. In contrast to the previous case, in welding a single crystal of the given orientation an increase of the welding speed is accompanied by growth of perfection of single-crystal structure of the welded joint.

Analysis of the data generated in the case of EBW of tungsten single crystals shows that the optimal results are obtained for single crystals with a welded surface (111) at low welding speeds. We failed to produce welds with a structure close to that of the single crystal welded at fusion surface orientation {112}. Therefore, it can be concluded that in a case of welding tungsten single crystals each initial crystallographic orientation is characterised by its optimal welding conditions and parameters, which provide the welded joints with the most perfect inherited structure.

EBW of single crystal samples of a heat-resistant nickel alloy was performed in such a way that its direction did not coincide with the high symmetry axes. Pole figures {220} shown in Figures 6 and 7 indicate only those reflections that correspond to single-crystal structure of the initial crystal. In EBW of nickel alloy single crystals, the welded joint retains, as a rule, the single-crystal structure of an initial alloy

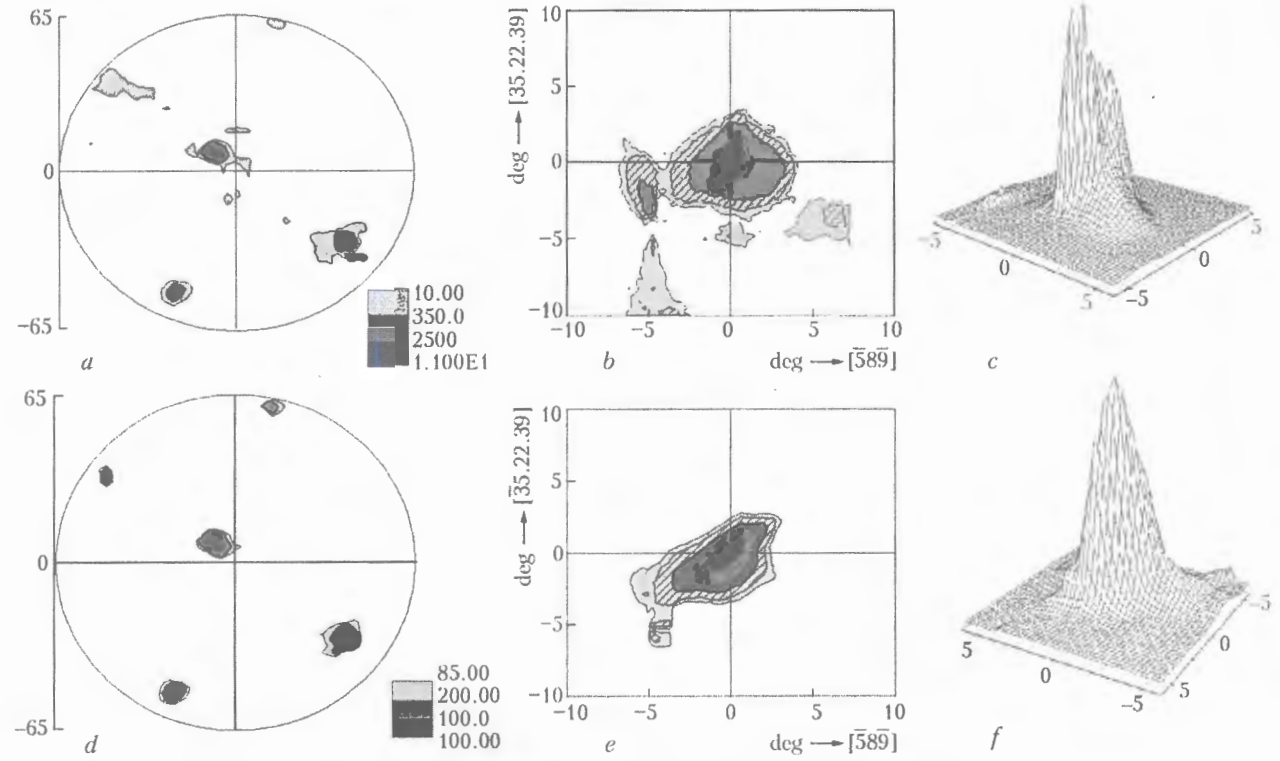

Figure 7. Pole figures {220} (*a, d*), spatial distribution of intensity I (*c, f*) of reflection (331) and iso-intensity lines $I_{q\perp}$ (*b, e*) of scattered X-ray radiation in azimuthal plane of weld metal in nickel alloy; *a, b, c* — length of the weld made at 40 m/h; *d, e, f* — same at 20 m/h

(Figure 7, *a, d*). However, under certain welding conditions a large amount of grains (Figure 8) with the crystallographic orientation other than that of the initial material may be formed in the weld metal. Intensive formation of these grains causes, as a rule, increase in the welding speed. Violation of single-crystal structure may be related to two processes, i.e. loss of stability at the solidification front and fragmentation of the material, provided that a heterogeneous dislocation structure is formed in it. Distributions of $I_{q\parallel}$ and $I_{q\perp}$ for the welds made at different welding speeds, at which the lattice parameters of the γ- and γ′-phases and positions of maxima of the $I_{q\parallel}$ lines coincide, allow a conclusion that structure with coherently related phase components is formed in the major part of the weld, and, hence, favourable conditions for formation of the single-crystal structure are established at the solidification front. Decrease in $\delta_{q\parallel}$ (half width of the distribution of intensity $I_{q\parallel}$) with increase in $\delta_{q\perp}$ (half width of the distribution of intensity $I_{q\perp}$) in the welds made at high speeds is related to growth of local stresses in a narrow region of the welded joint. This leads to fragmentation of crystalline grains of the weld metal (Figures 7 and 8).

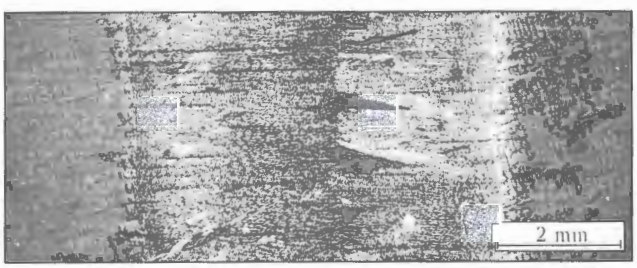

Figure 8. Microstructure of welded joint in single-crystal nickel alloy Ni–Cr–Al–W–Co (total content of aluminium, titanium and niobium is 9 %)

The value and direction of thermal and deformation gradients in welded joints are known to depend upon the welding conditions. Resulting welding stresses induce shear stresses in slip planes at an asymmetric orientation of the weld pool. Crystallographic asymmetry of the weld pool that determines direction of a maximal thermal gradient leads (according to the Schmid factor [9]) to different tangential stresses formed on different sides from the weld axis. The level of these stresses effective in potential slip systems may be substantially different, despite the fact that the rate of cooling of the weld metal and shape of the solidification front remain unchanged. Shear stresses in the slip planes are most different in a case where the direction of the maximal thermal gradient changes from <111> to <100> or <110> (in a case where the direction from <112> to <011> corresponds to the welding direction), and least different in a case of its change from <100> to <110> (welding direction along <001>). The experimental distributions of intensity $\delta_{q\perp}$ demonstrate a different homogeneity of the dislocation ensemble in the weld metal depending upon the welding conditions. Smooth shapes and isointensive curves of the distributions of $\delta_{q\perp}$ resulting from the welding condition at a low speed reflect, according to [3], statistical homogeneity of the dislocation ensemble, i.e. sufficient averaging is seen within the X-ray radiation zone over all parameters of the dislocation distribution. In a case where this condition is not met, the structure under consideration

is a heterogeneous dislocation ensemble with a comparatively coarse mosaic structure. The distribution of $\delta_{q\perp}$ is represented by multi-peak or asymmetric curves, which is the case of high welding speed. The shape of the distribution of $\delta_{q\perp}$ in heterogeneous dislocation ensembles greatly depends upon the relationship of sizes and angles of disorientation of coarse and finer fragments and blocks forming this structure. This allows homogeneity of the dislocation ensemble at different structural levels to be estimated from the distribution of $\delta_{q\perp}$, i.e. type of the distribution of $\delta_{q\perp}$ is a qualitative indicator of plurality of the dislocation systems and homogeneity of their distribution in a material. Local regions of a high scalar dislocation density are formed in the dislocation structures having heterogeneous disorientation (high welding speed). This leads to acceleration of deformation under the effect of temporary and residual welding stresses, and, hence, fragmentation of the material. Homogeneity of the dislocation structure and dislocation density are determined by temperature-stress conditions in the weld metal. Their level depends upon the welding conditions which create premises for formation of a relatively high-temperature structure at low welding speeds, and a low-temperature mechanism of its formation at high welding speeds. The dislocation density in metal of the weld made at low welding speeds ($\Delta\delta_{q\perp} \cong 0.3$–$0.5°$) corresponds to a 6–8 times increase in the dislocation density, compared with the initial value, whereas in welding at a high speed the dislocation density grows by a factor of 15–20.

Therefore, stresses in the weld at an asymmetric location of the weld pool lead to different values of the dislocation density in primary and secondary slip systems, and determine their distribution in metal of a welded joint. Increase in the dislocation density caused by the polygonisation processes and peculiarities of the sub-structure formation cause development of heterogeneous disorientations of the sub-structure elements and generation of different sub-structure levels. The locally measured scalar dislocation density in different regions of the heterogeneous multi-level sub-structure grows substantially, compared with an average dislocation density, which leads to fragmentation and probable initiation of defects in the form of micro tears or embryo cracks.

CONCLUSIONS

1. In fusion welding of structure-oriented metallic materials, the solidifying weld metal may inherit the structural and crystallographic orientation of the initial material. This is caused by a controlled epitaxial growth of crystalline grains of the weld metal from a melted surface of the fusion zone.

2. For bcc (molybdenum, tungsten) and fcc (nickel alloys) single crystals, the welded joint may retain its single-crystal structure if the welding direction coincides with the high symmetry directions of a single crystal welded.

3. Tangential stresses differing in values are formed in asymmetric orientation of the weld metal to different sides from the welded joint axis. Differences in shear stresses may lead to violation of perfection of single-crystal structure of the welded joint.

1. Palme, R. (1971) Effect of deformation textures on properties of refractory metals. In: *New refractory metallic materials*. Moscow: Mir.
2. Gaumann, M., Bezencon, C., Kurz, W. (2001) Columnar to equiaxed transition in solidification processing. *Sci. and Techn. of Advan. Materials*, **2**, 185–191.
3. Krivoglaz, M.A. (1996) *X-ray and neutron diffraction in nonideal crystals*. Berlin: Springer.
4. Karasevskaya, O.P. (1999) Orientation X-ray experimental method for phase analysis of polycrystals. *Met. Phys. and Techn.*, 21(**8**), 34–39.
5. Fewster, P.F. (2000) Commission on powder diffraction: Int. union on crystallography, microstructure of materials. *Newsletter*, 24 Dec., 17.
6. Karasevskaya, O.P. (2000) Multi-level structures. *Metallofizika i Nov. Tekhnologii*, 22(**11**), 44–53.
7. Trefilov, V.I., Milman, Yu.V., Ivashchenko, R.K. et al. (1983) *Structure, texture and mechanical properties of deformed molybdenum alloys*. Ed. by V.I. Trefilov. Kiev: Naukova Dumka.
8. Zadery, B.A., Kotenko, S.S., Marinchenko, A.E. et al. (2002) Formation of crystallographic texture in metal of welded joints on molybdenum alloys. *The Paton Welding J.*, **11**, 12–16.
9. Schmid, E., Boas, V. (1938) *Plasticity of crystals, metallic crystals in particular*. Moscow: GONTI KKTP SSSR.

SEMI-AUTOMATIC DEVICE M30 FOR MECHANISED TIG WELDING

Semi-automatic device M30 consists of a feeding mechanism, hose with a nozzle and a power source for electromagnet. The feeding mechanism provides feed of a 1.0–1.5 mm dia. filler wire at a preset speed to the welding zone. The electromagnet controls the spatial position of the arc by making it move along the weld axis. The arc movement amplitude can be varied in real time with variations in size of the joint gap.

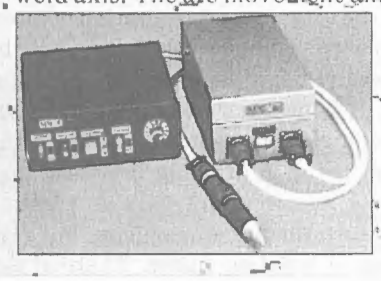

M30 can be used with any standard DC power supply.

Application. Semi-automatic device M30 is intended for mechanised TIG welding of titanium and titanium-base alloys, as well as other non-magnetic materials in any spatial position. It is especially indicated for field welding.

Mechanised welding using M30 improves weld formation in the case of improper fit-up, reduces losses of filler wire, and decreases requirements to the welders' skill.

ADVANCED METHODS FOR INVESTIGATION, PREDICTION AND EVALUATION OF PROPERTIES OF WELDING FLUX-CORED WIRES*

V.N. SHLEPAKOV
E.O. Paton Electric Welding Institute, NASU, Kiev, Ukraine

The article shows urgency of improvement of methods for prediction and evaluation of properties of welding consumables to achieve further progress in their application for mechanised and automated welding processes.

Keywords: *arc welding, welding consumables, flux-cored wires, efficiency of application, investigation methods, prediction and evaluation of properties*

Improvement of the efficiency, qualitative and quantitative indicators of welding technologies results in the need to stiffen requirements to welding consumables. Application of the known principles of metallurgy and technology of fusion arc welding can serve as a main but insufficient basis for comprehensive solution of problems in welding engineering.

Advances in welding using flux-cored wire, achieved during the last two decades, have led to the development of new types of this electrode material and specialised technologies involving it [1–3], which contributed to expansion of the application fields and scopes for this welding method, as well as increase in its competitiveness compared with other processes. Addressing the problems associated with upgrading of the method required development and utilisation of advanced approaches to prediction of properties, analytical methods and experimental procedures ensuring generation of quantitative data and dependencies correlating with the obtained results.

Processes accompanying flux-cored wire melting. In flux-cored wire welding, the current flows mainly through the sheath. Therefore, its density and melting efficiency are higher than in the case of using solid wires of the same diameter. Considering a high melting rate, heating and melting of the core occur primarily as a result of heat transfer from the melted wire tip and, to a lesser degree, from the sheath. The share of heat transferred to the core from the sheath grows with increase in the wire extension [4]. Specific conditions of melting of the flux core determine the effect of its composition on melting characteristics of the wire, electrode metal transfer, as well as composition and properties of the gas and slag phases interacting with molten metal. To predict the above processes, the E.O. Paton Electric Welding Institute uses to advantage the method for integrated thermal analysis of components and powder mixtures, i.e. wire core models.

Investigations were conducted to study kinetics of the processes of thermal destruction of carbonates, fluorides and organic materials, melt formation, oxidation of metal powders, and evaporation of moisture. This led to generation of the data bank on physical-chemical properties of the core materials in continuous heating. Development and implementation of the method for prediction of reactions occurring at the real rates of heating and melting of wire, amounting to 10^4–10^6 K/min, were an important step forward in elaboration of notions of the real processes. The developed computation software is based on the data of dynamic thermogravimetric analysis conducted at different heating rates, providing the information on the activation energy of the reactions, mechanisms and sequence of the occurring processes. The computations made it possible to plot kinetic diagrams showing the extent of development of the reactions of dissociation of carbonates and fluorides, playing an important role in metallurgical processes [5].

The comprehensive thermal analysis of powder mixtures (wire core models) resulted in establishing the principles of development of reactions between components and the effect of composition of a mixture on the kinetics of the processes occurring in heating and melting. Investigation of the processes of oxidation of iron powders and ferroalloys shows that the oxidation rates are low, and the effect of a gas evolved in dissociation of carbonates on the process is insignificant. The composition of a mixture has a substantial impact on the kinetics of gas evolution, which makes it possible to regulate the processes of formation of carbon dioxide and volatile fluorides during wire melting [6].

Investigation of the kinetics of evaporation of moisture from the core materials shows that heating at the wire extension allows removal of only part of water vapours. Therefore, it is necessary to take extra metallurgical and technological measures to decrease the hydrogen content of metal. A drawing lubricant present on the surface of wire acts not only as a source of hydrogen getting into the arc atmosphere, but also as one of the sources of welding fumes. Thermal de-

*The article is based on the paper presented at the 3rd International Conference on Welding Consumables of the CIS countries (Dnepropetrovsk, June 1–4, 2004).

© V.N. SHLEPAKOV, 2005

struction of the drawing lubricant occurs in several stages at a rate that fails to ensure its complete burnout in heating at the extension.

Results of investigations of properties of the core materials and powder mixtures make it possible to predict composition of the gas and slag phases entering into reaction with molten metal, as well as characteristics of melting of the wire.

Reactions of molten metal with gases. In fusion arc welding, the processes of absorption of gases (oxygen, nitrogen, hydrogen) by metal are determined by a large number of factors, this making analysis of their effect on the gas content of the weld metal much more complicated. Peculiarities of melting of flux-cored wire caused by arrangement of powder materials inside a metal sheath and development of reactions during heating and melting of a powder composite require a mandatory allowance for special conditions of interaction between metal and gases. Under conditions of a steady-state welding process, it is permitted to accept thermodynamic parameters (distribution of temperatures, concentrations and pressure) close to the state of dynamic equilibrium within the melting zone. Under these conditions, absorption of gas can be described by a smooth kinetic function of the gradient system [7]. The function can be determined from an integral value through the concentration gradient, when using a scheme of contact of the phases. For the flux-cored wire welding conditions, allowing for existence of stages of a drop of the electrode and weld pool metals, it is expedient to regard the process of interaction of metal with gases as a two-stage one with a common gas phase. Dilution of the electrode metal with a melted part of the base metal, typical of the fusion welding methods, takes place at the pool stage. At the same time, dilution with metal powders takes place at the drop stage, in addition to continuous renovation of the drop metal from a melted sheath. The slag phase at the drop stage is heterogeneous to a substantial degree, which results from continuous melting of solid particles of non-metallic components of the core and occurrence of the reactions of interaction and thermal destruction of materials. In modelling of absorption of gases in metal, it is more convenient to make computations using weights in mole fractions, which allows avoidance of errors in their re-calculation into volume or weight percent, and provides an in-depth analysis of the two-stage process.

The following baseline principles can be distinguished among those formulated during the computations. In terms of decreasing absorption of gases in metal, it is necessary to maintain constant proportions of the weight of metal in mole fractions and gas when changing the wire melting rate and properties of the slag phase formed in melting of the core. Absorption of gases by metal from the arc atmosphere in spray transfer occurs more intensively. At the pool stage, the principles of absorption of gases by metal coincide with those established for gas-shielded welding using covered electrodes and solid wires. Absorption of gases by metal at the drop stage in flux-cored wire welding strongly depends upon the properties of the core and melting conditions, including welding parameters. This is most pronounced in welding using self-shielding flux-cored wire, where the special consideration in development of compositions is given to measures of a metallurgical character aimed at decreasing the content of gases (using nitride-forming elements together with active deoxidisers, complex fluorides, combinations of carbonates, etc.).

Properties of flux-cored wires. Normally, three main groups of properties of welding flux-cored wires are taken into account. They are welding-technological (operational) and sanitary-hygienic properties, as well as composition and properties of the weld (welded joint) metal. Corresponding requirements are specified in national and international standards, such as GOST 26271–91, AWS/SFA A5.20 and A5.29, Eurostandard EN 758, etc. The standards include only those technical requirements which can be verified by a manufacturer, customer and independent specialised examination body ensuring a sufficient extent of objectivity.

As to the group of welding-technological properties, the standards include primarily requirements for a technological quality (absence of pores, cracks, slag inclusions), which can be verified by non-destructive testing methods, examination and destruction of test samples. Some standards comprise optional requirements to operational properties, as no generally accepted procedures are available.

The need to achieve high welding-technological properties becomes increasingly urgent in view of a more strict competition in the market of welding consumables. At the same time, noteworthy are studies on the arc stability and methods of estimation based on statistical analysis [8], as well as evaluation of the effect of metallurgical factors, such as surface tension and viscosity of slags, on welding-technological properties in flux-cored wire welding performed in different spatial positions [9].

Special attention today should be given to the problem of ensuring the most secure sanitary-hygienic welding conditions. Requirements for this group of properties are specified in a corresponding section of GOST 26271–91 and Sanitary Welding Code. Procedures for evaluation of sanitary-hygienic properties are used mainly by specialised organisations. Available publications cover the problems of the effect of different factors primarily on precipitation of a solid phase of the welding fumes, as well as application of modern ventilation devices and individual protection means in arc welding. Pendency of some problems associated with improvement of sanitary-hygienic properties in fusion arc welding may become one of the factors that limit application of the technology.

Requirements to composition and properties of the weld and welded joint metal are most comprehensively formulated in standards for welding flux-cored wires. Procedures used to determine the properties are stand-

ardised, except for analysis of the content of diffusible hydrogen in the weld metal. The chromatographic analysis procedure takes the priority position. There is no lack of publications on the hydrogen problem. Urgency of the problem of decreasing the hydrogen content of metal is determined by a continuous increase of the scope of application of high-strength steels [10], in welding of which the achievement of low and ultra low contents of diffusible hydrogen in the weld metal adds much to the probability of cold cracking.

Modern standards for steels specify requirements to mechanical properties of the weld and welded joint metal (classification by yield stress, determination of impact toughness on specimens with a sharp notch, etc.). Despite the sufficiently large number of publications concerning the problems of investigation of different aspects associated with meeting of the requirements to the properties, a systematic approach to addressing the problems has an insufficient coverage. Among the most significant publications, we can distinguish the publications on prediction of strength and toughness values of steel welded joints using neuron networks [11], as well as methods for prediction of properties of the weld metal allowing for the composition of metal, cooling rate, peculiarities of solidification and formation of non-metallic inclusions [12].

Development, upgrading and wide application of the advanced methods for prediction and evaluation of properties of welding consumables, welding wires in particular, will accelerate the progress in mechanised and automated welding processes, improvement of quality and extension of life of welded structures.

1. Pokhodnya, I.K. (2003) Welding consumables: State-of-the-art and tendencies of development. *The Paton Welding J.*, **3**, 2–13.
2. Heywood, J. (1996) Cored wire review. *Svetsaren*, **1/2**, 3–5.
3. Myers, D. (2002) Metal cored wires: Advantages, disadvantages. *Welding J.*, **9**, 39–42.
4. Pokhodnya, I.K., Suptel, A.M., Shlepakov, V.N. (1972) *Welding with flux-cored wire*. Kiev: Naukova Dumka.
5. Shlepakov, V.N., Suprun, S.A., Kotelchuk, A.S. (1986) Kinetics of gas evolution in welding with flux-cored wire. In: *Information documents of CMEA*. Issue 1. Kiev: Naukova Dumka.
6. Pokhodnya, I.K., Shlepakov, V.N. (1995) Welding with flux-cored wire. In: *Welding and Surfacing Rev. Series*, Vol. 4, Part 4. Ed. by B.E. Paton. Harwood A.P.
7. Shlepakov, V.N. (1990) Kinetics of processes of interaction between metal and gases in welding with flux-cored wire. In: *Transact. on Problems of Welding and Special Electrometallurgy*. Kiev: Naukova Dumka.
8. Shlepakov, V.N., Kotelchuk, A.S., Suprun, S.A. (1999) Identification of flux-cored wire composition by electric signals of arc welding. *Avtomatich. Svarka*, **8**, 37–42.
9. Shlepakov, V.N., Naumejko, S.M. (2001) Effect of surface tension of welding slags of salt-oxide system on characteristics of welding-technological properties of self-shielding flux-cored wire. *The Paton Welding J.*, **11**, 21–24.
10. Paton, B.E. (2003) Current trends of research and development in the field of welding and strength of structures. *Ibid.*, **10/11**, 5–11.
11. Metzbower, E.A., De Loach, J.J., Lalam, S.H. et al. (2001) Neural network analysis of strength and ductility of welding alloy shipbuilding steels. *Sci. and Technology of Welding*, **6(2)**, 116–124.
12. Olson, D.L., Metzbower, E., Liu, S. et al. (2003) Developments in property predictions for weld metal. *The Paton Welding J.*, **10/11**, 31–37.

TIG WELDING OF TITANIUM AND ITS ALLOYS OVER THE FLUX LAYER (TIG-F)

Welding is performed by the TIG method with flux preliminarily deposited on the weld edges. The flux provides widening of the technological capabilities of the arc, increase in the penetration depth in particular. TIG-F welding is carried out using standard TIG welding equipment. TIG-F welding can be performed with or without filler wire. Fluxes ANT-23A and ANT-25A can be used for welding, depending upon the base metal thickness and alloy type.

TIG-F welding provides welds with reinforcement and, what is especially important, in one pass without groove preparation on metal 0.8 to 6.0 mm thick. Compared with parameters of conventional argon-arc welding, TIG-F welding provides:

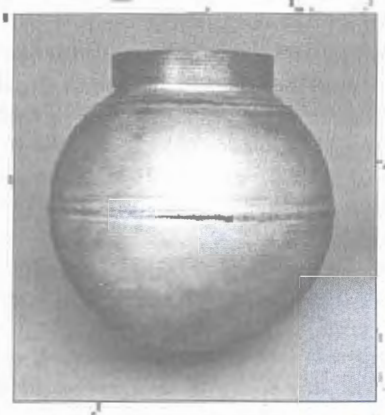

Typical example of TIG-F-welding

- 1.5–2 times decrease in welding current;
- 1.5–2 times decrease in weld and HAZ width;
- weld shape factor equal to about 1.0–0.9.

The use of flux prevents formation of pores in welds, which leads to a substantial improvement of fatigue properties of welded joints. Fatigue limit of samples welded by using the flux is always higher compared with cases when no flux is used.

Application. Application of these technological processes is indicated for making butt, overlap, T- and plug joints. The use of flux is especially efficient for manufacture of thin-walled sections of the T-, lattice and other types. Welding can be performed on the horizontal and vertical planes. The consumption of flux is 7–10 g per metre of the weld.

Proposals for co-operation. Transfer of the developed technology on a contract base.

CALCULATION ALGORITHM FOR ESTIMATION OF ACCEPTABLE SIZE OF LACK OF PENETRATION IN WELDED JOINTS OPERATING UNDER COMPLEX CYCLIC LOADING*

E.A. VELIKOIVANENKO, G.F. ROZYNKA and N.I. PIVTORAK
E.O. Paton Electric Welding Institute, NASU, Kiev, Ukraine

Calculation algorithm for estimation of acceptable lack of penetration in welded joints under a complex set of cyclic loading (forces and momenta) at a base of $2 \cdot 10^8$ cycles is considered with respect to welded joints in frames of wind-driven power plants. The use is made of the experimental data on a range of amplitudes of six types of loads by Q_j ($j = 1, \ldots, 6$), as well as numerical solution for nominal membrane and bending stresses in the weld zone, induced by single loads Q_j, according to which stresses in the HAZ induced by all loads in a given loading cycle are synthesised by superposition.

Keywords: *arc welding, thick-walled parts, welded joints, weld root, lack of penetration, acceptable size, cyclic loading, calculation algorithm*

Issues of estimation of acceptability of revealed defects in welded joints, particularly at a stage of manufacture (operation), where their repair involves much difficulties, are highly topical and attract considerable international interest [1–4, etc.]. In welding of thick-walled parts, one of such typical defects may be a lack of penetration in the weld root (Figure 1). In a number of cases parts with such lacks of penetration, having limited size $2a < [2a]$, can be accepted for operation, unless they affect the safe operation of a structure. As determination of the value of $[2a]$ depends upon the individual peculiarities of a structure, loading, service conditions, etc., i.e. requires a detailed case study, most solutions for the value of $[2a]$ in critical structures are of a conservative prohibitive character, i.e. $[2a] \approx 0$, although in the majority of the regulations for such structures it is not ruled out that $[2a]$ may be more than 0, if it is proved that a joint will operate safely. To prove it, study [5], for example, recommends to use only the methods of fracture mechanics for bodies containing cracks. The experience of application of these methods showed their wide capabilities in terms of reliable handling of such problems.

In the present study this approach was employed to generate data on acceptable values of $[2a]$ for welded joints shown in Figure 1, which are used in a frame of wind-driven power plants (WPP) with a capacity of about 2550 kW developed by the Nordex Energy Company (Figure 2). The frame is made from steel S235J263 + N + Z25 according to DIN EN10025, 1993. Butt and fillet welded joints were made by CO_2 arc welding using welding wire of the EMK6 grade (Boehler). Data on chemical composition of base metal and welds, as well as their mechanical properties, are given in Table 1. Thickness of the members joined in different connections of the frame varies from 12 to 70 mm.

Loads in welds on the frame are related to operation of WPP, and determined by values of three forces F_j and three momenta M_j ($j = x, y, z$) at the drive shaft, as shown in Figure 3. Below the vector of these loads will be designated as Q_j ($j = 1, \ldots, 6$). Extreme combinations of these loads are given in Table 2, and positive direction of Q_j is shown in Figure 3. Rotation of the shaft, as seen from Table 2, is accompanied by variations in loads Q_j. They vary in an asynchronous

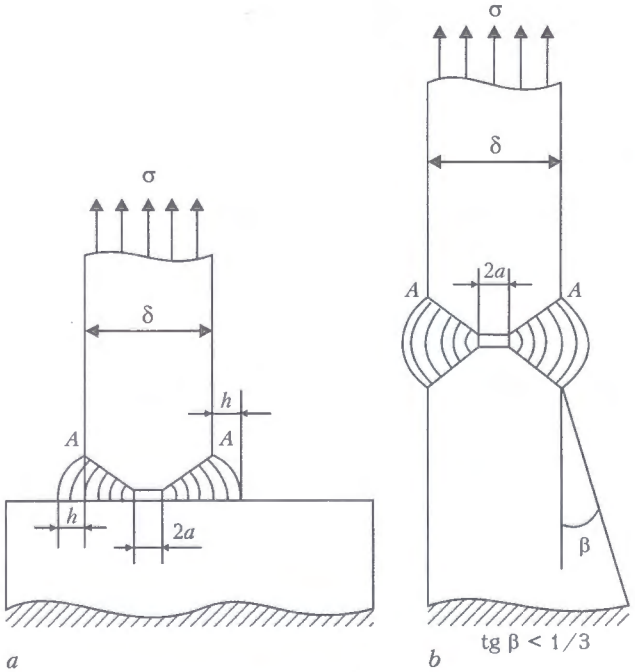

Figure 1. Schematics of welds with lack of penetration in T- (*a*) and butt (*b*) welded joints: *A–A* — zone of least fatigue crack resistance at $a \to 0$

*The article is based on data of the paper presented at the 2nd International Conference «Mathematical Modelling and Information Technologies in Welding and Related Processes» (Katsiveli, Crimea, Sept. 13–17, 2004). Kiev: PWI.

© E.A. VELIKOIVANENKO, G.F. ROZYNKA and N.I. PIVTORAK, 2005

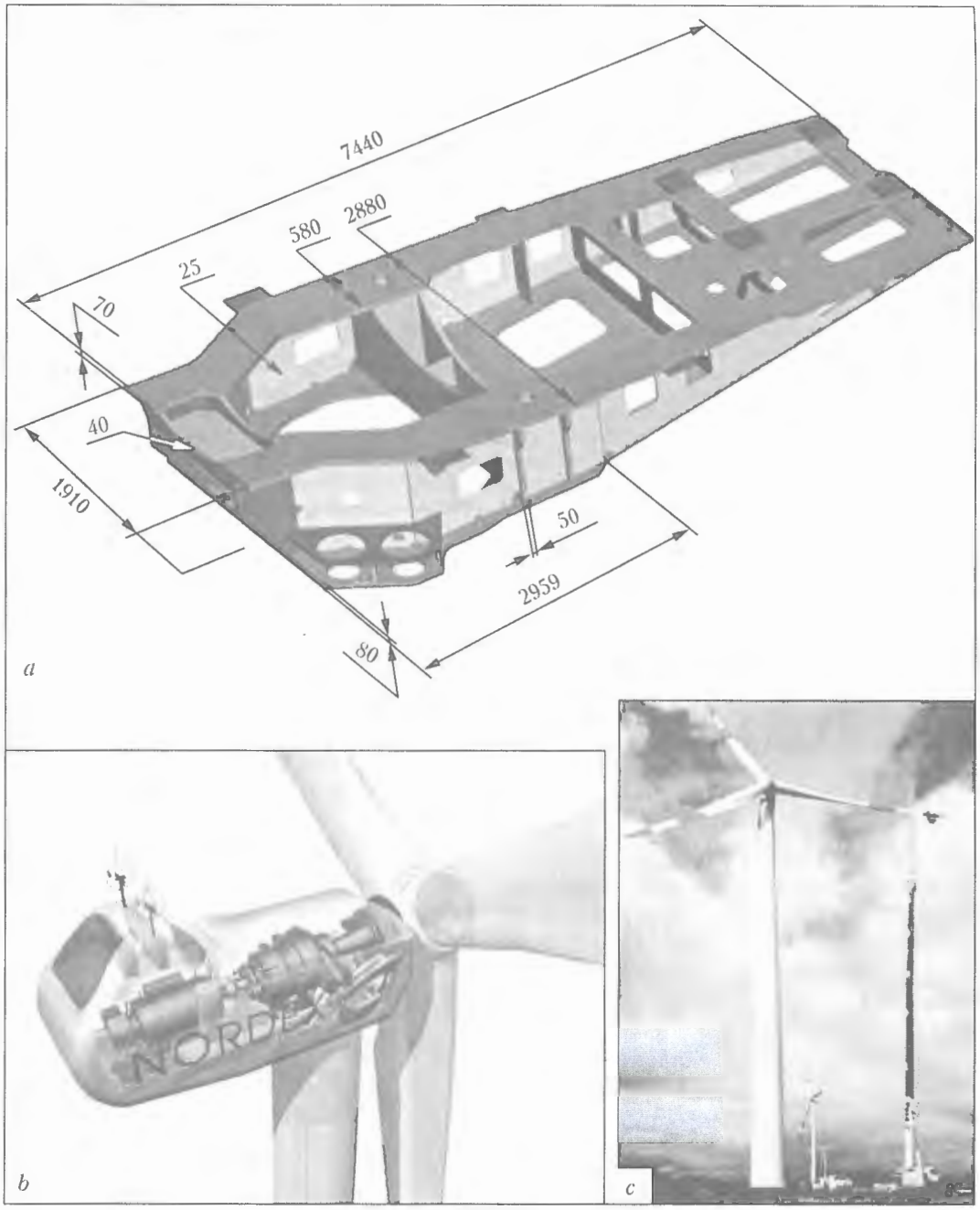

Figure 2. Wind-driven power plant with a capacity of 2550 kW: *a* — sketch of the frame; *b* — layout of devices mounted on the WPP frame; *c* — general view

way from Q_j^{min} to Q_j^{max} in one revolution of the shaft, the $Q_{j\alpha}/Q_j^{max} = R_{j\alpha}$ ratio being almost unchanged, where α is the angle of rotation of the shaft (Table 3). The following relationship, according to Table 2, exists between load variation amplitude ΔQ_j and Q_j^{max}:

$$\Delta Q_j = Q_j^{max}(1 - R_{j\alpha}^{min}). \quad (1)$$

If we determine components of stress tensor $\overline{\sigma}_{pq}^{(j)}$ caused by single load Q_j at corresponding points x, y, z of a welded joint by the elasticity theory methods, then, using the superposition method, we can find

Table 1. Chemical composition and mechanical properties of base and weld metals in WPP frame

Metal	*Content of elements, wt.%*						*Mechanical properties*			
	C	*Mn*	*Si*	*S*	*P*	*Al*	$\sigma_{0.2}$, *MPa*	σ_t, *MPa*	δ, %	KCV_{-40}, *J/cm²*
Base	0.14–0.17	0.68–1.03	0.23–0.29	0.010–0.023	0.009–0.020	0.027–0.420	285–339	424–470	24–33	–
Weld	0.07–0.10	1.47–1.54	0.85–0.90	0.013–0.015	0.010–0.012	–	> 400	480–600	> 22	> 47

Table 2. Extreme combinations of loads Q_j

Combination No.	Load case	$j = 1$	$j = 2$	$j = 3$	$j = 4$	$j = 5$	$j = 6$
		F_x, kN	F_y, kN	F_z, kN	M_x, kN·m	M_y, kN·m	M_z, kN·m
1	E1.1d1	441	186.4	102.2	2188	−4689	1374
2	S1.1a1	307.4	16	84.8	−34.4	−179.3	2136
3	E1.1d1	413.2	155.4	52.2	3748	−2911	1272
4	E1.11	374	134	123	1480	−3860	1180

total stresses $\sigma_{pq}^{(\alpha)}$ $(p, q = x, y, z)$ at point x, y, z for different angles α, i.e.

$$\sigma_{pq}^{(\alpha)} = \sum_{j=1}^{6} \bar{\sigma}_{pq}^{j}(x, y, z) Q_j^{\max} R_{j\alpha}. \qquad (2)$$

Therefore, nominal normal stresses that affect normal to the plane of lack of penetration, $\sigma_{qq}^{(\alpha)}$, at different points along the weld both on the inside and outside surface can be found for each weld on the frame under consideration. Membrane force $P_i^{(\alpha)}$ and momentum $M_i^{(\alpha)}$, where i is the number of a point along the weld, can be calculated from nominal stresses $\sigma_{qq}^{(\alpha)}$.

The $P_i^{(\alpha)}$ and $M_i^{(\alpha)}$ values are basic characteristics of external loading for the welds under consideration. Data on $\bar{\sigma}_{pq}^{(j)}(x, y, z)$ induced by single forces Q_j, which are necessary for their calculation, were obtained from numerical solution of elastic problems. Calculations were made using the finite element model shown in Figure 4.

To illustrate, Table 4 gives results of such calculations with respect to nominal $\bar{\sigma}_{xx\,\text{in}}^{(j)}$ and $\bar{\sigma}_{xx\,\text{out}}^{(j)}$ (index «in» stands for inside surface, and «out» — for outside surface of a corresponding member) for weld # 19 $(q = x)$ on the WPP frame at $j = 1, \ldots, 6$. Point number i is related to co-ordinate y through relationship $(i = y = -885/\Delta y)$.

Similar tables for $\bar{\sigma}_{qq}^{(j)}$ are available for all 60 welded joints made on the WPP frame. They are used as a basis for calculation of $P_i^{(\alpha)}$ and $M_i^{(\alpha)}$ depending upon Q_j.

Table 3. Variations of loads Q_j depending upon the shaft rotation angle α

α, deg	$R_{j\alpha} = Q_{j\alpha}/Q_j^{\max}$					
	$j = 1$	$j = 2$	$j = 3$	$j = 4$	$j = 5$	$j = 6$
0	0.4	0	0.55	0	1	0.2
90	0.7	1	1	1	0	0.6
180	1	0	0.55	0	−1	1.0
270	0.7	−1	0.1	−1	0	0.6
$R_{j\alpha}^{\min}$	0.4	−1	0.1	−1	−1	0.2

Loads Q_j may vary over wide ranges during operation. The Nordex Energy Company offers data on a spectrum of variations of amplitudes ΔQ_j in operation of the considered WPP. The calculation spectrum of amplitudes ΔQ_{jm} (Table 5), consisting of $m = 1, 2, \ldots, 23$ lines characterised by identical ΔN_m for all j at a base of approximately $N = 2 \cdot 10^8$ cycles, was formed on the basis of these data. Here ΔN_m is the number of cycles for a corresponding amplitude ΔQ_{jm} over the total lifetime of a structure. Using dependencies (1) and (2), they are employed to determine $P_{im}^{(\alpha)}$ and $M_{im}^{(\alpha)}$, which are the characteristics of loading at the corresponding i-th point in a specific weld, induced by the m-th component of spectrum of an external load.

In addition to the external load, residual welding stresses σ_{res} are also effective in the weld zone. It was assumed that for heat-treated welded joints the level of transverse stresses, averaged through thickness, is

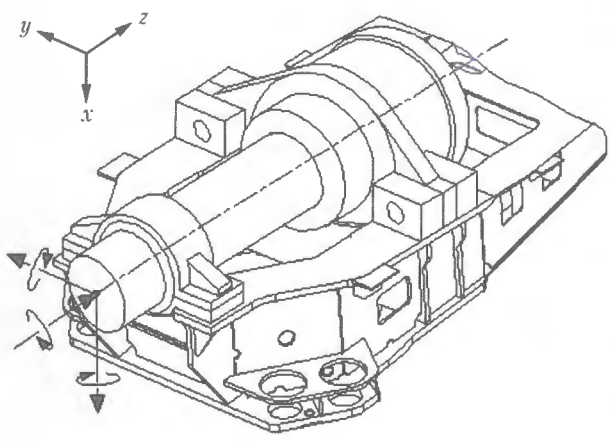

Figure 3. Schematic of application of loads on the drive shaft

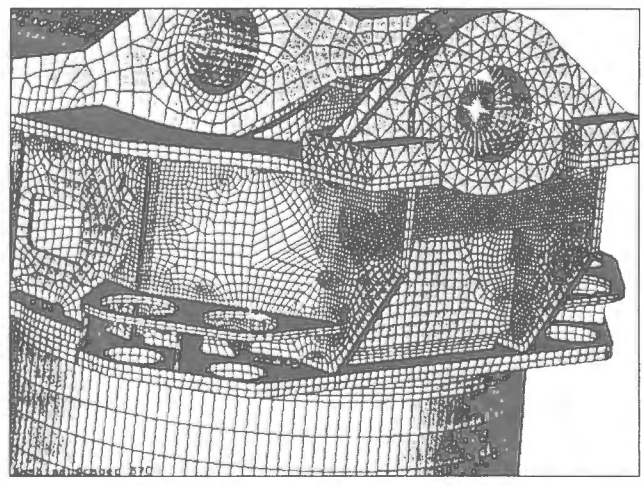

Figure 4. Model of WPP frame for FEM

Table 4. Values of $\bar{\sigma}^{(j)}_{xx\,in}\cdot 10^3$ and $\bar{\sigma}^{(j)}_{xx\,out}\cdot 10^3$ along weld # 19 (axis y) under single loads Q_j

i	$\bar{\sigma}^{(j)}_{xx\,in}\cdot 10^3$, *Pa*						$\bar{\sigma}^{(j)}_{xx\,out}\cdot 10^3$, *Pa*					
	$j=1$	$j=2$	$j=3$	$j=4$	$j=5$	$j=6$	$j=1$	$j=2$	$j=3$	$j=4$	$j=5$	$j=6$
1	8894	−2236	−5355	−624	−10770	12910	12790	−1462	−13080	−880	−12460	12660
2	7848	−2427	−3842	94	−10210	12480	12150	−1605	−12270	−174	−12130	12250
3	6639	−2458	−2515	472	−9206	11510	11180	−1620	−11320	197	−11270	11300
4	5459	−2395	−1430	618	−8056	10370	10090	−1549	−10350	335	−10170	10170
5	4404	−2285	−572	637	−6943	9269	9026	−1435	−9422	344	−9039	9082
6	3491	−2148	102	596	−5934	8290	8023	−1305	−8530	294	−7971	8110
7	2707	−1993	634	535	−5037	7430	7082	−1177	−7663	219	−6981	7259
8	2029	−1821	1056	473	−4236	6661	6187	−1060	−6802	137	−6061	6507
9	1441	−1630	1389	420	−3513	5956	5318	−962	−5929	56	−5197	5831
10	929	−1415	1642	380	−2853	5290	4459	−889	−5027	−23	−4376	5213
11	494	−1169	1811	355	−2245	4647	3590	−848	−4076	−104	−3587	4644
12	139	−888	1885	338	−1686	4012	2703	−838	−3068	−187	−2820	4117
13	−112	−542	1822	347	−1174	3369	1776	−876	−1976	−289	−2065	3636
14	−305	−151	1702	339	−686	2720	821	−886	−799	−371	−1316	3173
15	460	625	4	662	−530	1907	1	−1193	99	−669	−690	2900
16	1557	1304	−2375	254	−320	1112	−1152	−779	1557	−279	236	2278
17	−194	778	126	−426	573	982	−1119	−557	1049	−717	680	1642
18	−1439	425	1726	−765	1300	642	−928	−254	405	−1163	1012	1050
19	−1960	383	2078	−1164	1886	185	−895	31	−83	−1514	1449	440
20	−2438	439	2357	−1473	2490	−360	−1031	285	−320	−1796	1956	−198
21	−2998	572	2718	−1605	3186	−1066	−1500	486	−94	−1921	2628	−925

$\sigma_{res} \approx 0.2\sigma_y$, whereas for untreated joints it is equal approximately to $0.5\sigma_y$.

Estimation of acceptable size $2a$ of lack of penetration is made using a number of assumptions:

- lack of penetration is a flat crack with width $2a$ and length $l >> a$;
- normal to the crack plane coincides with the direction of effect of transverse stresses σ_{qq};
- stresses σ_{qq} gradually vary along the weld, thus, $P^{(\alpha)}_{im}$ and $M^{(\alpha)}_{im}$ can be assumed to be constant within the i-th point zone;
- the «crack» considered grows under service loading only due to increase in size $2a$;
- by the end of the specified service life at $N = 2\cdot 10^6$ cycles, the $2a$ size should not exceed $2a_{st}$, the value of which is determined from conditions of maintenance of static equilibrium of the crack at quasi-static application of extreme loads.

Consider determination of the critical values of $2a_{st}$.

Allowing for the brittle-tough behaviour of the material at the «crack» apex, the known procedure R6 [1] also recommended in [6] is used to determine critical size $2a_{st}$.

In this case, the value of $2a_{st}$ will be determined from solution of the following non-linear equation:

$$K_r = (1 - 0.14L_r^2)\,[0.3 + 0.7\exp(-0.6L_r^6)],$$

$$K_r = 0 \begin{cases} \text{at } L_r \le L_{r\,max}, \\ \text{at } L_r > L_{r\,max}, \end{cases} \qquad (3)$$

where $L_r = \sigma_{net}/\sigma_{0.2}$; σ_{net} is the effective stress in the net section, at which the possibility exists of a plastic collapse; $\sigma_{0.2}$ is the calculated value of yield stress of the material equal to $\sigma^{rat}_{0.2}/\gamma_M$; $\sigma^{rat}_{0.2}$ is the rated value of the material yield stress; γ_M is the safety factor; $L_{r\,max} = \dfrac{\sigma^{rat}_{0.2} + \sigma^{rat}_t}{2\sigma^{rat}_{0.2}}$; σ^{rat}_t is the rated value of tensile strength of the material; $K_r = K_I/K_c$, where K_I is the maximal value of the stress intensity factor; K_c is the calculated value of critical K_I equal to K^{rat}_c/γ_M; and K^{rat}_c is the rated value of K_c for the given material.

For the considered joints (see Figure 1), the values of $\sigma_{net,\,i}$ and $K_{I,\,i}$ can be determined at point i along the weld using nominal values of forces P_i and momenta M_i corresponding to the extreme loads taken from Table 1, or using the first line $m = 1$ of the load spectrum from Table 5, but at different α, based on the following dependencies [5]:

$$\sigma_{net,\,i} = \frac{P_i}{W - 2a^{(i)}_{st}} + \frac{6|M_i|}{W^3 - (2a^{(i)}_{st})^3}\,W, \qquad (4)$$

Table 5. Values of ΔQ_j in the formed spectrum of loads depending upon ΔN

m	$lg\,\Delta N$	ΔN	$j = 1$	$j = 2$	$j = 3$	$j = 4$	$j = 5$	$j = 6$
			F_x, kN	F_y, kN	F_z, kN	M_x, kN·m	M_y, kN·m	M_z, kN·m
1	0	1	271.8	304.8	304.7	4694	4556	1788
2	1	10	271.8	304.8	252.5	4690	4556	1328
3	2	100	268	304.8	207.2	4600	4556	1296
4	2.5	316	267	304.8	205.6	4570	4556	1270
5	3	1000	266	304.8	204.1	4553	4556	1269
6	3.5	3162	261	304.8	202.9	4506	4556	1198
7	4	10,000	262	274.3	201.7	4107	4214	1144
8	4.25	17,780	258	259.1	200.4	3943	4009	1090
9	4.5	31,620	248	243.8	199.2	3755	3826	1037
10	4.75	56,230	220	222.5	198	3567	3645	1010
11	5	100,000	217	198.1	195	3380	3417	983
12	5.25	177,830	190	183	186	3192	3257	930
13	5.5	316,230	177	164.6	176.7	3000	3007	894
14	5.75	562,340	163	152.4	170.6	2816	2825	822
15	6	1,000,000	149	140.2	158.4	2582	2597	778
16	6.25	1,778,280	129	128	143.2	2394	2392	715
17	6.5	3,162,280	115	114.3	128	2159	2164	681
18	6.75	5,623,410	103	99.1	115.3	2018	2005	590
19	7	10,000,000	97	91.4	97.5	1784	1822	536
20	7.25	17,783,000	81,5	79.2	82.3	1596	1595	492
21	7.5	31,624,000	68	67.6	70.1	1338	1367	393
22	7.75	56,234,000	58	54.8	54.8	1126	1113	358
23	8	100,000,000	47	45.7	42.6	938.8	911	304

$$K_{I,i} = \left(\frac{P_i}{\delta} + \sigma_{res}\right) B_i \sqrt{\pi a_{st}^{(i)} \sec \frac{\pi a_{st}^{(i)}}{W}} + \frac{3|M_i| a_{st}^{(i)} D_i}{4\left[\left(\frac{W}{2}\right)^3 - (a_{st}^{(i)})^3\right]} \sqrt{\pi a_{st}^{(i)} \left(1 - \frac{2a_{st}^{(i)}}{W}\right)}, \quad (5)$$

where

$$B_i = \frac{A_1 + A_2^2 a_{st}^{(i)} \cdot W}{1 + 2h/\delta},$$

$$A_1 = 0.528 + 3.287\frac{h}{\delta} - 4.361\left(\frac{h}{\delta}\right)^2 + 3.696\left(\frac{h}{\delta}\right)^3 - 1.875\left(\frac{h}{\delta}\right)^4 + 0.415\left(\frac{h}{\delta}\right)^5,$$

$$A_2 = 0.218 + 2.717\frac{h}{\delta} - 10.171\left(\frac{h}{\delta}\right)^2 + 13.122\left(\frac{h}{\delta}\right)^3 - 7.755\left(\frac{h}{\delta}\right)^4 + 1.783\left(\frac{h}{\delta}\right)^5,$$

$$D_i = \left[1 + \frac{a_{st}^{(i)}}{W} + \frac{3}{2}\left(\frac{a_{st}^{(i)}}{W}\right)^2 - \frac{11}{2}\left(\frac{a_{st}^{(i)}}{W}\right)^3 + 0.464\left(\frac{a_{st}^{(i)}}{W}\right)^4\right];$$

$W = \delta + 2h$ (h is determined from Figure 1).

The calculations of $2a_{st}$ were made for all joints under the extreme loads indicated in Table 1, four values of α and loads $m = 1$, according to Table 5. The least value was selected from eight versions of the $2a_{st}$ values.

Table 6 gives values of $2a_{st}$ for welded joint # 19 ($\delta = 50$ mm, $h = 4$ mm). To generate these data, it was assumed that $\sigma_{0.2}^{rat} = 300$ MPa, $\sigma_t^{rat} = 480$ MPa, $K_c^{rat} = 1400$ MPa·mm$^{1/2}$, and $\gamma_M = 1.4$, being the most severe situations according to [5]. In addition, the following limitation was assumed:

$$2a_{st} < 0.8W. \quad (6)$$

Table 6. Calculated values of $2a_{st}$ and $[2a^{(i)}]$ along the weld for welded joint # 19

y, mm	$2a_{st}$, mm	$[2a^{(i)}]$, mm	y, mm	$2a_{st}$, mm	$[2a^{(i)}]$, mm
885.3	36.5	3.3	1062	46.4	11.9
910.6	36.8	3.6	1087	46.4	14
936	38.1	4.4	1112	46.4	16.3
961	39.8	5.6	1138	46.4	18.9
986	41.7	6.9	1163	46.4	22
1011	43.4	8.5	1188	46.4	25
1037	45.1	10.1	1390	46.4	23.1

It can be seen that the values of $2a_{st}$ in Table 6 for zone $y \geq 1062$ mm were determined using equation (6).

Consider the algorithm of growth of the crack, i.e. lack of penetration. The rate of growth of the considered defect at the i-th point along the weld can be determined on an assumption that the spectrum of loads according to Table 5 always takes place.

Therefore, if we subdivide the total lifetime into K stages of tracing the propagation of the crack, at one stage the number of cycles for the m-th component will be $\Delta N_m/K$, where ΔN_m is determined from Table 5. Then the rate of growth from the m-th component of the spectrum per cycle in the i-th zone of the weld, according to [5], will have the following form:

$$v_m^{(i)} = \left(\frac{da^{(i)}}{dN}\right)_m = \frac{C_0 \Delta K_{I\,im}}{(1 - R_{im}) - \dfrac{\Delta K_{I\,im}}{K_c}} \quad (7)$$

$$\text{at } \Delta K_{I\,im} \geq \Delta K_{\text{th}\,im},$$

$$v_m^{(i)} = 0 \text{ at } \Delta K_{I\,\text{im}} < \Delta K_{\text{th}\,im}, \quad (8)$$

where $C_0 = 5 \cdot 10^{-13}$; $n = 3$ at $\Delta K_{I\,im}$ (MPa·mm$^{1/2}$); $\Delta K_{I\,im} = K_{I\,im}^{\max} - K_{I\,im}^{\min}$; $R_{im} = K_{I\,im}^{\min}/K_{I\,im}^{\max}$; $\Delta K_{\text{th}\,im}$ is the calculated threshold value determined as $\Delta K_{\text{th}\,im} = \Delta K_{\text{th}\,im}^{(0)}/\gamma_M$; and $\Delta K_{\text{th}\,im}^{(0)} = (190-144)R_{im}$, but not less than 62 MPa·mm$^{1/2}$, according to [5, p. 100].

Dependencies (5) were used to calculate $K_{I\,im}^{\max}$ and $K_{I\,im}^{\min}$, i.e. $K_{I\,im}$ were determined for four positions of the shaft characterised by angle α. $K_{I\,im}^{\max}$ and $K_{I\,im}^{\min}$ were found from these values. If $K_{I\,im}^{\min} < 0$, the use is made of the $K_{I\,im}^{\min}$ value, as under compression conditions the fatigue crack hardly propagates, i.e. in this case $R_{im} = 0$.

As the crack growth rate is usually $v \approx 10^{-8}$ mm/cycle for structural steels at a level of $\Delta K_I = \Delta K_{\text{th}}$, where the use of condition (8) does not lead to substantial errors for a lifetime base of $N < 10^7$ cycles, at the base of $N = 2 \cdot 10^8$ cycles it is better (more conservative) to write down this condition in the following form:

$$v_m^{(i)} = 10^{-8} \text{ mm/cycle at } \Delta K_{I\,im} < \Delta K_{\text{th}\,im}. \quad (8')$$

The total increment of size $\Delta a_k^{(i)}$ at the k-th tracing step, where $k = 1, \ldots, K$, is

$$\Delta a_{ik} = \sum_{m=1}^{23} v_m^{(i)} \frac{\Delta N_m}{K} \quad (9)$$

accordingly,

$$a_k^{(i)} = a_{k-1}^{(i)} + \Delta a_k^{(i)}, \quad (10)$$

if tracing is done from the set initial $a_0^{(i)}$ sizes of lack of penetration.

In this case, it is necessary to keep to inequality $2a_k^{(i)} < 2a_{st}^{(i)}$.

This sequence is convenient for estimation of acceptability of specific sizes $2a$ of the revealed defects. But if the task is to determine acceptable values of $[2a^{(i)}]$ under the set loading conditions, where it is possible to calculate $2a_{st}^{(i)}$, it is more convenient to conduct the process in a reverse order: $a_0^{(i)} = a_{st}^{(i)}$, accordingly $a_0^{(i)} = a_{st}^{(i)} - \Delta a_1^{(i)}$, etc. up to $k + K$, i.e. in this case

$$[2a^{(i)}] = 2a_K^{(i)}. \quad (11)$$

The quantity of tracing (integrating) cycles, K, is selected following the rules of numerical integration.

The described algorithm was applied to all 60 welded joints on the WPP frame under consideration.

It can be seen from Table 6 that $[2a^{(i)}]$ along the weld length may vary over considerably wide ranges. Availability of these data for all welded joints on the frame allows a rational planning of its repair in terms of maintaining the dimensional stability.

1. Harrison, R.P., Loosemore, K., Milne, J. et al. (1980) Assessment of the integrity of structure containing defects. In: *Report P/H R6*. Rev. 2 of Central Electricity Generating Board. Berkeley.
2. Harrison, J.D. (1984) Fracture mechanics developments related to the weld defect acceptance methods given in British standard PD 6493: Fract. and Fract. Mech. Case Study. In: *Proc. of 2nd Math. Conf.* (Johannesburg, Nov. 27, 1984).
3. *M-01–88*: Procedure of calculation of acceptable defects in metal of equipment and pipelines in operation of APP. Moscow: NIKIET.
4. *MP-125-01–90*: Calculations of stress intensity factors and section weakening factors for defects in welded joints. Kiev.
5. (1996) Recommendations for fatigue design of welded joints and components. *IIW Doc. XIII*.
6. IIW Guidance on assessment of the fitness for purpose of welded structures. *IIW/IIS-SST-1157–90*.

OPTIMIZATION OF TRANSFORMER WITH DEVELOPED TRANSVERSAL MAGNETIC STRAY FLUXES

S.V. RYMAR
E.O. Paton Electric Welding Institute, NASU, Kiev, Ukraine

An optimization model of a single-phase transformer with intensive transverse stray fluxes flowing from core to core in the magnet core has been developed. The model allows calculation of transformers optimum by weight, volume and cost, both with mobile and with stationary windings, while ensuring the specified value of stray inductance.

Keywords: *transformer, transversal magnetic stray fluxes, stray inductance, parameters, welding machinery, optimization*

Single-phase transformers with developed transversal magnetic stray fluxes (DTMSF) running from rod to rod of the magnet core are most widely used in the welding power sources for stick electrode welding. Theory of their calculation was developed at the E.O. Paton Electric Welding Institute by Prof. V.K. Lebedev and published in [1–4]. Studies on distribution of magnet fluxes in a transformer [5] and modernization of the procedure for calculation of stray inductances [6] developed this theory. Problems on optimization of such transformers were considered in [7], however in this case it was required to calculate a large number of variants to find the optimal transformer.

Full separation of dependent and independent parameters in the optimization model of the transformer with flat external characteristic was carried out by Prof. I.V. Pentegov under analytical calculation of the optimal transformer [8–13], which allowed unambiguously finding an optimal variant. However, these methods as applied to the transformer under consideration do not guarantee obtaining an optimal variant with the required level of stray inductance. This problem has not been solved so far because of rigid parameter, namely a preset value of the stray inductance, whose consideration is an essential problem under differentiation of the optimization function. The problem was solved by means of the developed optimization model intended for numerical methods of optimization.

The aim of this work is to describe the developed optimization model of a single-phase transformer with DTMSF with movable and stationary windings, tough restriction by a preset level of stray inductance and a full separation of dependent and independent variables.

DTMSF in the transformer under consideration are provided by separating primary and secondary winding by a length of rods of magnet core (Figure) due to which the fluxes run from one rod to another. Stray inductance smoothly changes because windings are moving apart by the length of the rods. When windings are converging the stray inductance is decreasing, when they are moving apart it is increasing, respectively, the welding current increasing and decreasing. The following designations are presented in the Figure: a, b are the thickness and width of the magnet core rod; h_{op}, l_{op} are the height and width of the magnet core opening; h_{c1} and h_{c2}, C_{c1} and C_{c2}, C_{cw1} and C_{cw2} are the height, thickness and total thickness of coils with primary and secondary windings; l_{c1}, l_{c2} are the preset distances between lateral surfaces of the coils with primary and secondary windings in the opening of magnet core; Δh_1, Δh_2 are the preset lengths the magnet core parts protruding from the coils with primary and secondary windings; $\Delta h_{1,2}$ is the distance between the faces of the coils with primary and secondary windings; d_{w1}, d_{w2} are the preset distances between the magnet core rods and primary and secondary windings.

Let us consider two-winding transformer powered by industrial mains with sinusoidal voltage. Effect of the current ousting to the winding conductor surface

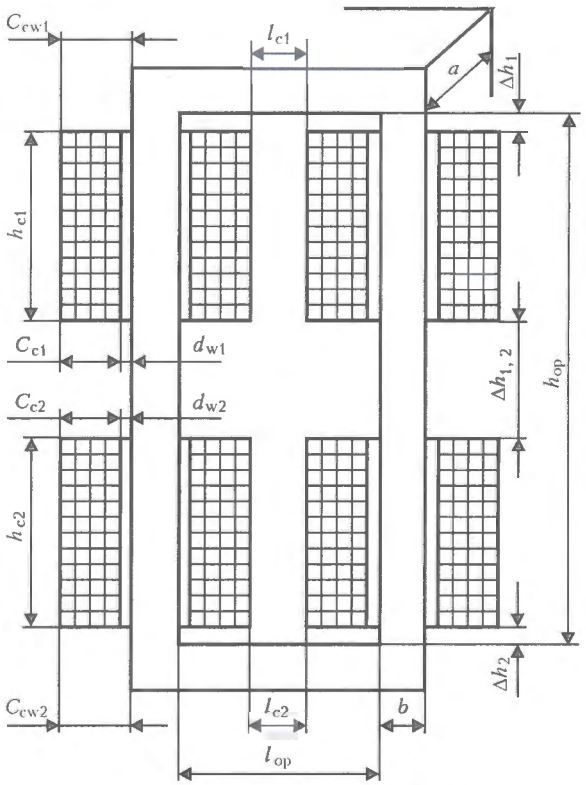

Diagram of a single-phase transformer with DTMSF (for designations see the text)

© S.V. RYMAR, 2005

is negligible. Only active materials of the transformer, such as electric steel of the magnet core, copper or aluminium of the conductors of its winding conductors are considered in optimization.

The optimization model of the transformer is a procedure of the global cycle, which begins by assigning to an intermediary variable F' a starting value of the optimization function F, while in subsequent transformations assignment of the value of the optimization function calculated at the previous step of the cycle is

$$F' = F. \tag{1}$$

Initial value $\Delta w = 0.1w_1$ of the step is also preset by turns of the primary winding of the transformer (with initial value the number of turns of the primary winding of the transformer being w_1), after which there follow the expressions of the first local cycle starting from the calculation of the active cross-section of the rod and the yoke of the magnet circuit [14]:

$$S_s = \sqrt{2U_1}/(\omega w_1 B_m), \tag{2}$$

where U_1 is the preset active value of the voltage on the primary winding of the transformer; ω is the angular frequency of the supply mains voltage calculated by the preset value of the mains f_{mains} equal to $2\pi f_{mains}$; B_m is the preset amplitude value of the magnet inductance in the magnet core.

Thickness of the rod and the yoke of magnet core is [14]

$$a = S_s/(k_s b), \tag{3}$$

where k_s is the preset coefficient of the magnet core filling with plates of the electrical steel.

Cross-sections of the active material of the primary and secondary winding in the opening of the magnetic core [13] are determined from the correlation:

$$S_{w1} = w_1 I_{1l}/J_{1l}; \quad S_{w2} = w_1 I_{2l}/(k_{tr} J_{2l}), \tag{4}$$

where I_{1l}, I_{2l} and J_{1l}, J_{2l} are, respectively, the long-term active values of currents and preset density currents in the primary and secondary windings of the transformer; k_{tr} is the transformation coefficient equal to U_1/U_2; U_2 is the preset active value of the phase voltage on the secondary winding in the open-circuit mode.

Long-term active values of phase currents in the primary and secondary windings of the transformer are equal to

$$I_{1l} = I_1\sqrt{X/100\ \%}; \quad I_{2l} = I_2\sqrt{X/100\ \%}, \tag{5}$$

where I_1, I_2 are the active values of currents in the primary [15] and secondary windings of the transformer (current I_2 for welding transformers is usually preset); X is the assigned duty cycle of the transformer, %.

Height of the coil with the primary winding is equal to

$$h_{c1} = S_{w1}/(2k_{w1}C_{c1}), \tag{6}$$

where k_{w1} is the coefficient of filling of the primary winding with the conduction material (k_{w1} = 0.50–0.95).

Total thickness of the coil with the primary winding is

$$C_{cw1} = d_{w1} + C_{c1}; \tag{7}$$

while the width of the magnet core opening is determined from the expression

$$l_{op} = 2C_{cw1} + l_{c1}; \tag{8}$$

thickness of the coil with the secondary winding is

$$C_{c2} = (l_{op} - l_{c2})/2 - d_{w2}; \tag{9}$$

total thickness of the coil with the secondary winding is

$$C_{cw2} = d_{w2} + C_{c2}; \tag{10}$$

height of the coil with the secondary winding is

$$h_{c2} = S_{w2}/(2k_{w2}C_{c2}), \tag{11}$$

where k_{w2} is the coefficient of filling of the secondary winding with the conduction material.

Average lengths of turns of primary and secondary windings are determined from the following correlations:

$$\begin{aligned} l_{av.t1} &= 2(a + b) + 2\pi(d_{w1} + C_{c1}/2); \\ l_{av.t2} &= 2(a + b) + 2\pi(d_{w2} + C_{c2}/2). \end{aligned} \tag{12}$$

Formulas (1), (10) and (21) from [16] are used to calculate the least values of the inductances of the transformer (L_c^{min} — the stray inductance (inductance of short circuit); L_s^{min} — the stray inductance of transversal fluxes propagating between the rods of the magnet core; ΔL_{fr}^{min} — the component of the inductance of the frontal flow of stray running from face to face of every coil outside magnet core at a preset minimal distance between windings $\Delta h_{1,2} = \Delta h_{1,2}^{min}$), the number of turns of the primary winding of the transformer is defined:

$$w_1 = \begin{cases} w_1 + \Delta w, & \text{if } L_c^{min} < L_{sh.c}^{min}, \\ w_1 - \Delta w, & \text{if } L_c^{min} > L_{sh.c}^{min}, \end{cases} \tag{13}$$

where $L_{sh.c}^{min}$ is the least assigned value of the stray inductance.

The expression (13) forms a sub-cycle to enter into which requires the use of only one of its current conditions with unchanged value Δw with recalculating the value L_c^{min} at every step. The sub-cycle should be performed as long as the current condition is true. After this a value of the step by turns of the primary winding decreases $\Delta w = 0.5\Delta w$. A condition for exit from the first local cycle has the form of

$$|L_{sh.c}^{min} - L_c^{min}|/L_{sh.c}^{min} < \varepsilon_1, \tag{14}$$

where ε_1 is the preset accuracy of calculations in the first local cycle.

The expressions (2)–(14) forms the first local cycle, which is performed until the condition (14) is met.

To provide the highest assigned value of the stray inductance $L_{sh.c}^{min}$ it is necessary to determine a maximal distance between the faces of the coils with primary and secondary windings $\Delta h_{1,2} = \Delta h_{1,2}^{max}$.

Initial value of the stray inductance between the rods of the magnet core of the transformer is calculated by the formula (1) from [6]:

$$L_s^{max'} = L_{sh.c}^{max} - \Delta L_{fr}^{min},$$

where instead of L_{fr}^{max} there is ΔL_{fr}^{min} calculated previously at $\Delta h_{1,2} = \Delta h_{1,2}^{min}$ since the value $\Delta h_{1,2}^{max}$ is still unknown. In the considered case the initial value $\Delta h_{1,2}^{max}$ obtained by formula (10) from [6] solved in relation to $\Delta h_{1,2}$ is equal to

$$\Delta h_{1,2}^{max} = L_s^{max'}/(\mu_0 \omega_1^2 g_y) - (h_{c1} + h_{c2})/3,$$

where μ_0 is the magnet constant; g_y is the specific geometrical conductivity between the rods of the magnet core.

Initial value for determination of the distance between the faces of the coils with primary and secondary windings $\Delta h_{1,2}^{max}$ is $\Delta_{1,2} = 0.1\Delta h_{1,2}^{min}$.

To refine the value of $\Delta h_{1,2}^{max}$ the second local cycle is used starting from calculation of the values of stray inductances of the transformer L_s^{max}, ΔL_{fr}^{max} and L_c^{max}, respectively by the formulas (1), (10), (21) from [6] by substituting there the value $\Delta h_{1,2} = \Delta h_{1,2}^{max}$:

$$\Delta h_{1,2}^{max} = \begin{cases} \Delta h_{1,2}^{max} + \Delta_{1,2}, & \text{if } L_c^{max} < L_{sh.c}^{max}, \\ \Delta h_{1,2}^{max} - \Delta_{1,2}, & \text{if } L_c^{max} > L_{sh.c}^{max}. \end{cases} \quad (15)$$

The expression (15) forms a sub-cycle the entrance to which requires the use of one of its current conditions with unchanged value $\Delta_{1,2}$ with recalculation of $\Delta h_{1,2}^{max}$ at every step. The sub-cycle is performed as long as the current condition of the sub-cycle is true. After this the value of the step $\Delta_{1,2} = 0.2\Delta_{1,2}$ decreases and the performance of the condition on exit from the second local cycle is checked:

$$|L_{sh.c}^{max} - L_c^{max}|/L_{sh.c}^{max} < \varepsilon_2, \quad (16)$$

where ε_2 is the preset accuracy of calculations at the second local cycle.

The expressions (15) and (16) form the second cycle, which is performed until the condition (16) is met.

After this a height of the opening of the magnet core is determined:

$$h_{op} = \Delta h_1 + h_{c1} + \Delta h_{1,2}^{max} + h_{c2} + \Delta h_2, \quad (17)$$

average length of magnetic field line in magnet core:

$$l_{av} = 2(h_{op} + l_{op}) + 4b, \quad (18)$$

volume, weight and cost of active materials of the magnet core and windings:

$$V_s = l_s S_s;\ M_s = \gamma_s V_s;\ C_s = c_s M_s; \quad (19)$$

$$V_w = l_{av.t1} S_{w1} + l_{av.t2} S_{w2};\ M_w = \gamma_w V_w;\ C_w = c_w M_w, \quad (20)$$

where γ_s, γ_w are the density of active materials of magnet core and windings; c_s, c_w are the specific cost of active materials of magnet core and windings, cmu/kg (cmu is the conditional monetary unit).

Volume, weight and cost of active materials of the transformer is determined by the correlations:

$$V = V_s + V_w;\ M = M_s + M_w;\ C = C_s + C_w. \quad (21)$$

Optimization function of the transformer has the following form [13]:

$$F = M_s + k_g M_w, \quad (22)$$

where k_g is the generalized weight coefficient assigning a correlation between the weights of active material of magnet core and the windings.

Condition for exit from the global cycle has the following form:

$$|F - F'|/F < \varepsilon, \quad (23)$$

where ε is the preset accuracy of calculations in the global cycle.

Analysis of the optimization model of the transformer (1)–(23) allows a conclusion that the two values b and C_{c1} are independent variables while the rest of them are either preset or dependent. Independent variables are determined as a result of minimization of the function F. Minimal values of the optimization function may be found by using numerical methods of optimization, for example, the Gauss–Seidel method (coordinate descent) [16] with assigned primary valuables of independent variables b and C_{c1}. The minimization of the function F permits determining the optimal values of the variables b, C_{c1} and other values constituting the optimization model.

At the coefficient $k_g = 1$ the calculation of the transformer is carried out for the minimum weight of the active materials; at γ_s/γ_w — for minimum volume of the active materials, at c_w/c_s — at the minimum cost of the active materials. In the general case the coefficient k_g may assume any other values [13].

For optimization calculation of the transformers with stationary windings it is possible to use the obtained optimization model but excluding from it the expressions (15), (16) which calculate the maximal distance between the faces of the coils with primary and secondary windings $\Delta h_{1,2}^{max}$ to provide the highest value of the stray inductance L_c^{max} and to remove indices min and max in the remaining expressions (13), (14) and (17).

The elaborated optimization model was used for calculation of transformers of the welding power

sources developed at the E.O. Paton Electric Welding Institute. Let us consider the data of the welding transformer with mobile windings calculated by means of the elaborated optimization model for minimum weight of the active materials. These data may be used for production of a transformer with smooth current regulation for stick electrode welding intended for repair shops and for every day use.

The transformer has the following parameters: U_1 = 220 V; U_2 = 60 V; f_{mains} = 50 Hz; X = 25 %; k_{tr} = 3.667; L_c^{min} = 13.91 mH; L_c^{max} = 31.22 mH (reduced to primary winding) with a possibility to regulate the welding current within I_2 = 75–160 A. Then the values for the parameters for the nominal current 160 A are presented: I_1 = 45.58 A; I_{1l} = 23.76 A; J_{1l} = = 2.27 A/mm^2; J_{2l} = 2.58 A/mm^2; no-load current is 1.943 A (4.26 %); transformer power is 9.6 kV·A; arc voltage is 26.4 V; efficiency is 94 %; B_m = 1.63 T; electrical steel 3414 (0.35 mm thick); c_s = = 1.4 cmu/kg; copper winding; c_w = 3.3 cmu/kg; M_s = 22.5 kg; M_w = 11.7 kg; M = 24.2 kg; C_s = = 27 cmu; C_w = 28 cmu; C = 55 cmu.

Parameters of the windings are as follows: coils of primary winding are connected in sequence, w_1 = 198 (the number of turns in one coils is 99, 13 turns are in the layer, 8 turns in the last layers, the number of layers is 8); coils of secondary winding are connected in parallel (coils are mobile), $w_2 = w_1/k_{tr}$ = 54 (the number of turns in one coil is 54, 14 turns are in the layer, 12 turns are in the last layer, the number of layers is 4); conductor of the primary winding is 2.65 × 4 mm in dimension (thickness of the insulation by two sides is 0.27 mm); conductor of the secondary winding is 3.15 × 6 mm in dimension (thickness of the insulation by two sides is 0.5 mm); thickness of the inter-layer insulation is 0.15 mm; length of the wire of primary winding is 66.5 m, that of the secondary winding is 19.5 m.

Geometrical dimensions of the transformer are as follows: a = 65 mm; b = 50 mm; h_{op} = 310 mm; l_{op} = = 75 mm; h_{c1} = 63 mm; C_{c1} = 26 mm; C_{cw1} = 29 mm; h_{c2} = 87 mm; C_{c2} = 18 mm; C_{cw2} = 28 mm; l_{c1} = = 16 mm; L_{c2} = 18 mm; d_{w1} = 3 mm; d_{w2} = 10 mm; $\Delta h_1 = \Delta h_2$ = 6 mm; $\Delta h_{1,2}^{min}$ = 8 mm; $\Delta h_{1,2}^{max}$ = 148 mm; dimensions of the transformer are 230 × × 130 × 405 mm.

Heat characteristics are as follows: an average temperature of the primary winding is 140 °C, of the secondary one is 130 °C and of the magnet core is 75 °C with ambient temperature 40 °C; insulation class is F [14].

CONCLUSION

The optimization model of a single-phase transformer with DTMSF with stationary and mobile windings and with full separation of dependent and independent variables is proposed.

The model allows optimizing the transformer for a minimum weight, volume and cost of its active materials providing the assigned values of the stray inductance. The optimization model will be helpful for designers of new welding power sources.

1. Paton, B.E., Lebedev, V.K. (1953) *Elements of design of alternating-current circuits and apparatuses for arc welding*. Kiev: AN Ukr. SSR.
2. Paton, B.E., Lebedev, V.K. (1966) *Electric equipment for arc and slag welding*. Moscow: Mashinostroenie.
3. Lebedev, V.K., Koritsky, V.A. (1961) Design of short-circuit resistance of welding transformer with moving winding. *Avtomatich. Svarka*, **7**, 21–24.
4. Lebedev, V.K., Koritsky, V.A. (1965) Power losses in casings of welding transformers with developed leakage. *Ibid.*, **7**, 1–6.
5. Pentegov, I.V., Rymar, S.V. (1997) Specifics of design of transformers with developed transverse magnetic leakage fluxes. *Tekhn. Elektrodinamika*, **2**, 41–48.
6. Pentegov, I.V., Rymar, S.V. (2004) Specifics of design of leakage inductance of transformers with developed magnetic leakage fluxes. *Elektrotekhnika i Elektromekhanika*, **2**, 38–45.
7. Feder, E.S., Pesenson, A.E. (1965) On design of arc welding transformers with moving windings. *Avtomatich. Svarka*, **7**, 7–10.
8. Pentegov, I.V. (1962) On design of resistance welding transformers. *Ibid.*, **9**, 13–17.
9. Pentegov, I.V. (1960) Determination of optimal sizes of transformers. *Izvestiya Vuzov. Elektromekhanika*, **8**, 69–76.
10. Pentegov, I.V., Stemkovsky, E.P., Shejkovsky, D.A. (1980) Design of capacitor-discharge resistance welding transformer. *Ibid.*, **3**, 26–30.
11. Pentegov, I.V., Stemkovsky, E.P., Shejkovsky, D.A. (1981) Determination of optimal number of secondary turns of transformers for alternating-current resistance welding and capacitor-discharge welding. *Ibid.*, **4**, 11–15.
12. Pentegov, I.V., Stemkovsky, E.P., Shejkovsky, D.A. (1983) Determination of optimal parameters of welding transformers of resistance machines with predetermined turns resistance. *Avtomatich. Svarka*, **11**, 35–40.
13. Pentegov, I.V., Rymar, S.V., Stemkovsky, E.P. (2002) Optimized mathematical model of three-phase transformer and selection of its designed version in multicriterion optimization. *Tekhn. Elektrodinamika*, **1**, 22–28.
14. Tikhomirov, P.M. (1986) *Design of transformers*. Moscow: Energoatomizdat.
15. Rymar, S.V. (2005) Optimization of transformer with developed yoke magnetic leakage fluxes. *The Paton Welding J.*, **7**, 27–30.
16. Koryachko, V.P., Kurejchik, V.M., Norenkov, I.P. (1987) *Theoretical principles of CAD*. Moscow: Energoatomizdat.

PRODUCING A FLAME-SPRAYED COATING USING HYDROGEN-OXYGEN FLAME

V.N. KORZH and **Yu.S. POPIL**
National Technical University of Ukraine «Kiev Polytechnic Institute», Kiev, Ukraine

Influence of the combustible mixture composition and nature of its flow on the energy state of a spraying particle is considered. Conditions are established of producing flame-sprayed coatings of materials with different melting temperatures, using hydrogen-oxygen flame, generated when burning a mixture produced by water-electrolysis generators.

Keywords: *hydrogen-oxygen flame, water-electrolysis generator, laminar flow, turbulent flow, particle velocity, adhesion strength, coating porosity*

One of the conditions to produce a sound flame-sprayed coating is provision of the required energy level of particles of the spraying material on the item surface. Energy state of the particles is determined by the sum of energies, namely thermal energy, characterized by the heating temperature, and kinetic energy [1–3].

In flame spraying with powder material, the spraying material particle is heated up to the temperature of plastic state or melting temperature due to convective heat exchange between the plume flame combustion products and particle. This proceeds in the temperature range of effective temperatures, where the temperature of the combustion products is by 300 °C higher than that of melting [4]. The plume area, in which the particle temperature is not lower than that of material melting, and does not drop below this temperature, determines the working zone of the flame plume for flame spraying of coatings.

Investigations conducted by the Chair of Reconditioning of Machine Parts of the Welding Department of NTUU «Kiev Polytechnic Institute» [5], showed that the length of the effective temperature zone and working zone depends on the plume combustion mode and combustible mixture composition. For the hydrogen-oxygen flame generated at combustion of a mixture produced by a water-electrolysis generator, the length of the zone of effective temperatures at spraying of materials at melting temperature is up to 1000 °C and higher at laminar mode of combustion product flow. It increases, if hydrocarbon compounds are added to the vapour mixture.

In spraying of materials with the melting temperature above 1000 °C, the length of effective temperature zone is greater at turbulent flow of the combustion product jet.

Velocity distribution of the combustion product flow along the flame plume was established by experimental-design method. Calculation was performed using experimental data on distribution along the plume of temperature [5, 6] and head pressure of the combustion product gas jet, obtained using a water-cooled probe (Pito–Prandtl tube) [7]. Maximum velocity of spraying particles was experimentally established using ISSO-1 instrument [8]. Experimental data differed from the design data by ± 5 %.

Influence of the combustible mixture composition and mode of combustion product flow on the velocity of 20–40, 20–63 and 63–100 μm spraying particles of copper, iron (PZh-1) and nickel alloy (PG-AN-33) powders, respectively, was studied. The above materials were selected on the basis of analysis of powder materials widely used in flame spraying of coatings, which have different ranges of melting temperatures, characteristic of flame spraying.

Analysis of distribution of particle movement velocity W_p along the flame plume length showed that it has three zones, namely zone of acceleration where the particle acquires the velocity from the minimum to the maximum; stable motion, where the velocity varies in the range from 5 to 10 %; and braking where the particle velocity decreases.

Study of the velocity of motion of a copper powder particle showed that at laminar mode of flow of combustion products of hydrogen-oxygen mixture (HOM) and HOM + 16 % ethyl alcohol vapours, the particles acquire the maximum velocity of motion at distance L = 300 mm from the edge of the torch nozzle, and at combustion of a mixture of HOM + 5.5 % benzene vapours — at 250 mm distance. Maximum velocity of particle motion at spraying powder with 20 to 40 μm particle size and laminar flow of HOM combustion products is equal to 95 m/s at 250 mm distance.

Adding hydrocarbon compounds to the combustible mixture increases the velocity of particle motion up to 117 m/s (Figure 1, *a*). At laminar mode of combustion product flow of HOM and HOM + 16 % alcohol vapours, the zone of particle acceleration is the most extended, while the zone of stable motion of a particle is practically absent, and forms only at combustion of a mixture of HOM + 5.5 % benzene vapours.

At transition of the gas jet flow mode into the turbulent mode the acceleration zone is reduced to 100–150 mm, i.e. it is practically two times smaller than with the laminar flow. Accordingly, the maximum velocity of particle acceleration is 10 % lower (Table 1). Zone of stable particle motion extends prac-

© V.N. KORZH and Yu.S. POPIL, 2005

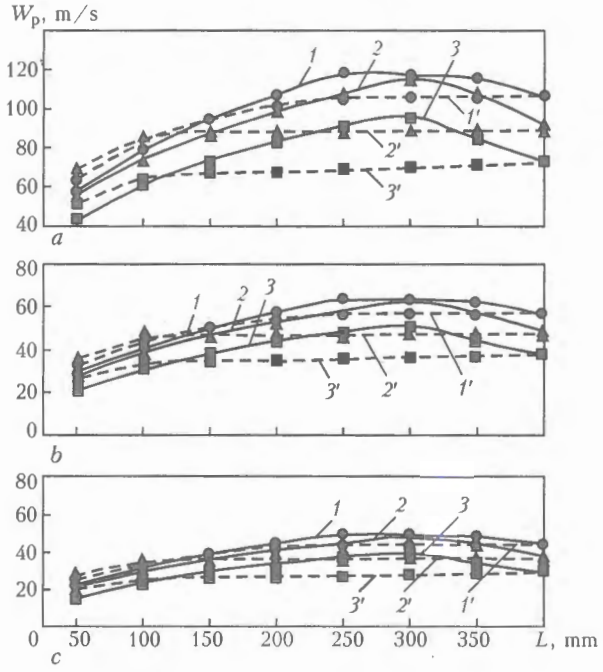

Figure 1. Dependence of motion velocity of powder particles of sizes 20–40 (*a*), 20–63 (*b*) and 63–100 μm (*c*) on the gas plume length at laminar (*1–3*) and turbulent (*1′–3′*) mode of the flow, respectively: *1*, *1′* — HOM + 5.5 % benzene vapours; *2*, *2′* — HOM + 16 % alcohol vapours; *3*, *3′* — HOM

tically to the entire working length of the plume, remaining after the acceleration zone (see Figure 1).

With increase of particle size, the general regularity of distribution of the velocity of particle motion along the plume length is preserved, but the maximum velocity of motion is significantly decreased (Figure 1, *b*, *c*).

Studying the velocity of iron powder particle motion showed that the mode of its distribution along the plume length does not change compared to copper powder, but the velocity of iron powder particles is higher. Maximum velocity of motion of iron powder particles of 20 to 40 μm size is achieved at laminar mode of the combustion product flow of the mixtures of HOM + 5.5 % benzene vapours and HOM + 16 % alcohol vapours at about 250 to 300 mm distance from the nozzle edge (Figure 2) and is equal to 125 m/s.

Analysis of particle motion velocity when using nickel alloy powder (Figure 2, Table 3) showed that they preserved the general regularity of motion in the gas flow of the combustion products, similar to other studied materials. Maximum velocity of particle motion is lower compared to iron powder and higher than that for copper powder. For powder with particle size of 20 to 40 μm the maximum velocity of particle motion is approximately 120 m/s at combustion of a

Table 1. Maximum velocity of motion of various metal powder particles (m/s) depending on particle size and mode of combustion product flow

Combustion product composition	*Powder particle size, μm*					
	20–40		*20–63*		*63–100*	
	Design	*Experiment*	*Design*	*Experiment*	*Design*	*Experiment*
	Copper powder					
HOM	95/70	90/65	50/35	45/30	40/30	35/25
HOM + benzene vapours	117/105	110/100	65/55	65/50	50/45	45/35
HOM + alcohol vapours	115/90	110/85	60/50	55/45	45/35	40/30
	PZh-1 iron powder					
HOM	105/80	100/75	60/40	55/35	50/30	45/25
HOM + benzene vapours	127/117	120/110	70/65	65/60	60/50	55/45
HOM + alcohol vapours	125/100	120/95	70/60	65/55	55/45	50/40
	PG-AN-33 nickel alloy powder					
HOM	102/75	95/70	55/40	50/35	40/30	35/25
HOM + benzene vapours	120/110	115/105	65/60	60/55	50	45
HOM + alcohol vapours	120/95	115/90	65/50	60/45	50/38	45/30

Notes. 1. Numerator gives the values at laminar mode of gas flow, denominator — at turbulent mode. 2. Measurement by experimental procedure was conducted at 400 and 150–200 mm plume length at laminar and turbulent mode of combustion product flow, respectively.

mixture of HOM + 5.5 % of benzene vapours and laminar mode of the combustion product flow.

When benzene vapours are added to the combustible mixture, a pronounced zone of a stable particle motion is found, and the maximum velocity of their motion is higher than when other gas mixtures are used.

Proceeding from the energy state of the spraying particles, the probability of producing a sound coating from various metals may be evaluated by analyzing the length of the flame plume working zone L_{FWZ}, acceleration zone L_{PAZ} and of the zone of stable particle motion L_{SPMZ}, as well as maximum velocity of spraying particle motion on the working zone boundary. There exist three variants of the ratio between the working zone of the flame plume and velocity zones, by which it is possible to evaluate the possibility of producing a sound coating:

$$L_{FWZ} = L_{PAZ} + L_{SPMZ};$$
$$L_{FWZ} < L_{PAZ} + L_{SPMZ};$$
$$L_{FWZ} > L_{PAZ} + L_{SPMZ}.$$

Analysis of the length of the plume working zone, zones of acceleration and stable particle motion, allowing for the maximum velocity of the spraying particles on the working zone boundary (Table 2), showed that producing a sound coating is the most probable at spraying of a copper powder with 20 to 40 μm particle size and laminar flow mode of the combustion products of HOM + 5.5 % benzene vapours and HOM + 16 % alcohol vapours (Table 2, variants 3 and 5) with about 300 mm optimum spraying distance. In this case, the energy state of the spraying particle is maximum, namely movement velocity at the working zone boundary is more than 100 m/h; working zone length is 300 mm; lengths of acceleration and stable motion zones are commensurate with that of the working zone.

In the case of a turbulent mode of combustion product flow, the flame working zone length is reduced to 160 mm in copper spraying. And although the zone of powder particle acceleration is commensurate with it, the maximum velocity of particle motion at the working zone boundary is higher than 50 m/h only for particles of 20 to 40 μm size in combustion of HOM (W_p = 65 m/s) and HOM + 16 % alcohol vapours (W_p = 90 m/s). Hence, the probability of producing the coating in this case is much lower than at laminar flow of the combustion products, as in the case of more than 160 mm spraying distance the particles are cooled down.

If iron powder is used, coating formation can only be anticipated at powder particle size of 20 to 40 μm and turbulent mode of combustion of HOM + 5.5 % benzene vapours or HOM + 16 % alcohol vapours. In this case, the maximum velocity of powder particle motion on the working zone boundary is not higher than 95 m/s at the working zone length of 100 to 110 mm. Spraying distance should fall within this range, as at a greater spraying distance the particles cool down. At a short distance the probability of producing a sound coating is much lower than at copper powder spraying.

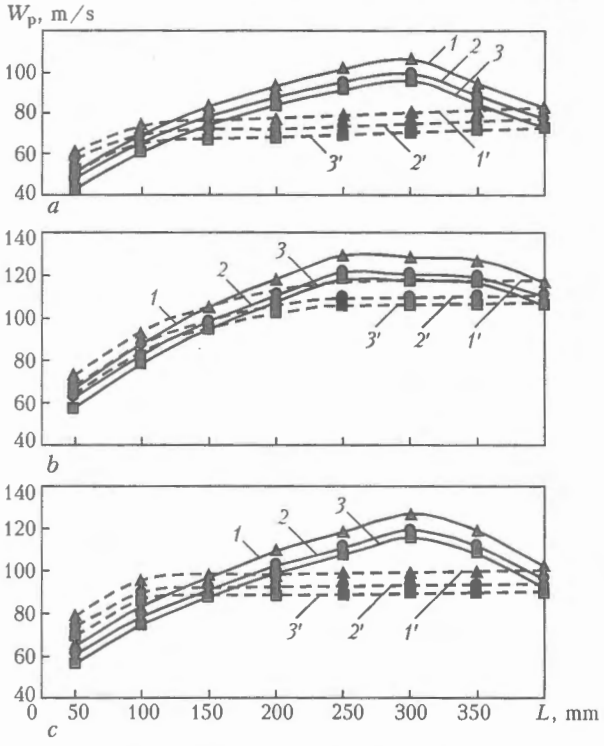

Figure 2. Influence of the composition of combustible mixtures of HOM (*a*), HOM + 5.5 % benzene vapours (*b*) and HOM + 16 % alcohol vapours (*c*) on the velocity of motion of powders with 20–40 μm particle size at laminar (*1–3*) and turbulent (*1′–3′*) flow modes: *1*, *1′* — copper powder; *2*, *2′* — iron powder; *3*, *3′* — nickel alloy powder

In spraying of a PG-AN-33 nickel alloy powder the length of the flame working zone is greater compared to that of the working zone in spraying of iron powder. Therefore, the probability of producing a sound coating is higher in this case than in iron powder spraying. Use of the laminar mode of the combustion product flow of the considered combustible mixtures is preferable, as the maximum velocity of the spraying particles on the working zone boundary is higher than with the turbulent flow, and outside of the working zone the particles continue moving with acceleration, which leads to a spraying distance of not less than 160–190 mm.

Suggestions of the possibility of using for flame spraying the flame generated at combustion of HOM produced by water-electrolysis generator were confirmed experimentally during investigation of the quality of coatings spray-deposited under the optimum conditions of flame burning selected after analysis of variants from Table 2.

Results of studying the quality of sprayed coatings are given in Table 3. Strength of coating adhesion to the base and porosity are taken as the criteria of coating quality evaluation. Strength of coating adhesion was determined by the adhesive method (using 65 % of EPU-TEKHKO adhesive and 35 % of hardener with the press-down force of 50 kPa at heating up to 70 °C). Hardening took 5–6 h, the coating thickness was 300 μm ± 10 %. Spraying was performed on standard

Table 2. Maximum velocity of particle motion (m/s) on the boundary of plume working zone and length of velocity zones of particle motion

Variant No	Combustion product composition	Jet flow mode	Powder particle size, μm			Working zone length L_{FWZ}, mm	Length of velocity zones of particle motion in gas flow, mm			Optimum spraying distance, mm
			20–40	20–63	63–100		L_{PAZ}	L_{SPMZ}	L^*_{PBZ}	
Copper powder										
1	HOM	Laminar	85	45	30	200	300	20	100	~200
2		Turbulent	65	35	25	160	150	250	100	160
3	HOM + benzene vapours	Laminar	117	65	50	300	250	100	50	300
4		Turbulent	100	55	45	180	200	200	50	180–200
5	HOM + alcohol vapours	Laminar	115	62	50	300	300	20	100	~300
6		Turbulent	90	45	35	160	150	250	100	150–160
PZh-1 iron powder										
7	HOM	Laminar	60	35	30	75	290	20	90	–
8		Turbulent	70	38	30	95	100	275	90	–
9	HOM + benzene vapours	Laminar	90	60	50	105	250	100	50	≥ 105
10		Turbulent	95	50	40	100	100	130	50	≥ 100
11	HOM + alcohol vapours	Laminar	85	50	40	110	300	20	75	≥ 110
12		Turbulent	95	55	45	110	100	275	75	≥ 100
PG-AN-33 nickel alloy powder										
13	HOM	Laminar	80	45	35	160	290	20	80	≥ 160
14		Turbulent	70	40	35	125	100	275	80	≥ 100
15	HOM + benzene vapours	Laminar	105	60	50	175	250	100	50	≥ 175
16		Turbulent	100	55	45	150	110	150	90	≥ 150
17	HOM + alcohol vapours	Laminar	100	55	45	190	300	10	90	≥ 190
18		Turbulent	90	50	40	140	110	290	90	≥ 110

*L_{PBZ} – length of particle braking zone.

samples made from steel 45 of 25 mm diameter, after abrasive-jet treatment. Samples were tested in TIRAtest 2151 machine with the loading rate of 2.5 mm/min. Total porosity of the coating was measured by the method of hydrostatic weighing [9]. Before spraying the studied samples were preheated up to the temperature of 150 °C [10].

Maximum adhesion strength of the coating was 28–30 MPa. It was achieved in spraying a copper powder with 20 to 40 μm particle size at laminar mode of combustion of HOM + 5.5 % benzene vapours and HOM + 16 % alcohol vapours at spraying distance of 300 mm (Tables 2 and 3, variants 3 and 5). Total porosity in this case was 3–4 %. With increase of the copper powder particle size, the strength drops to 20 and 22 MPa at the same spraying distance, respectively, while porosity increases to 7–8 %.

Obtained results are on the level of coating adhesion strength and porosity in spraying of non-ferrous materials, using acetylene-oxygen flame. By the data of Sulzer Metco Company, adhesion strength of the coating in deposition of non-ferrous powder materials is equal to 7–34 MPa, while porosity is 10–15 % [11].

Metallographic analysis of the structure of a copper coating spray-deposited with powder of 20–40 μm particle size (Figure 3, *a*) showed that the particle microstructure after spraying is sufficiently monolithic, and oxide inclusions are practically absent. In spaying with powder with 63–100 μm particle size (Figure 3, *b*) oxide inclusions are observed, and boundaries of individual particles are visible, which is attributable to insufficient particle energy.

Studying the coating quality when spraying with PZh-1 iron powder with 20 to 40 μm particle size showed that the strength of the coating adhesion to the base is higher with the turbulent mode of the combustion product flow in the case of using the mixtures of HOM + 5.5 % benzene vapours and HOM + 16 % alcohol vapours.

At spraying distance of 100 mm the strength of the coating adhesion to the base is up to 22 MPa in combustion of a mixture of HOM + 5.5 % benzene vapours and turbulent combustion mode coating porosity being 5 %. At combustion of a mixture of HOM + 16 % alcohol vapours and turbulent mode of the combustion product flow at spraying distance of 110 mm, the strength and porosity are equal to 24 MPa and 4 %, respectively. Such adhesion strength and porosity of the coating are on the level of similar quality characteristics in spraying of iron-base metal powders by acetylene-oxygen flame. By the data of Sulzer Metco [11], the adhesion strength in flame spraying of ferrous metal powders is equal to 14 to 21 MPa, and porosity is 10 to 15 %.

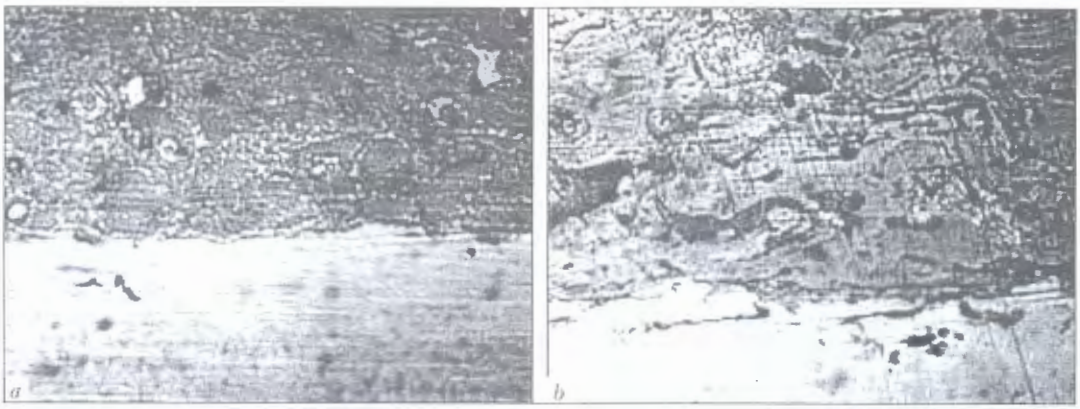

Figure 3. Microstructure of a coating produced by spraying of copper powder with 20–40 (*a*) and 63–100 (*b*) μm particle size at laminar flow mode of combustion products of HOM + 5.5 % benzene vapours and spraying distance of 300 mm (×300)

Metallographic analysis of the coating showed that in spraying of powder with 20 to 40 μm particle size, a rather dense coating microstructure is found, featuring a low content of oxide inclusions with a sufficiently pronounced deformation of particles, which is indicative of a good energy state of the particles for coating formation (Figure 4). The coating microstructure shown in Figure 5, demonstrates oxide inclusions on the coating–base interface and between the coating layers, undeformed and unmolten particles, and a pronounced laminated structure of the coating. Spraying of powder of the same particle size does not yield any positive results, even using a flame of HOM + 5.5 % benzene vapours, this being confirmed by a low adhesion strength and high porosity.

PG-AN-33 nickel-base powder is designed for deposition by spraying of wear- and corrosion-resistant coatings with their subsequent surface melting. In flame spraying with acetylene-oxygen flame, the coating adhesion strength is 10–20 MPa without melting, and 400 to 450 MPa with melting [12].

Deposition of a coating by hydrogen-oxygen flame without melting using PG-AN-33 powder showed that the maximum adhesion strength is on the level of coatings spray-deposited by acetylene-oxygen flame, and reaches 10 to 15 MPa, both with the turbulent and with the laminar nature of the gas mixture combustion product flows.

In deposition by spraying of PG-AN-33 powder with 20–40 μm particle size at the laminar mode of

Table 3. Quality of coatings spray-deposited using optimum variants of combustion conditions depending on the composition and nature of combustion product flow

Variant No	*Combustion product composition*	*Jet flow mode*	*Spraying length, mm*	*Coating adhesion strength, MPa, at consumed powder particle size, μm*			*Coating porosity, %, at consumed powder particle size, μm*		
				20–40	*20–63*	*63–100*	*20–40*	*20–63*	*63–100*
Copper powder									
1	HOM	Laminar	200*	22*	–	–	8	–	–
2		Turbulent	160*	18*	–	–	12	–	–
3	HOM + benzene vapours	Laminar	300**	30**	26**	22**	3**	5**	7**
4		Turbulent	180*	20*	16*	–	10*	12*	–
5	HOM + alcohol vapours	Laminar	300**	28**	24**	20**	4**	6**	8**
6		Turbulent	160*	20*	–	–	8*	–	–
PZh-1 iron powder									
9	HOM + benzene vapours	Laminar	105*	22*	20*	14*	9*	12*	16*
10		Turbulent	100**	24**	18**	–	7**	10**	–
11	HOM + alcohol vapours	Laminar	110*	20*	16*	–	8*	14*	–
12		Turbulent	110**	25**	18**	–	6**	10**	–
PG-AN-33 nickel alloy powder									
13	HOM	Laminar	160*	8*	–	–	8*	–	–
14		Turbulent	125*	6*	–	–	20*	–	–
15	HOM + benzene vapours	Laminar	175**	14**	12**	10**	8**	10**	12**
16		Turbulent	150**	12**	–	–	10**	–	–
17	HOM + alcohol vapours	Laminar	190**	15**	–	–	7**	–	–
18		Turbulent	140*	10*	–	–	12*	–	–

Notes. 1. Adhesion strength and porosity of PG-AN-33 powder coating were measured without melting after spraying. 2. * – spraying is possible, but quality is low; ** – spraying is possible.

Figure 4. Microstructure of a coating produced by deposition of PZh-1 iron powder with particle size of 20–40 μm at turbulent mode of the flow of combustion products of HOM + 16 % alcohol vapours and spraying distance of 110 mm (×300)

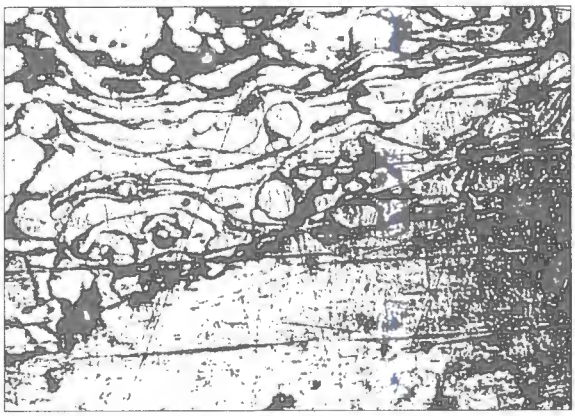

Figure 5. Microstructure of a coating produced by deposition of PZh-1 powder with 63–100 μm particle size at turbulent mode of combustion product flow of HOM + 5.5 % benzene vapours and spraying distance of 100 mm (×300)

Figure 6. Microstructure of a coating produced by deposition of PG-AN-33 nickel powder with 63–100 μm particle size at laminar flow of HOM combustion products and 170 mm spraying distance (×300)

the flow of combustion products of HOM with additives of hydrocarbon compounds, the coating adhesion strength was equal to 14–15 MPa, this being on the level of the strength of coatings spray-deposited without melting using acetylene-oxygen flame. Increase of powder particle size lowers the adhesion strength of the coating. Unmolten particles of the powder are readily visible in Figure 6, which is indicative of an insufficient energy state of the particle. Powder melting is required to produce a sound coating.

CONCLUSIONS

1. In flame spraying using hydrogen-oxygen flame, the maximum velocity which the particle acquires in the gas flow at the laminar mode of the combustion product flow is 10 % higher compared to the turbulent flow. In the case of adding benzene vapours to the combustible mixture at the laminar mode of the combustion product flow, a pronounced zone of stable motion of particles is observed. The maximum velocity of particles is higher than when using the considered gas mixtures.

2. Hydrogen-oxygen flame generated at combustion of a mixture produced by water-electrolysis generators, can be used for spraying materials with melting temperature below 1000 °C in the case of a laminar mode of flame burning at combustion of HOM + 5.5 % benzene vapours or HOM + 16 % ethyl alcohol vapours and about 300 mm spraying distance. Strength of coating adhesion to the base decreases with increase of particle size. At flame spraying of copper powders with 20 to 40 μm particle size it is 28 to 30 MPa, and in the case of 63–100 μm it drops to 20–22 MPa, and porosity increases from 3–4 to 7–8 %, respectively.

3. At spraying of powder materials with 20 to 40 μm particle size with about 1500 °C melting temperature, a coating can be produced to have the adhesion strength not lower than that when acetylene-oxygen flame is used at turbulent mode of the flow of combustion products of HOM + 5.5 % benzene vapours or HOM + 16 % ethyl alcohol vapours and about 100–110 mm spraying distance.

1. Antsiferov, V.N., Bobrov, G.B., Druzhinin, L.K. et al. (1987) *Powder metallurgy and sprayed coatings*. Moscow: Metallurgiya.
2. Kharlamov, Yu.A. (1983) About role of particle velocity and temperature in thermal spraying. *Fizika i Khimiya Obrab. Materialov*, **3**, 12–17.
3. Dorozhkin, N.N., Abramovich, T.M., Sakhnovich, V.T. (1989) Theoretical evaluation of time of powder particle heating in thermal spraying of coatings. *Doklady AN BSSR*, 33(**1**), 44–47.
4. (1964) *Application of acetylene substitute gases in thermal spraying of metals*. Ed. by I.A. Antonov. Moscow: Mashinostroenie.
5. Korzh, V.N., Popil, Yu.S. (2004) Influence of hydrocarbon additives on the structure of hydrogen-oxygen flame and temperature distribution along the plume length. *The Paton Welding J.*, **11**, 32–36.
6. Kudryavtsev, E.V. (1959) Measurement of temperature of high rate gas flux using the thermocouples. In: *Gas dynamics and combustion physics*. Moscow: AN SSSR.
7. Abramovich, G.N. (1976) *Applied gas dynamics*. Moscow: Nauka.
8. Donskoj, A.V., Klubnikin, V.S. (1979) *Electric plasma processes and units in machine-building*. Leningrad: Mashinostroenie.
9. Krechmar, E. (1966) *Spraying of metals, ceramics and plastics*. Moscow: Mashinostroenie.
10. Makarevich, S.S., Kozhuro, L.M., Mrochek, Zh.A. et al. (2001) Study of residual stresses in the coating, base and on their interface. In: *Theoretical and technological principles of hardening and reconditioning of machine-building products*. Minsk: Tekhnoprint.
11. (1996) *Thermal coating processes*. Wasteurry: Sulzer Metco.
12. Vityaz, P.A., Ivashko, V.S., Manojlo, E.D. et al. (1993) *Theory and practice of thermal spraying*. Minsk: Navuka i Tekhnika.

PRODUCTION AND APPLICATION OF THIN-WALLED SPIRAL-WELDED PIPES

A.S. PISMENNY, V.V. POLUKHIN, Vl.V. POLUKHIN, Yu.V. POLUKHIN, A.S. PROKOFIEV and V.G. UDOVENKO
E.O. Paton Electric Welding Institute, NASU, Kiev, Ukraine

Features of manufacturing thin-walled spiral-welded pipes, their advantages and applications are considered.

Keywords: *high-frequency welding, spiral-welded pipes, technology, equipment, application, articles*

Metal saving every day becomes more pressing because of continuous growth of metal consumption and price. One of the ways to save metal is to use round thin-walled pipes and different closed thin-walled sections for creation of various metalwork and mechanisms. The use of thin-walled spiral-welded pipes (SWP) produced with application of high-frequency welding (HFW) [1–5] is promising in this respect because often it is not technologically possible to produce longitudinal welded (LWP) or weldless pipes with small wall thickness meeting the needed requirements. Besides, they are much more expensive than welded pipes including SWP. Lines for production of SWP by using HF currents allow producing specially thin-walled pipes when a correlation of the diameter to the wall thickness may be large. In practice the correlation of the wall thickness to the diameter in the SWP is from 1:50 up to 1:1200. A pipe 3200 mm in diameter with wall thickness of 2.5 mm may serve as an example. In practice, both shells were employed as outer housings for manufacturing ultraportable premises for exploration of difficult-to-access regions. The smallest diameter of SWP produced at the E.O. Paton Electric Welding Institute was 25 mm. There is an experience for producing such pipes of special non-magnetic alloy, which serve as protective cases for microcircuits.

The E.O. Paton Electric Welding Institute produces technological lines for production of electric-welded spiral pipes of different grades. Simple design and easy maintenance of these lines allow producing such pipes in conditions of non-specialized pipe production with a possibility to easily adjust these lines for producing of pipes of different diameter and wall thickness.

Possibilities and advantages of thin-walled SWP. Special units are used for producing SWP by means of HF currents. Production of SWP has its advantages over production of other types of pipes including electric-welded longitudinal ones. Their production is more universal and allows producing pipes of different diameter and of a very wide range from a strip of the same width. It is possible to produce pipes with different wall thickness on the same units without any additional adjustments or replacement of parts. Besides, it is possible to produce pipes of one standard grade from the strips of different width. Inaccuracies in the width of the coils from different supplies are easily compensated by the provided adjustments. Technological lines for production of SWP are much easier for maintenance than the lines for production of LWP.

Metal consumption of lines for production of SWP is 6–7 times smaller as against lines for LWP. The number of equipment components participating in shaping the strip into the pipe is 10 times less. The number of especially precise hard-to-produce parts, forming rolls mainly, is less about 20 times.

Extension of lines for producing LWP of 20–76 mm in diameter is about 50 m long. Line for production of SWP occupies the area of 10×10 m in the shop. Owing to much smaller metal consumption these lines can be accommodated into small production areas and easily tailored into existing technological processes without creation of additional shops necessary for their work and maintenance.

All equipment for production of pipes up to 1000 mm in diameter together with the power supply may be accommodated in the automobile trailer and produce pipes directly there (Figure 1). These is no problem in allocating this equipment on other transport facilities, such as flat-cars, barges and others and to use it in the difficult-to-access regions producing pipes in situ and saving enormous funds needed for their transportation (in fact, air transportation) from the welded pipe production site.

Lines for production of SWP allow welding pipes of different diameter, wall thickness and of different materials. The lines provide continuous coiling of strip into the pipe of the preset diameter with simultaneous formation of the weld and automatic cutting into sections of the required length. In this case one does not need to use shielding gases, fluxes and fillers. The absence of fluxes and harmful fumes makes this production compatible with other types of production without the need to separate to them.

Besides, the process of production of SWP is very high-productive, fully automated and sufficiently unified; it does not require the involvement of highly qualified personnel. Pipes produced by this method may be used as pipelines for transportation of different materials and structural elements for different metalwork.

© A.S. PISMENNY, V.V. POLUKHIN, Vl.V. POLUKHIN, Yu.V. POLUKHIN, A.S. PROKOFIEV and V.G. UDOVENKO, 2005

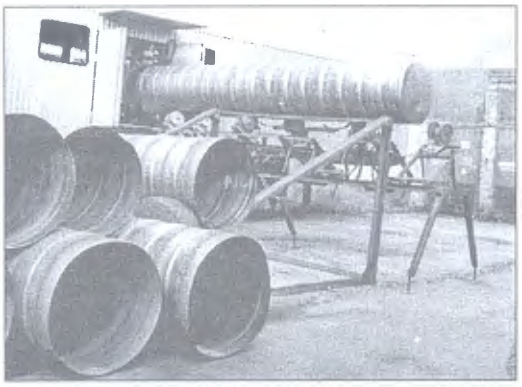

Figure 1. Mobile pipe-producing complex on the basis of semi-trailer 13 m long

Geometry accuracy of SWP is a distinguishing feature in their production. SWP produced by the method of HFW are highly precise in diameter within a wide range of standard grades. Accuracy of their production by diameter is within 0.1 mm and higher (Figure 2).

Strength characteristics of SWP are in most cases exceed those of pipes produced by other technologies. SWP have, as a rule, higher strength characteristics and rectilinearity in production as compared with LWP. Joints made using HFW in production of SWP of low-carbon steel have 100 % of strength in relation to the parent metal.

High strength of welds on SWP used for the pressure vessels is explained by the fact that the spiral weld is practically located in the direction of the tangential stresses therefore it does not cause rapture. The safety margin coefficient of spiral welds as against welds located along the axis of the pipe is 1.6–1.8 and depends on the width of the strip, therefore the vessels produced of SWP are distinguished with high strength. High density of the weld metal is provided by observing all technological parameters of the welding and forming: overlapping, heating, upsetting pressure. Joining of the heated edges is accompanied in welding by rolling. Thermomechanical strengthening as an inevitable component of the HFW provides high strength of the weld, which, as a rule, is higher than that of the parent metal.

Lines for production of SWP (Figure 3) have the following characteristics:

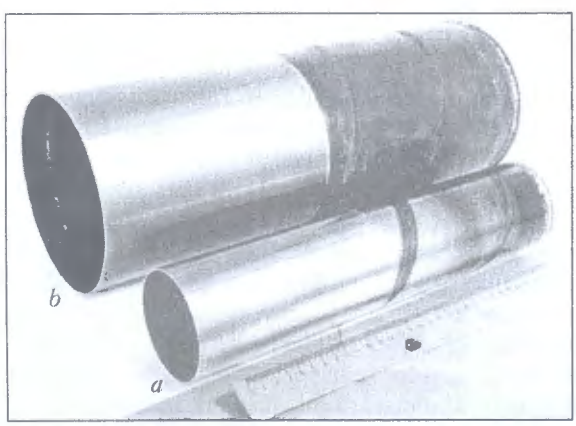

Figure 2. SWP of 75 (*a*) and 152 (*b*) mm in diameter with walls 1.5 mm thick after lathing

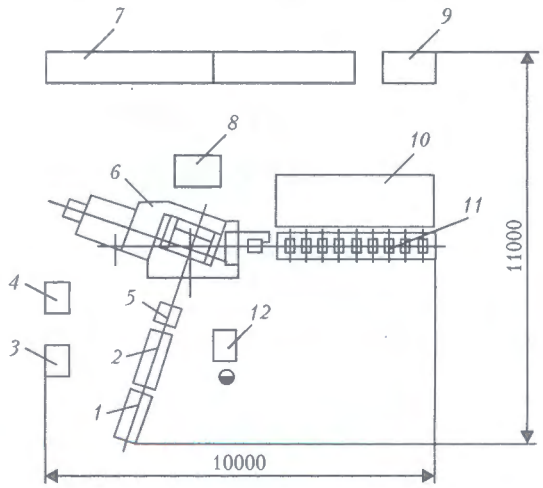

Figure 3. Diagram of production line for SWP: *1* — recoiling machine; *2* — feeding machine; *3* — control box for line; *4* — control box for plasma cutting; *5* — butt-welding machine; *6* — forming-welding machine; *7* — welding generator; *8* — welding head; *9* — heat exchanger; *10* — accumulating mechanism; *11* — receiving roll table with a cutting device; *12* — control panel

Diameter of pipes to be produced, mm	75–460
Accuracy in diameter, mm	0.1–0.3
Pipe wall thickness, mm	0.5–3.0
Strip width, mm	100–200
Pipe yield rate, m/min	5–30
Energy consumption, kW	170–220

Technological process. A process for production of SWP starts from recoiling the strip by the feeding machine located right after the recoiling machine. Next the butt-welding machine is located for lineup the coils to prevent the reloading of the strip into the forming-welding machine and thereby to save time. The feeding machine, which may straighten the strip when required, is intended for smooth feed of the strip into the forming-welding machine and is mainly used for the coils of relatively large weight and strip with thickness of more than 2 mm or when it has increased tension. The forming-welding machine, which is the main component in the line for production of SWP, performs the function of forming the strip into the pipe (Figure 4). Alongside with forming the butts in welding are being heated and joint. The preset diameter of the pipe is provided by this or other method depending on the type of the machine.

Then the welded pipe is automatically cut into cut-to-length sections without termination of the process by a special sensor synchronizing the pipe yield rate and the speed of the cutting mechanism displacement. The line allows using different equipment for cutting. One of the possible variants is the use of plasma cutting, which does not exclude the application of other equipment and methods, for example, cutting wheels of different configuration and others (Figure 5).

Units of two types are used for producing SWP. These units differ by a principle for maintaining the preset diameter of the formed pipe, namely:

- a-type units are equipped with the scroll forming element. These units are mostly used for production of pipes of up to 400 mm in diameter;
- b-type units are not equipped with the forming element but they have the device for automatic control

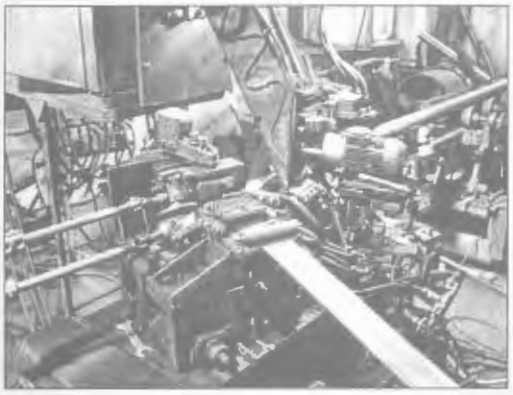

Figure 4. Forming-welding machine for producing SWP

for the preset diameter in the forming zone. These units used for producing pipes with diameter of more than 400 mm are more complicated but they allow producing pipes of unlimited diameter providing high surface condition and observing the shape.

In addition to the main types of units the E.O. Paton Electric Welding Institute produces customized units by individual orders. Such units take into account the requirements of the clients to the quality and sizes of the pipes. All units are serviced by one operator.

Grade of the produced SWP. The wall thickness of SWP most often used in machine building is usually from 0.5 to 2.5 mm. The most demanded are the pipes with diameter from 76 up to 250 mm with wall thickness from 1 to 2 mm. In most cases the strip 100 and 200 mm wide are used. For producing pipes with diameter of more than 400 mm it is appropriate to employ the strip of 500 or 700 mm wide.

A correlation of wall thickness and diameter of SWP may vary within a wide range (Table).

The HFW is the main method of welding used for production of pipes of low-carbon steel, though the use of argon-arc welding is also possible. Other methods of joining may be used if the high productivity is not required. Power sources for arc welding set are much cheaper and smaller in size though not easier in operation. Arc welding methods are more applicable for producing pipes of special steels and aluminium alloys or when there is no need in production of large volumes of pipes.

Application of SWP. Thin-walled SWP have gained a wide application in different industry

Figure 5. Cutting mechanism in operation

Most used SWP diameters and wall thicknesses

Pipe diameter, mm	*Wall thickness, mm*	*Strip width, mm*
75–100	0.5–2.0	100
100–200	0.8–2.5	100
200–600	1.0–3.5	200
600 and higher	2.0–4.0	500 and higher

branches due to simplicity of their production and a wide range of standard sizes.

Ventilation systems. A possibility to produce pipes of small thickness strips with simultaneous knurling of the spiral corrugation creates additional possibilities for saving metal (due to decrease of thickness) owing to the increase of the pipe rigidity. This in its turn allows producing draw-off ventilation of the metal of much less thickness than it was previously recognized without using expensive thick-walled pipes for these purposes. For example, it is possible to decrease the wall thickness of the draw-off ventilation pipe 820 mm in diameter to 2 mm. Large amount of metal is saved due to the absence of the beading seam as it is done by the Nokia technology. The use of telescope joint of pipes due to high accuracy of their geometry has allowed refusing from conventional assembling of air ducts by using flanges (Figure 6) while the use of galvanized and aluminized strip for such pipes gives a very good protection against corrosion. Corrosion properties of the weld in this case remain at the level of the parent metal (Figure 7).

Containers, barrels. Specially thin-walled SWP gained their application for producing containers for the paint and vanish industry and for chemical industry. Shells 300 mm in diameter are employed to produce barrels for paints, and pipes 560 mm in diameter are used for producing barrels with 200 l capacity for storing and transportation of combustible and lubricant materials.

Supports. Thin-walled SWP were used for production of reinforced concrete supports (columns). Tests showed that strength increase of such columns exceeded the designed indicators by 100 %.

Mining poles may also be produced from SWP. Compression tests showed that SWP proved to be stronger than weldless or longitudinal welded pipes. It is explained by the tendency of SWP to convolve under pressure, which requires additional work.

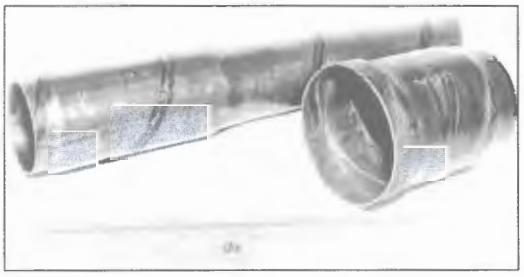

Figure 6. SWP produced with expansion of diameter in the end part

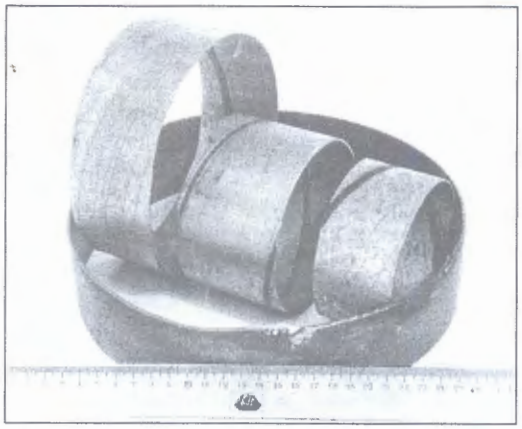

Figure 7. SWP produced from galvanized and aluminized steel

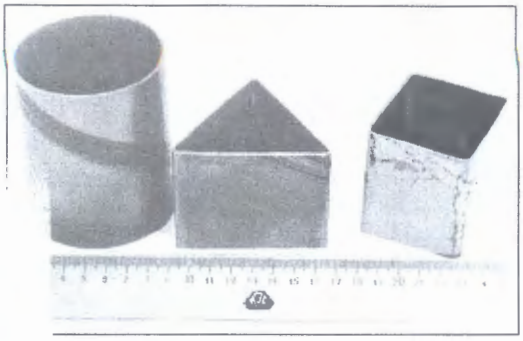

Figure 8. Re-profiled SWP

...l signs in some regions are installed on the ...s also made of SWP.

Irrigation systems. The use of SWP in the irrigation systems several times decreases their metal consumption. In this case the service life of the systems does not decrease because it is possible to use galvanized and aluminized strip for production pipelines.

Heating mains and pipelines. It is promising to use thin-walled SWP for heating mains and pipelines. It was calculated that the use of enameled thin-walled pipes is economically more profitable than the laying of thick-walled insulated pipes with regard to their possible corrosion. Especially thin-walled SWP in this case may be used for protection (casing) of heating mains. Pipes with the corrugation applied during their production may be used for manufacturing thermal compensators.

Thin-walled SWP find their application in the agricultural machine-building as the auger bodies in grain harvesters (Kherson Plant for Agricultural Machine Building, Ukraine), and in the flour-milling industry as flour and grain piping.

Vessels, receiver, cylinders, fire extinguishers. Body frames of certain types of fire extinguishers are produced from SWP. High demand for them provides high effectiveness of this production.

Multi-layer pressure vessels endure the load higher than the one-layer thick metal of the same thickness as the total thickness of the multi-layer vessels. Therefore, multi-layer pressure vessels produced of a set of SWP may be of great interest. A possibility to produce SWP of high accuracy allows assembling (inserting into each other) separately welded pipes with shrink fit and with shift of the welds. Inner part of such

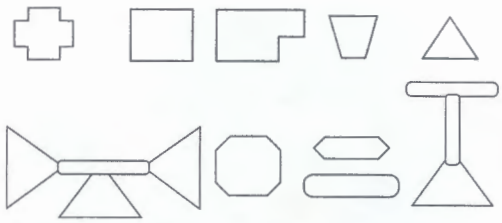

Figure 9. Diagram of beams and profiles produced by shaping of round pipes and their combinations

multi-layer vessels can be made of corrosion-resistant steel and then these vessels may be used for storage and transportation of corrosive substances saving expensive stainless steels.

Panels and casings. SWP may be used for production of different panels and shells with or without their subsequent forming. For example, pipes 3200 mm in diameter and 10 m long were the casings for round houses intended for exploration of difficult-to-access regions. If to cut such pipe lengthwise one can get a metallic sheet 100 m^2 in area.

Beams, sections, frames. One of the new directions in using the thin-walled SWP is to produce different sections, which are the components of metalwork, different beams and frames. Shaped into triangle, square, rectangular or other form the pipe will have an increased rigidity in the required direction (Figure 8). Such pipes are used for producing window and door frames. It is necessary to take into account that profiles produced of the pipes will have the closed section, which increases their rigidity and corrosion resistance. Different variants of coupling of the preliminary shaped pipes (Figure 9) open new potentialities for their use in the metalwork. It is especially effective in combination with anticorrosion metallization of the structure, which altogether gives an opportunity to perform their complete assembly in the industrial conditions. A low specific weight of these structures allows their cheaper delivery to difficult-to-access regions.

Currently the SWP are used in the rural locality as different pipelines, containers, vessels, machine-building elements, construction components (as independent beams and in composition of frames). Units for production of these pipes are universal equipment since they can produce pipes of different ranges.

For more information, please, contact:
E.O. Paton Electric Welding Institute,
Department 43
11, Bozhenko Str., 03680, Kiev-150, Ukraine
Tel./fax: (38044) 289 10 89; 220 10 89; 287 42 20
E-mail: pismenny@paton.kiev.ua

1. Shamov, A.N., Lunin, I.V., Ivanov, V.N. (1991) *High-frequency welding of metals*. Leningrad: Politekhnika.
2. Pismenny, A.S. (1997) *High-frequency welding of metals*. Amsterdam: Harwood A.P.
3. Skachko, Yu.N., Moshkin, V.F., Garkalyuk, R.I. et al. (1970) High-frequency spiral welding of pipes with butt joining of edges. *Avtomatich. Svarka*, **1**, 63–65.
4. Skachko, Yu.N., Moshkin, V.F., Popov, N.V. (1972) High-frequency spiral welding of pipes with beveled joint. *Ibid.*, **7**, 70, 71.
5. Skachko, Yu.N., Popov, N.V., Moshkin, V.F. et al. (1975) Analysis of approaching of edges in forming and high-frequency butt spiral welding of pipes. *Ibid.*, **6**, 30–32.

TECHNOLOGY OF WET MECHANIZED WELDING IN CONSTRUCTION OF IRSSP «PRIRAZLOMNAYA»

V.Ya. KONONENKO
Company «Ekotekhnologiya», Kiev, Ukraine

Information is given on application of the technology of wet mechanized welding with self-shielded flux-cored wires in mounting of superblocks of IRSSR «Prirazlomnaya».

Keywords: *wet mechanized welding, self-shielded flux-cored wires, welding in dry caisson, sea platform*

Ice-resistant stationary sea platform (IRSSP) «Prirazlomnaya» constructed by the Severodvinsk Federal State Unitary Enterprise «Production Association Sevmashpredpriyatie» (customer is «Rosshelf», Ltd.) was laid in December 1995.

«Sevmorneftegaz» and «Sevmashpredpriyatie» concluded on July 13, 2002 the contract on production of the bearing part for sea platform. For accelerating the construction works and making them cheaper IRSSP «Prirazlomnaya» decided to construct the lower part of the platform together with Russian specialists (about 30 % of the project cost) and to cut the upper part (housing area, drilling site technological modules) from the foreign sea platform that was shut down. The upper part of the platform was delivered to the water area of the «Sevmashpredpriyatie» in August 2003. Alongside with this the caisson was being produced at the enterprise. The caisson presented a welded structure of cold-resistant steel 126 × × 126 × 24.3 m by size and 70,000 t by weight providing storage of 700,000 barrels of oil and their shipment to the tankers. The modernized upper part of the platform would be installed on this structure. It is not possible to assemble the caisson of such sizes on the building cradles of the «Sevmashpredpriyatie» plant at present. Therefore, it was decided to divide the caisson into four super-blocks, each being 126 × × 31.5 × 24.2 m by size. The second super-block of the platform «Prirazlomnaya» caisson (Figure 1) was produced on February 27, 2004, and the third one — on May 28. Three out of four super-blocks of the caisson are now in the tank basin of «Sevmashpredpriyatie». In 2004 the company «SVP Interakva» registered in Russia began implementing the project on assembling the super-blocks [1]. It is not possible to assemble such structure on the building cradles of the «Sevmashpredpriyatie» plant at present. The technology, which is employed abroad but has not yet been used in the territory of the CIS countries, was used for joining the super-blocks. It consists in stage-by-stage assembling with the use of dry caisson, which is a device for sealing of the butt (DSB). A half of the DSB (eventually removed) is fixed to the lower part of the section during its manufacturing on the building cradle (Figure 2). Two DSB halves produced of steel RSA GOST 5521–93 are joint under the water at the depth of 8 m using the technology of wet mechanized welding with self-shielded flux-cored wire. The welding is supervised by the Maritime Register of Shipping of the Russian Federation. The divers-welders with qualification not lower than the second class of the specialization groups I and II, who were specially trained and passed practical exams in welding in vertical and overhead positions at the «Sevmashpredpriyatie» were allowed to do the work.

Flux-cored wires of grades PPS-AN1, PPS-AN2 and PPS-AN5 developed at the E.O. Paton Electric

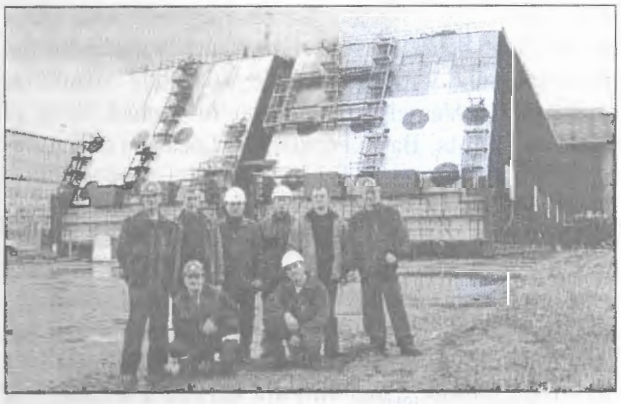

Figure 1. Super-blocks 2 and 3 in the tank basin

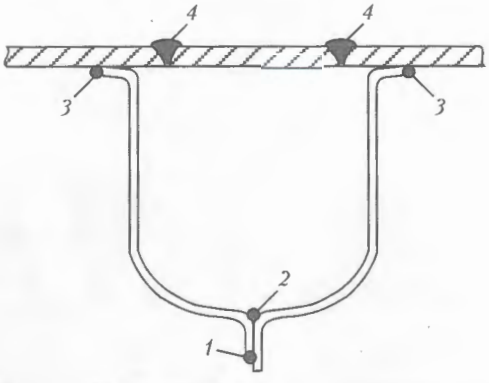

Figure 2. General layout of the DSB: *1* — three-layer weld formed under water in mechanized welding with self-shielded flux-cored wire; *2* — additional weld made after drying DSB by the electrodes UONII-13/45R; *3* — assembling fillet weld made on the building cradle in preparation of the DSB; *4* — multi-run butt weld made in dry conditions when joining bottom and board parts of the caisson super-blocks

© V.Ya. KONONENKO, 2005

Welding Institute do not provide the necessary predicted level of the joint quality in underwater welding in the overhead position. In this situation the flux-cored wire PPS-EK1 developed by the Company «Ekotekhnologiya» (TU 14288312.003–97) was used for creation of the bearing part of the base [2]. Corresponding technological documents and specifications were developed and agreed upon, specimens of the flux-cored wires were produced and tested, divers-welders were trained during a year and a half of work. All consulting activities in this projects, development and supply of the flux-cored wires as well as training of experts were carried out by the experts of the «Ekotekhnologiya».

Work on joining of two parts of DSB included welding in the overhead (126 m) and vertical (16 m per section) positions. All operations are carried out in the wet heated diving outfit (water temperature did not exceed 4 °C). Air for breathing and water for heating of the diving outfit are supplied by the hose bundle. When doing the work the diver has to swim away from the place of diving at a distance of up to 70 m for transportation of the semi-automatic welding machine and dressing machine. Some problems arise because of a large length of the welding circuit (200 m). Additional active resistance in the welding circuit decreases stability of the arc process and increases sensitivity to disturbances related to irregular feed of the flux-cored wire into the welding zone under heavy sea [3]. It is not possible to decrease the length of the welding circuit because of the mutual location of super-blocks and servicing vessels.

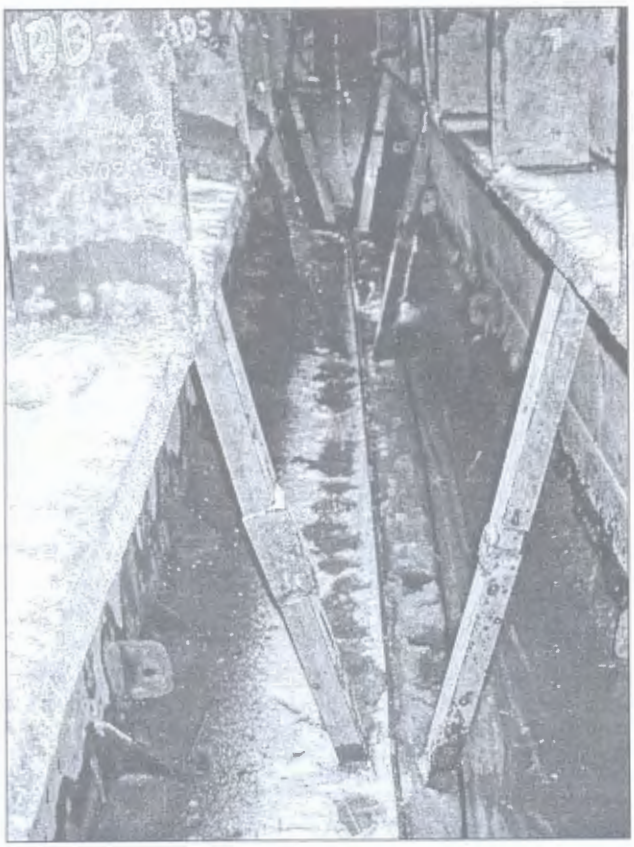

Figure 3. DSB after drying

Semi-automatic machines for underwater welding A1660 and PSP-3 (being manufactured now in Russia instead of A1660) are used for operations. The design of the submersion unit of the semi-automatic machine A1660 was finished providing its zero buoyancy (weight of the standard submersion unit of the semi-automatic machine in the water is more than 35 kg together with the wire stock). Welding cable with section of 70 mm^2 tied into a common bundle with the control circuit cable has also zero buoyancy due to the floats. Rectifier VS 300 was used as power source for the arc. Welds under the water were dressing by the hydrodynamic tools MNS-30 and DP-16, and by metallic brushes and abrasive wheels 306 mm thick.

Working technology includes the following stages:

- dressing the outer surface of the elements to be welded;
- installation of cramps and reduction of the welded parts of DSB for the whole length of the structure;
- dressing DSB parts (weld is at least 100 mm long) every 200–300 mm;
- dressing the tack welds and their visual control;
- dissembling of cramps and 100 % quality control of assembling quality by means of underwater video and TV equipment with recording on video recorder;
- welding the root weld with dressing from slag and 100 % quality control of welding by visual inspection to make sure that there are no inadmissible external defects by means of underwater video and TV equipment with recording the results on the video recorder;
- welding the second and third layer with dressing and 100 % quality control of welding by visual inspection of the whole joint to make sure that there are no inadmissible external defects by means of underwater video and TV equipment with recording the results on the video recorder.

Every day before starting the welding operation the welder performs the test specimen at least 100 mm long. By this procedure the correctness of the welding conditions is confirmed and the quality of the weld formation is estimated. Once a week the welded specimens are tested to fracture according to GOST 6996–66. In case the defects are detected they are corrected in compliance with RD 5.1078–76: Body Structures of Metallic Vessels. Correction of Defect Sites of Welding Joints. Basic Provisions. Location of the corrected defects is recorded in the log.

Assembling and welding of the DSB between second and third super-blocks (sections) was carried out in November–December 2004 (Figure 3). Underwater welding in vertical and overhead (Figure 4) positions was performed at 110–180 A welding current and 24–29 V arc voltage. Voltage losses in the welding circuit due to active resistance did not exceed 9 V. Speed of three-pass welding in the overhead position (without considering preparation and completion time) was

8.3 (root run), 6.8 (second weld) and 6.25 (third weld) m/h.

Mechanical properties of the weld metal obtained when using a batch of the flux-cored wire PPS-EK1 supplied for doing the work are as follows:

σ_t = 461.2 (448.8–480.2) MPa;

σ_y = 373.1 (371.3–375.8) MPa;

KCV_{20} = 75.5 (70.4–77.7) J/cm^2.

Relative elongation and reduction in area were not specified.

Weight fraction of elements in the deposited metal (the sixth layer) was, %: 0.015C, 0.04Si, 0.12Mn, 1.14Ni, 0.026S, 0.016P.

Welding of control butt specimens of steel VSt3sp (semi-killed) 14 mm thick and six-layer deposition were performed by the author in the fresh water at the depth about 5 m.

Lateral parts of the caisson were joint by the two-run fillet weld in the vertical position, the average welding speed being 4 m/h. The main problems in welding arose when the weld was formed in the zone of variable wetting.

After completion of underwater welds and control for their leak-proofness the caisson was dried and the welding was carried out in the inside area in «dry» conditions by the electrodes UONII-13/45R. Then the specialists of the «Sevmashpredpriyatie» started welding of sections of super-blocks by the standard technologies adopted at the enterprise. The thickness of the metal to be welded was 32 mm in the bottom and in board. Welding of the second and third super-blocks was carried out in March 2005. After carrying out the welding operations and control of quality of the obtained joint the DSB (dry caisson) between the second and the third super-blocks was removed using the technology of underwater cutting by the exothermic electrodes.

Figure 4. Appearance of three-layer weld made under water in the overhead position

Joining the first and second super-blocks of the caisson of the platform «Prirazlomnaya» using the described technology was scheduled for June 2005, and the third and fourth ones — for August 2005. It is planned to transport the platform «Prirazlomnaya» to the place of its installation in 2005.

1. Kononenko, V.Ya. (2004) *Technology of underwater welding and cutting*. Kiev: Ekotekhnologiya.
2. Kononenko, V.Ya. (1999) State-of-the-art of underwater welding and cutting. *Svarochn. Proizvodstvo*, **5**, 37–40.
3. Lebedev, V.K., Uzilevsky, Yu.A., Savich, I.M. et al. (1980) Analysis of possibilities of compensating by self-regulation system of typical disturbances of the arc length in underwater mechanized welding. In: *Underwater welding and cutting of metals*. Ed. by A.E. Asnis. Kiev: PWI.

PRESS WELDING OF DISSIMILAR METALS IN VACUUM

Welding is performed in vacuum chamber at a temperature close to 0.5 of the melting temperature of a lower-melting point metal welded, and at a pressure that is in excess of its yield stress under the welding conditions. Welding is carried out in a special device, i.e. tool, providing the required deformation degree in the contact zone, as well as retention of an assigned shape and size of a workpiece.

Quality joints between dissimilar metals are provided through applying the sufficient pressure to form a physical contact over the entire area of the mating surfaces at an initial welding period, achieving the assigned degree of plastic deformation and limiting the welding temperature. Selection of the welding time is based on the conditions of the recrystallisation processes occurring in metal of the contact zones.

Application. The method of press welding in vacuum is intended for joining metals with a limited mutual solubility. The method requires no interlayers and eliminates formation of brittle intermetallic phases within the contact zone.

Welding under the above conditions guarantees tensile strength of the joints at a level of that of a weaker metal joined.

Technological processes are available for press welding in vacuum of the following pairs of metals: titanium to aluminium, titanium to copper, titanium to austenitic, ferritic and low-carbon steels, titanium to tungsten and titanium to molybdenum.

WELDING OF TUBES WITH TUBE PLATES OF HEAT-EXCHANGE APPARATUSES OF TITANIUM ALLOYS

V.E. BLASHCHUK[1], G.M. SHELENKOV[2] and V.E. TROYANOVSKY[2]
[1]E.O. Paton Electric Welding Institute, NASU, Kiev, Ukraine
[2]OJSC «M.V. Frunze Sumy Machine Engineering SPA»

Results of the work on development of the technology and equipment for joining tubes to tube plates are presented. The main technological operations are described, which allow producing sound welded joints.

Keywords: *argon-arc welding, electron beam welding, titanium alloys, heat-exchange apparatuses, tube plates, pipes, selective assembling, expanding*

Heat-exchange apparatuses widely used in many branches of industry including nuclear power engineering are the inseparable elements of the thermal power plants. Heat-exchange apparatuses produced from titanium alloys find in the recent times a wider application in this branch of industry. Tough requirements are specified to their air-tightness proceeding from safety conditions of their operation. This, in its turn, conditions high requirements to the quality of the tube to tube plate joints insuring not only reliable air-tightness of joints but also meeting tough requirements to the main geometrical sizes of the heat exchanger (decrease of the flow section of the tubes, deviation from the tube plate plane etc.) [1].

Mainly two variants of fastening of the tubes in the tube plate are used when producing tube heat exchangers of titanium alloys: welding and welding + expanding [2]. The first variant is used mostly for production of heat exchangers operating in the stationary conditions and under the action of corrosive media, the second one — under operation in conditions of vibration loads and high pressures.

Welding of tubes with tube plates is carried out in two positions in relation to the tube plate — in the downhand and vertical positions. In the conditions of the shop the downhand welding is carried out in technological shafts or on the high special platforms. In the absence of technological tools or inappropriateness to use them because of dimensions of the article the welding is performed in the vertical plane locating the article on the idlers. In this case certain difficulties arise in automatic welding of tubes with the tube plate. These difficulties are related to the change of the geometrical parameters of the weld pool depending on the space position of the arc with its displacement by the tube face perimeter. In manual welding such welds are performed by the required manipulations of the electrode and change of the welding speed [3–5].

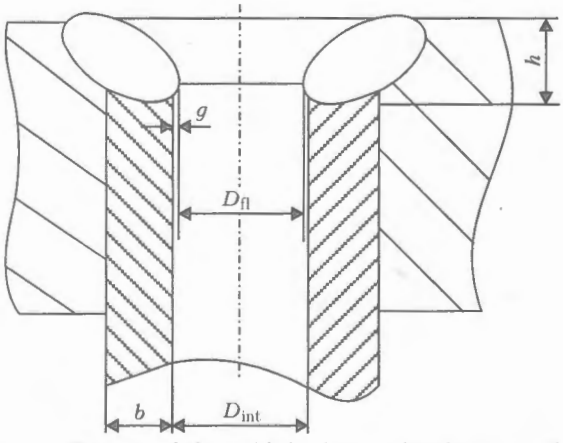

Figure 1. Diagram of the welded tube to tube plate joint: h — height of net section of weld; g — value of weld roll; b — tube wall thickness; D_{int} — internal diameter of tube; D_{fl} — diameter of flow section of tube

Obtaining of the preset height of the net section of the weld to provide a maximal openflow section of the tube is an important task in developing the technology of welding of tubes with tube plates (Figure 1). Height of the net section of the weld for the heat exchanges of general purpose is $h \geq 0.5b$ (b is the thickness of the tube wall). For heat exchangers with tough requirements to the tube fastening safety $h \geq b$. The highest reliability of the tube fastening is achieved with correlation of the penetration depth to the tube wall thickness $h/b = 3{:}4$. Special attention in the process of assembling of tubes with tube plates is attached to providing the required size of the clearance between the welded parts, which is achieved either by selective assembling or by mechanical rerolling of the tube ends.

When preparing the parts for assembling and in the process of assembling for welding the measures are taken to provide the required cleanness of the surfaces of the parts being assembled. With this aim the ends of the tubes before packing into tube plates are exposed to dressing and degreasing. The holes in the tube plates are treated in the same way. Preparation quality is estimated by cleaning the surfaces of the parts by the bleached calico napkin on which no traces of contaminations are allowed. Otherwise, the operation of degreasing and subsequent control is repeated. When assembling is performed for welding a clearance between the tube and the wall of the hole in the tube plate should not exceed 0.1–0.2 mm. Exceeding of the permissible clearance leads to the vio-

© V.E. BLASHCHUK, G.M. SHELENKOV and V.E. TROYANOVSKY, 2005

lation of the weld form, burn-through the tube wall and other defects. However, in the cases when the operational media may cause the development of the crevice corrosion, the clearances are obligatory removed by expanding (press-on) of the tubes by the whole thickness of the tube plate before or after welding, or the tube to tube plate joint is produced with the increased clearances.

In the process of the welding-in tube in tube plates the apparatus tube space is filled with argon to protect the weld root and adjacent heated zones of the parts being assembled from the contact with air. The welding is performed with minimal heating of the pipe plate (its temperature in the zones of the location of adjacent tubes should not exceed 100 °C).

In single production the welding-in tubes in the tube plates of heat-exchange apparatuses is carried out by the manual argon-arc welding. Disadvantages of this method include a low productivity, small and instable penetration depth, high porosity of the weld (especially in welding of preliminary expanded tubes), dependence of the welding quality on the individual skills of the welder. Partially, such drawbacks can be eliminated by using the flux reagents on the basis of fluorides of the alkaline metals of BMK-1 type. However, in this case the market condition of the weld is deteriorated, problems arise when detecting defects in leak testing while the process itself proceeds with emission of harmful substances and requires application of additional means for protection of the welder's breathing [6].

For obtaining a guaranteed index $h/b > 2$ in the welded joints of tube to tube plate, it is possible to use the known technology of the EBW in the local vacuum. For this purpose the weld guns are developed that orient the EB gun in space for welding of girth seams using the centralizers and compactors. The binary refraction allows guiding the beam to the butt with an error ± 0.2 mm. However, because of the impossibility to remove the root defects in the welds typical for the EBW such technology did not gain a wide application [7].

For obtaining the welded joints of the required quality of the $h/b \geq 1$ the M.V. Frunze Sumy Machine Engineering Company has applied the technology of welding-in the tubes into the tube plates by the immersed arc. For this purpose a batch of automatic machines «Kometa» (Figure 2) equipped with a system of automatic regulation of the arc voltage was developed and produced. Welding technology by the layer of the flux reagent using these machines provided the needed penetration depth with high productivity of the process, however, the drawbacks typical for this technology remained the same. Therefore, it was necessary to improve the technology and to develop new equipment for automatic welding of tubes to tube plates excluding the use of the flux reagent and allowing production of the welded joint that meets the requirements of the specifications. In this case it

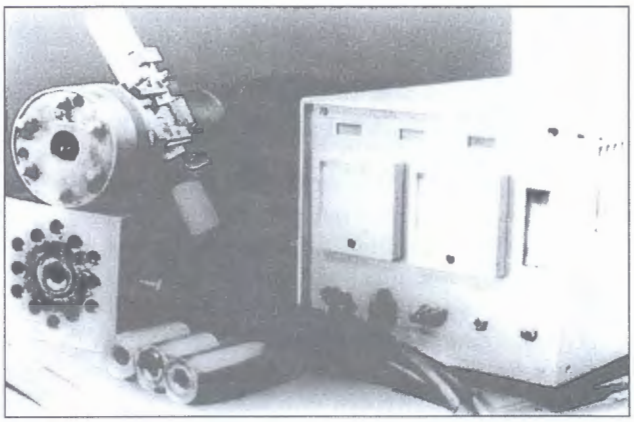

Figure 2. Automatic machine «Kometa-M» for welding tubes to tube plates by immersed arc

turned out that the automatic machines «Kometa» do not fully solve the set problem.

Analysis of the produced machines for welding of titanium tubes with tube plates has shown that the welding head of the AG series as a component of the commercially produced automatic machine «Agat-1» (design of the TsNIITMASh) has a number of advantages as compared to commercial import heads of the analogous class. Hence, this head was selected as the basic one for modernization of the welding machine. The brand «Agat-M1» was assigned to the automatic machine (Figure 3). The machine was modified to make it possible to operate with more powerful power

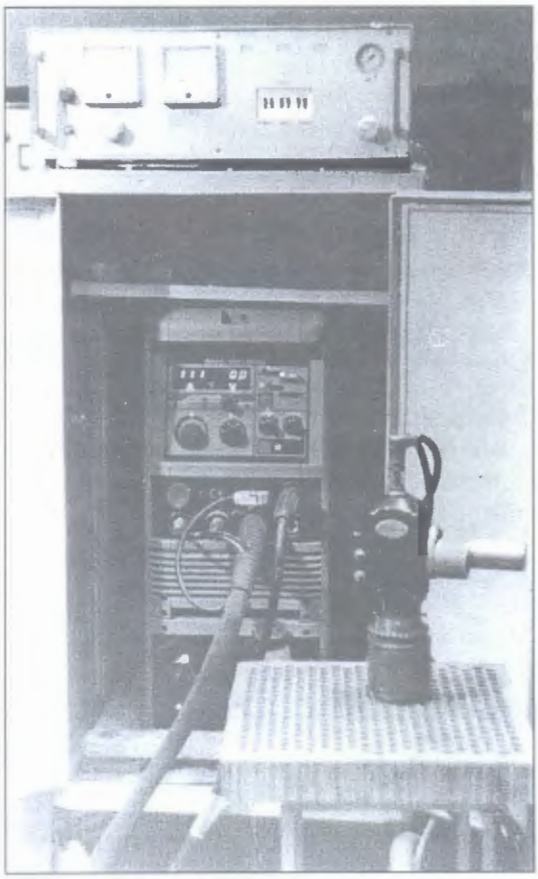

Figure 3. Automatic machine «Agat-1M» for pulsed welding tubes to tube plates with forced formation of weld

supply VSVU-315 and later with the Fronius power supply TT-3000 (Austria).

As a result of the testing and design operations new equipment was developed. It includes the following components:

- machine unit with expanded technological possibilities as against the basic model;
- water-cooled collet allowing not only alignment of the welding machine head relative to the welding-in tube but also forced formation of the weld;
- protection chamber providing a reliable gas shielding of the welding zone and the zone adjacent to the tube being welded and allowing regulation of the electrode tip in relation to the surface of the assembling;
- autonomous portable cooling unit.

The developed technology provides the welding process without flux reagent using the powerful current pulses with forced formation of the weld by the water-cooled collet, which excludes a possibility of burn-through of the tube wall and irregular formation of the weld typical for welding without forced heat removal from the weld pool. Welding conditions of the tubes of $\varnothing 10 \times 1.5$ mm with the tube plate are as follows: I_{pulse} = 280–300 A; I_{pause} = 20–30 A; τ_{pulse} = = 0.44 s; τ_{pause} = 0.24 s; v_w = 6.4–6.6 m/h; G_{Ar} = = 1–15 l/min.

Equipment and technology were checked in conditions of commercial production of heat-exchange apparatuses of titanium alloys. The statistical processing of the results showed that the welding technology permitted by 60–75 % decreasing porosity of the welded joints as compared to the previously employed technologies of fastening tubes in the tube plates. The welded joints have a good commercial condition and provide a constancy of the flow area of tubes in the weld zone even under the values h/b = 1.5–2.0. This is especially important for subsequent expanding of tubes by explosion or electric pulse since there is no need to calibrate the charges [8].

Considering the obtained results a batch of the automatic welding machines «Agat-1M» is produced. They have found their application in production of heat-exchange apparatuses of titanium alloys using the heat-exchange tubes with the external diameter of 10–56 mm and wall thickness of 1.0–2.5 mm.

1. Mikhajlov, V.I., Semyonov, V.A., Goldobaev, M.I. et al. (2002) Specifics of welding of thin-walled titanium tubes to titanium-steel bimetal tube sheets for heat-exchange equipment. *Metalloobrabotka*, **4**, 26–30.
2. Mazurovsky, B.Ya. (1980) *Electrohydropulse pressing-in of tubes in tube sheets of heat-exchange apparatuses*. Kiev: Naukova Dumka.
3. Tsaryuk, A.K. (1998) Welding of tubes to tube plates (Review). *Avtomatich. Svarka*, **4**, 25–29.
4. Tsaryuk, A.K. (2000) Equipment for welding of tubes to tube plates (Review). *Svarshchik*, **4**, 12–13.
5. Nenon, V.K. (1999) Orbital welding in record time. *Welding J.*, **3**, 51–55.
6. Troyanovsky, V.E. (1985) Experience of mechanized welding of tubes to tube sheets of heat-exchange apparatuses. In: *Current problems of welding of non-ferrous metals*. Kiev: Naukova Dumka.
7. Paton, B.E., Leskov, G.I. (2003) Some aspects of electron beam welding application (Review). *The Paton Welding J.*, **12**, 22–26.
8. Shelenkov, G.M., Blashchuk, V.E., Melekhov, R.K. et al. (1984) *Producing and service of titanium equipment*. Kiev: Tekhnika.

ELECTRON BEAM WELDING OF γ-TITANIUM ALUMINIDE

The technology and technological solutions developed for electron beam welding of heat-resistant alloy Ti–48Al–2Nb–2Mn provide welded joints with properties close to those of base metal.

As established, formation of cold cracks in welds can be prevented by using preheating of workpieces to 400–500 °C. To lower the level of residual stresses, it is necessary to subject the joints immediately after welding to annealing at a temperature of 800–900 °C for 10–15 min. Both preheating and postweld annealing are performed by the electron beam.

Long-time (25 h) annealing in vacuum furnace at a temperature of 1260 °C provides absolute elimination of structural heterogeneity in a welded joint with formation of a duplex structure, as well as high mechanical properties of the joints.

Mechanical tests of the welded joints made by the developed technology gave the following results:

- base metal – σ_t = 480–540.4 MPa, $\sigma_{0.2}$ = 457.5–469.5 MPa;
- welded joint – σ_t = 513–528 MPa, $\sigma_{0.2}$ = 480.8–499 MPa.

MECHANICAL PROPERTIES OF ALUMINUIM ALLOYS IN CONSUMABLE AND NONCONSUMABLE ELECTRODE ARC WELDING

V.S. MASHIN, A.G. POKLYATSKY and **V.E. FEDORCHUK**
E.O. Paton Electric Welding Institute, NASU, Kiev, Ukraine

Comparative analysis has been performed of mechanical characteristics of the joints on aluminium alloys of different alloying systems, produced by consumable and nonconsumable electrode arc welding, using batch-produced and test welding wires alloyed with zirconium and scandium.

Keywords: *arc welding, aluminium alloys, consumable and nonconsumable electrodes, scandium-containing fillers, mechanical properties, comparative analysis*

Two arc welding processes, namely consumable and nonconsumable electrode welding are the most widely used in fabrication of structures from modern aluminium alloys. They provide comparatively high levels of weld strength and ductility and the required performance of welded joints.

Use of nonconsumable electrode argon-arc welding (TIG process) allows producing a smooth weld surface with a gradual transition to the base metal. This process requires particularly thorough preparation of the surfaces of metal to be welded, edge fastening, as well as cathode breaking up of the oxide film, which has the main influence on development of characteristic defects, namely nonmetallic inclusions of oxide film in welds [1–3]. A high quality of welds can be ensured, when the appropriate technological requirements to edge preparation, conditions of butt fastening and electric parameters of the welding process are met.

In consumable electrode welding (MIG process) the efficiency increases, heat input into the metal being welded is reduced, and residual stresses and strains are decreased. In this case, however, the welds and zone of their fusion with the base metal often develop pores, resulting from gas saturation of the metal being welded or violation of the technological process of welding [1, 4].

The purpose of this study is comparative analysis of the main values of mechanical properties of the metal of welds and welded joints on aluminium alloys, made in optimum modes of MIG and TIG welding, using standard and promising test wires. Sheets of batch-produced and test aluminium alloys of different alloying systems were used for welding (Table 1). Mechanical properties of these alloys are given in Table 2.

Butt joints were produced by single-pass welding using standard and Sc-alloyed test welding wires (Table 3). Mechanized MIG welding was performed using ASTB-2m welding head powered by TPS-450 source, and TIG welding — by MW-450 source. After mechanical removal of the deposit in the weld root the joints were X-rayed. Sound weld sections were used to make samples for mechanical testing, allowing determination of ultimate strength of welded joints σ_t^{WJ}, weld metal σ_t^w, proof stress of weld metal $\sigma_{0.2}^w$, relative elongation δ^w, impact toughness a_n^w and joint bend angle α.

AMg6 alloy welded joints. Analysis of the results of joint mechanical testing showed that irrespective of the welding process, flat samples with weld reinforcement always fail in the zone of weld fusion with the base metal. Ultimate strength of welded joints made by TIG process with SvAMg6 wire, is on the level of 315 MPa (Figure 1). Application of wires alloyed with zirconium (SvAMg63) and scandium (AMg63Sc) provides an increase of welded joint

Table 1. Composition of aluminium alloys, wt.%

Alloy grade	*Alloying system*	*Cu*	*Mg*	*Mn*	*Fe*	*Si*	*Li*	*Zn*	*Sc*	*Ti*	*Zr*
AMg6	Al–Mg–Mn	–	6.4	0.6	0.4	0.4	–	–	–	0.1	–
1420	Al–Mg–Li	–	5.4	0.2	0.2	0.15	2.1	–	–	–	0.1
1201	Al–Cu	5.7	–	0.2	0.3	0.2	–	–	–	–	0.1
1460	Al–Cu–Li	3.0	–	0.1	0.12	0.1	2.0	–	0.1	0.1	0.1
1925 (TB)	Al–Zn–Mg	–	1.5	–	0.4	0.4	–	7.0	–	–	–
V96Ts (TB)	Al–Zn–Mg–Cu	2.3	1.9	–	0.2	0.2	–	8.1	–	–	0.1

© V.S. MASHIN, A.G. POKLYATSKY and V.E. FEDORCHUK, 2005

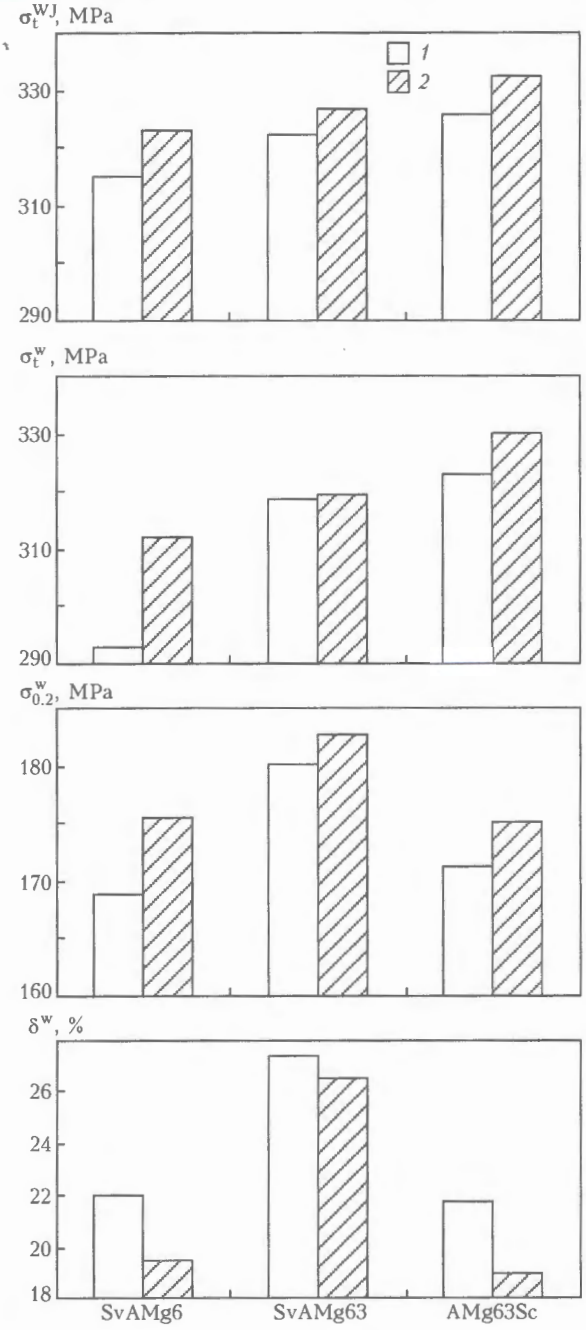

Figure 1. Mechanical properties of AMg6 alloy joints produced in TIG (*1*) and MIG (*2*) welding using wires of different compositions

strength by 6 and 11 MPa on average, and increase of weld metal strength by 26 and 30 MPa, respectively.

In MIG welding, average values of welded joint strength are somewhat higher than in TIG welding and are equal to 323 MPa. Strength of the metal of MIG welds made with batch-produced SvAMg6 wire (312 MPa) also is almost 20 MPa higher than that of TIG welds. Use of Sc-alloyed wire increases this index to 330 MPa. For all the welding processes, the proof stress and relative elongation of weld metal stay on the level of values obtained in welding with batch-produced wire SvAMg6.

Joints of 1420 alloy. Failure of flat samples with weld reinforcement made by both the welding processes always proceeds in the zone of weld fusion with

Table 2. Mechanical properties of aluminum alloys

Alloy grade	*Sheet thickness, mm*	σ_v, *MPa*	$\sigma_{0.2}$, *MPa*	δ, %	a_n, *J/cm2*	α, *deg*
AMg6	6	343.3	164.6	23.1	22.4	135
1420	4	463.8	352.5	5.8	11.8	37
1420	6	448.0	300.4	9.1	8.3	24
1201	6	435.7	353.6	9.6	8.8	29
1460	3	573.6	532.2	3.5	2.4	17
1460	6	511.7	463.8	4.5	4.0	28
1925 (TB)	3	472.9	426.0	9.3	17.2	54
V96Ts (TB)	3	616.5	579.4	10.0	4.5	15

Note. Average values are given by the results of testing 5 to 7 samples.

the base metal. Use of batch-produced wire SvAMg6 in TIG welding, provides the strength of 4 mm welded joints on the level of 319 MPa, and of 6 mm joints on the level of 271 MPa. Weld metal strength (similar to MIG welding) is on the level of 315–316 MPa (Figure 2). Application of Zr- and Sc-containing wires allows increasing the strength of the joints by 7 to 14 MPa and weld metal strength by 6–9 MPa. When all the studied wires are used, the impact toughness of the welds and bend angle of TIG-welded joints are superior to the appropriate indices for MIG-welded joints. Application of wires alloyed with zirconium and scandium, allows increasing the impact toughness of welds up to 26 J/cm^2 on 4 mm thick metal and up to 20 J/cm^2 on 6 mm thick metal. Bend angle of sheet metal joints is up to 90°.

In MIG welding with SvAMg6 wire average strength values of welded joint are higher than in TIG welding, and are equal to 322 and 295 MPa for 4 and 6 mm thick metal, respectively. Application of wires with zirconium and scandium allows an even higher increase (compared to TIG welding) of the strength characteristics of the welded joint and weld metal. On 4 mm thick metal σ_t^{WJ} and σ_t^w increase by 2 to 12 MPa compared to TIG, and on 6 mm metal by 25 and 35 MPa, respectively.

Joints of 1201 alloy. Irrespective of the welding process and wire composition, samples of 1201 alloy

Table 3. Composition of aluminium welding wires, wt.%

Electrode grade	*Cu*	*Mg*	*Mn*	*Sc*	*Ti*	*Zr*
SvAMg5	–	5.1	0.1	–	–	–
AMg5Sc	–	5.0	–	0.5	–	0.2
SvAMg6	–	6.2	0.4	–	0.1	–
SvAMg63	–	6.3	0.6	–	–	0.2
AMg63Sc	–	6.1	0.2	0.5	–	0.1
Sv1201	6.0	–	0.3	–	0.1	0.2
1201Sc	6.0	–	–	0.5	0.1	0.2

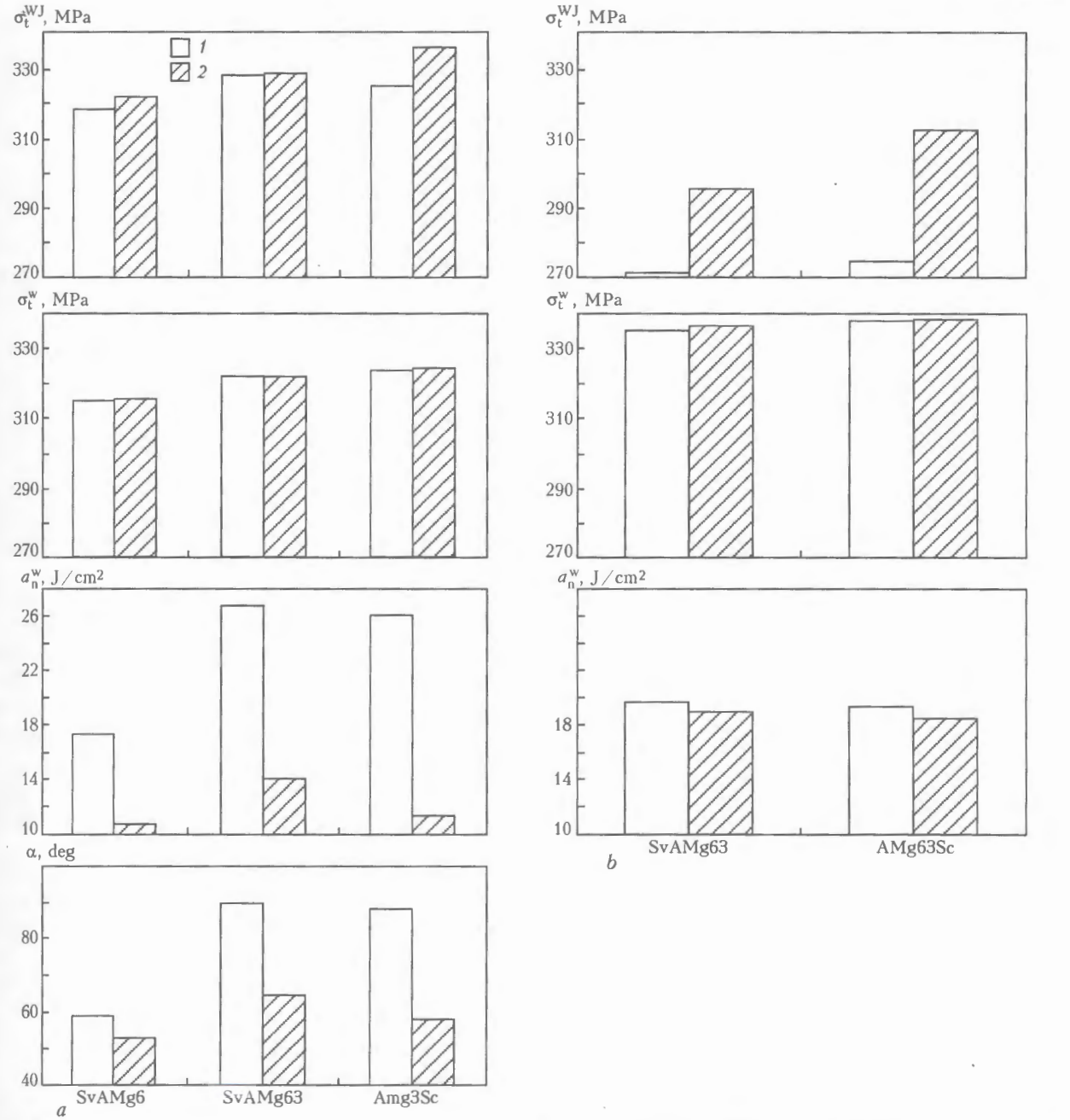

Figure 2. Mechanical properties of 1420 alloy joints 4 (*a*) and 6 (*b*) mm thick produced in TIG (*1*) and MIG (*2*) welding using wires of different compositions

welded joints fail at tension in the zone of weld fusion with the base metal. Ultimate strength of the joints made by TIG welding is on the level of 240 MPa (Figure 3). Scandium addition to the welds practically does not change the strength properties of welded joints (σ_t^{WJ}), but greatly increases the strength of welds (from 236 to 256 MPa), and noticeably lowers the metal impact toughness (from 12 to 9 J/cm^2).

Compared to TIG welding, application of MIG process allows increasing the ultimate rupture strength of welded joints to 266 MPa with batch-produced wire Sv1201 and to 279 MPa with Sc-containing wire. Strength and impact toughness of weld metal also are on a higher level in MIG welding. Use of Sc-alloyed wire leads to an increase of weld metal strength from 260 to 272 MPa and lowering of their impact toughness from 18 to 14 J/cm^2.

Joints of 1460 alloys. In TIG welding with Sv1201 wire, joint strength on the level of 307 MPa is provided for 3 mm sheets and of 275 MPa for 6 mm sheets (Figure 4). Wire alloying with scandium allows significantly increasing the ultimate strength and proof stress of the weld metal. In TIG welding of 3 mm thick metal, weld strength increases from 251 to 288 MPa, and for 6 mm thick metal from 248 to 275 MPa. Impact toughness of weld metal decreases from 14 to 10 J/cm^2, and welded joint bend angle from 174 to 79°.

Compared to TIG welding, MIG welding provides an increase of strength properties of welded joints.

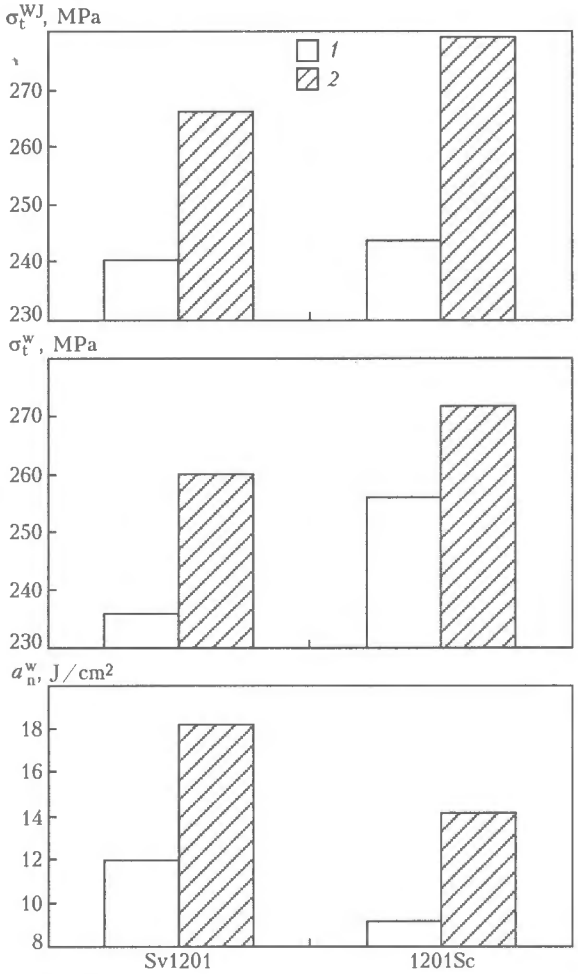

Figure 3. Mechanical properties of joints of 1201 alloy produced in TIG (*1*) and MIG (*2*) welding using wires of different composition

When Sv1201 wires are used, σ_t^{WJ} increases up to 312 MPa for metal 3 mm thick, and up to 289 MPa for metal 6 mm thick. Weld metal also has a higher strength in MIG welding both on sheet (280 MPa) and thicker metal (287 MPa). Proof stress and weld metal impact toughness are also higher.

Compared to TIG welding, weld alloying with scandium in MIG welding of 3 mm thick metal leads to σ_t^{WJ} and σ_t^w increase by 4 to 5 MPa, and for 6 mm metal to σ_t^{WJ} and σ_t^w increase by 20 to 23 MPa. Impact toughness of welds drops from 16.8 to 14.5 J/cm^2 and bend angle from 130 to 35°.

Joint of 1925 alloy (test batch). Irrespective of welding process and wire composition, samples with weld reinforcement fail in the base metal in the HAZ. Ultimate strength of welded joints made by TIG process with SvAMg5 wire is on the level of 358 MPa (Figure 5). Application of Sc-containing wire (AMg5Sc) provides increase of weld metal strength from 288 to 314 MPa and decrease of joint bend angle from 106 to 55°.

In MIG welding average values of joint strength σ_t^{WJ} are somewhat higher than in TIG welding, and are equal to 370 MPa. Strength of the metal of MIG and TIG welds with batch-produced wire SvAMg5 is approximately on the same level (288 MPa). When Sc-containing wire is used, σ_t^w increases to a greater extent for MIG welds than for TIG welds and is equal to 321 MPa. In all the cases, bend angle of joints produced by MIG is 5 to 25° lower than in TIG welding.

Joints of V96Ts alloy (test batch). All the samples with weld reinforcement fail in the zone of weld fusion with base metal. Ultimate strength of joints made by

Table 4. Coefficient *K* of mechanical properties of the joints in TIG and MIG welding

Alloy grade	*Sheet thickness, mm*	*Electrode grade*	*TIG*	*MIG*	*TIG*	*MIG*	*TIG*	*MIG*	*TIG*	*MIG*
			$\sigma_t^{WJ}/\sigma_t^{BM}$		σ_t^W/σ_t^{BM}		a_n^w/a_n^{BM}		α^{WJ}/α^{BM}	
AMg6	6	SvAMg63	0.94	0.95	0.93	0.93	–	–	–	–
		AMg63Sc	0.94	0.97	0.94	0.96	–	–	–	–
1420	4	SvAMg63	0.70	0.71	0.69	0.69	2.27	1.19	2.43	1.76
		AMg63Sc	0.71	0.73	0.70	0.70	2.20	0.97	2.38	1.57
	6	SvAMg63	0.61	0.66	0.75	0.75	2.48	2.39	–	–
		AMg63Sc	0.66	0.70	0.75	0.75	2.43	2.33	–	–
1201	6	Sv1201	0.55	0.61	0.54	0.60	1.36	2.07	–	–
		1201Sc	0.56	0.64	0.59	0.62	1.05	1.60	–	–
1460	3	Sv1201	0.54	0.54	0.44	0.49	–	–	10.24	7.76
		1201Sc	0.54	0.55	0.50	0.51	–	–	4.65	2.12
	6	Sv1201	0.54	0.57	0.48	0.56	3.60	4.20	–	–
		1201Sc	0.55	0.59	0.54	0.58	2.53	3.60	–	–
1925 (TB)	3	SvAMg5	0.76	0.78	0.61	0.61	–	–	1.96	1.46
		AMg5Sc	0.76	0.78	0.66	0.68	–	–	1.02	0.94
V96Ts (TB)	3	SvAMg5	0.49	0.57	0.47	0.49	–	–	2.87	2.07
		AMg5Sc	0.53	0.59	0.49	0.54	–	–	2.07	1.47

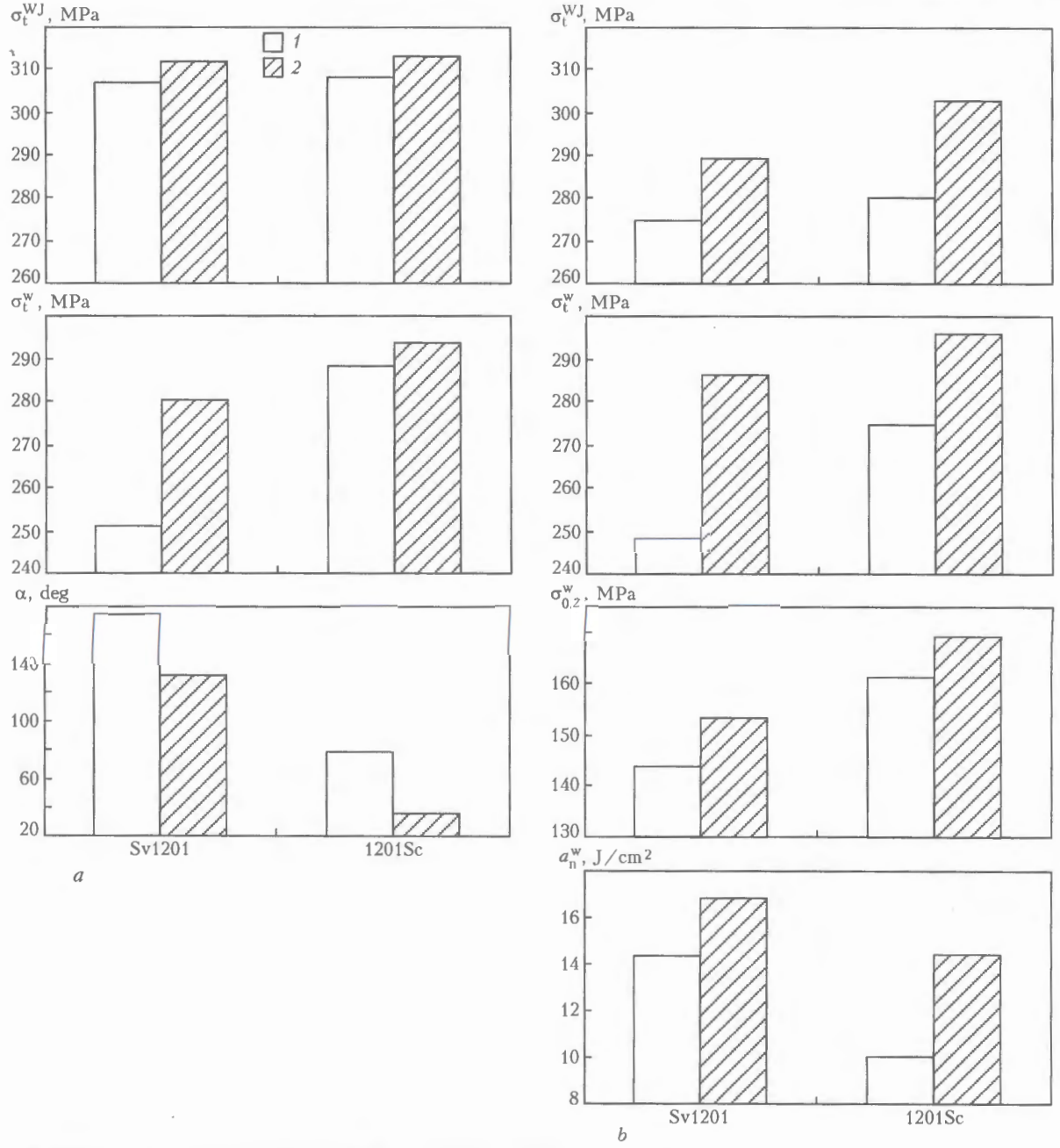

Figure 4. Mechanical properties of joints of 1460 alloy 3 (*a*) and 6 (*b*) mm thick produced in TIG (*1*) and MIG (*2*) welding using wires of different compositions

TIG process with batch-produced SvAMg5 wire is equal to 302 MPa, and with Sc-containing wire 324 MPa (Figure 6).

MIG process provides higher levels of welded joint strength: 350 MPa when using SvAMg5 wire, and 366 MPa when using AMg5Sc wire. Ultimate strength of weld metal is also higher in MIG welding, being equal to 305 and 363 MPa, respectively. Use of Sc-alloyed wire promotes strengthening of the metal of MIG welds by 28 MPa and TIG welds by 10 MPa. Bend angle of welded joints is low both when using batch-produced and Sc-alloyed wire.

K, *C* and *F* coefficients were used to perform comparative analysis. Coefficient *K* of joint mechanical properties was determined from the ratio of indices of TIG- and MIG-welded joint properties, to the indices of respective properties of the base metal (Table 4). Variation of mechanical properties of weld metal *C* at replacement of TIG process by MIG process (Table 5) was determined from the formula

$$C = [(MIG - TIG)/TIG] \cdot 100\ \%.$$

F coefficient used to evaluate the effectiveness of adding scandium to the filler wire (Table 6) was determined from the dependence

$$F = [(\text{filler with Sc} - \text{filler without Sc})/\text{filler without Sc}] \cdot 100\ \%.$$

Table 4 shows that AMg6 alloy joints produced by MIG welding using a scandium filler, have the highest strength factor, and joints of complex alloy

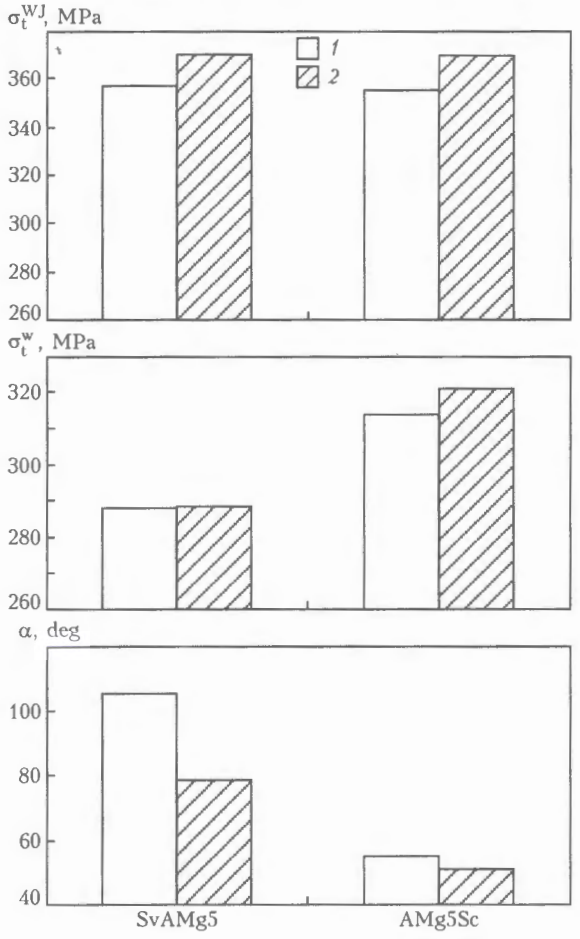

Figure 5. Mechanical properties of joints of 1925 (TB) alloy produced in TIG (*1*) and MIG (*2*) welding using wires of different compositions

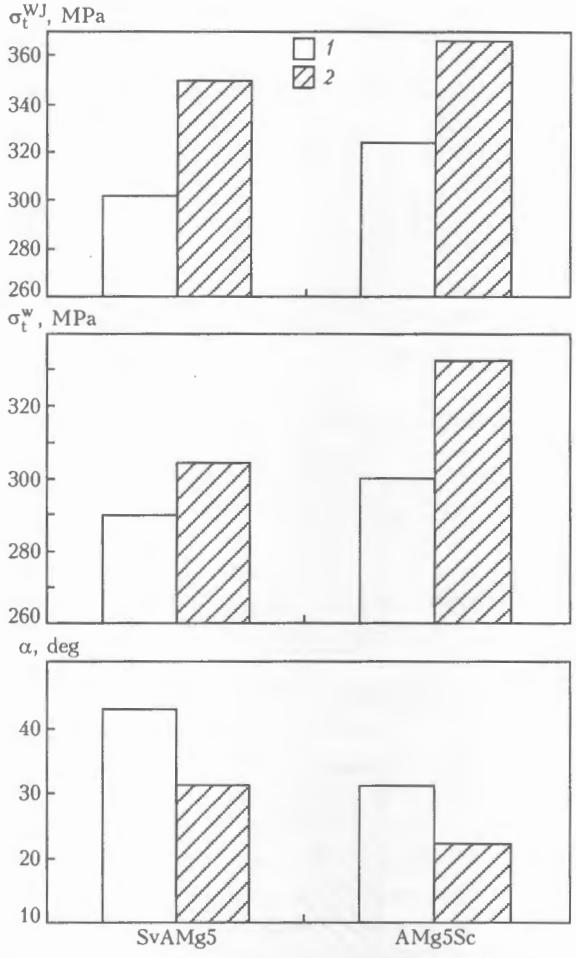

Figure 6. Mechanical properties of joints of 1925 (TB) alloy produced in TIG (*1*) and MIG (*2*) welding using wires of different compositions

Table 5. Change of mechanical properties of the joints and weld metal when MIG is used instead of TIG

Alloy grade	*Sheet thickness, mm*	*Electrode grade*	*Coefficient C, %*			
			σ_t^{WJ}	σ_t^{w}	a_n^{w}	α
AMg6	6	SvAMg63	1.3	0.3	–	–
		AMg63Sc	3.0	2.0	–	–
1420	4	SvAMg63	1.0	0.1	−47.8	−38.5
		AMg63Sc	2.3	0.1	−56.2	−51.7
	6	AMg63	8.9	0.4	−3.9	–
		AMg63Sc	5.8	0.2	−4.5	–
1201	6	Sv1201	10.6	9.3	51.7	–
		1201Sc	14.4	5.8	53.3	–
1460	3	Sv1201	1.6	10.3	–	−31.8
		1201Sc	1.6	1.7	–	– 119.4
	6	Sv1201	5.3	13.5	14.3	–
		1201Sc	8.2	7.0	29.9	–
1925 (TB)	3	SvAMg5	3.7	0.2	–	−34.2
		AMg5Sc	3.7	2.2	–	−7.8
V96Ts (TB)	3	SvAMg5	15.9	4.5	–	−38.7
		AMg5Sc	13.1	9.7	–	−40.9

V96Ts (TB) have the lowest factor. Generalization of the results leads to the conclusion that the higher is the base metal strength, the lower is the coefficient of welded joint strength. Alloy 1925 (TB) is an exception, which is related to its capability of self-quenching at cooling in air. At replacement of TIG welding by MIG welding (Table 5) the strength properties of the joints and weld metal increase, irrespective of the composition of metal being welded and filler wire grade. This dependence is manifested to the highest degree on aluminium alloys containing 2.3–5.7 % Cu. Ductile properties of the joints (in particular, impact toughness) can both increase and decrease. MIG welding of alloys of Al–Cu(Li) system provides and increase of a_n^{w} by 14 to 53 %, and for Al–Mg–Li system lowering of this index by 4 to 56 %. Advantages of MIG process increase with the thickness of the metal being welded (alloys 1420 and 1460).

Application of Sc-containing wires leads to a considerable drop of ductile properties of the joints and weld metal. For all the considered alloys, joint bend angle can decrease by 2 to 73 %, and weld impact toughness by 2 to 30 %. Scandium produces the least lowering of ductility in alloys of Al–Mg–(Mn, Li) system, in which the joint bend angle drops by 2.2 to 10.8 %, and impact toughness by 1.9 to 18.6 % (Ta-

Table 6. Change of mechanical properties of the joints and weld metal using scandium-containing filler instead of standard filler

Alloy grade	*Sheet thickness, mm*	*Coefficient P, %*			
		σ_t^{WJ}	σ_t^{w}	a_n^{w}	α^{WJ}
AMg6	6	0.1 / 1.7	1.4 / 3.3	–	–
1420	4	1.0 / 2.2	0.8 / 0.8	−3.0 / −18.6	−2.2 / −10.8
	6	8.9 / 5.8	0.7 / 0.5	−1.9 / −2.5	–
1201	6	1.3 / 4.8	8.5 / 4.4	−23.3 / −22.5	–
1460	3	0.3 / 0.3	14.8 / 4.7	–	−54.6 / −72.7
	6	1.9 / 4.7	10.9 / 3.2	−29.8 / −14.3	–
1925 (TB)	3	0	9.0 / 11.1	–	−48.1 / −35.4
V96Ts (TB)	3	7.2 / 4.6	3.4 / 9.3	–	−27.9 / −29.0

Note. The numerator gives the values for TIG process, and the denominator – for MIG process.

ble 6). Investigations showed that at a relatively low base metal strength and high strength coefficient of welded joints produced by regular TIG welding (when $\sigma_t^{WJ}/\sigma_t^{BM} \geq 0.9$) application of Sc-containing wires is an ineffective means of increasing the strength properties of the joints, and leads to a considerable drop of ductile properties of the metal – impact toughness of welds and joint bend angle.

Thus, comparative analysis of the results showed that strength of welded joints on high-strength aluminium alloys is always higher in MIG welding than in TIG welding. This is attributable to a lower level of heat input in consumable electrode welding and lower softening of the metal in the fusion zone and HAZ, respectively [5]. This is particularly evident at increase of sheet thickness of high-strength Al–Li alloys 1420 and 1460 sensitive to heat input.

Weld metal strength depends on welding wire composition and welding process. Scandium contained in the wire goes into the solid solution at weld metal solidification, increases the phases dispersity and promotes formation of subdendritic crystals, thus leading to increase of weld strength. A higher speed of liquid metal solidification achieved in MIG welding, provides a higher degree of solid solution saturation both by the main alloying elements, and by scandium [6]. As a result, such welds are superior to the welds made by a nonconsumable electrode in most of the cases. In addition, the strength and structural characteristics of welds have a certain influence on the fusion zone properties, which affects the welded joint mechanical properties as a whole.

CONCLUSIONS

1. Ultimate strength of welded joints of currently available aluminium alloys of the main alloying systems, produced by MIG welding is by 1 to 16 % higher than that of joints made with nonconsumable electrode. On the other hand, the ductile properties of welded joints (impact toughness of weld metal and bend angle of the joints) are higher in TIG welding.

2. Advantages of MIG process application increase with the welded metal thickness. In alloys 1420 and 1460 at sheet thickness of 3 to 4 mm the advantages of MIG process are equal to 1–2.5 %, and to 5–9 % at 6 mm thickness of the sheets.

3. Application of Sc-alloyed welding wires in arc processes of aluminium alloy welding allows improving the strength properties of the metal of welds and welded joints as a whole. Degree of weld strengthening as a result of scandium addition depends on the alloy composition, sheet thickness and structure of cast weld metal, while leading to a decrease of the weld metal impact toughness and welded joint bend angle.

1. Rabkin, D.M. (1986) *Metallurgy of fusion welding of aluminium and its alloys*. Kiev: Naukova Dumka.
2. Ishchenko, A.Ya., Poklyatsky, A.G., Yavorskaya, M.R. (1989) Prevention of oxide film inclusions in weld metal of aluminium alloys. *Avtomatich. Svarka*, **6**, 38–41.
3. Poklyatsky, A.G. (2001) Peculiarities of formation of macroinclusions of oxide film in weld metal of aluminium alloys (Review). *The Paton Welding J.*, **3**, 36–38.
4. Levchenko, O.G., Mashin, V.S. (2003) Sanitary-hygienic characteristic of process of consumable electrode inert-gas welding of AMg6 aluminium alloy. *Ibid.*, **1**, 46–48.
5. Labur, T.M., Bondarev, Andr.A., Lozovskaya, A.V. et al. (2001) Influence of welding process on fracture resistance of joints in aluminium-lithium alloys 1420 and 1460. *Ibid.*, **7**, 11–15.
6. Ishchenko, A.Ya., Lozovskaya, A.V., Mashin, V.S. et al. (2002) Increase in strength of welds in arc welding of alloy 1420 using the Sc-containing fillers. *Ibid.*, **1**, 10–14.

DEVICE FOR FORMATION OF WELD IN ELECTROSLAG WELDING

E.N. ERYOMIN
Omsk State Technical University, Omsk, Russia

New techniques, as well as equipment and fixtures are described, which are used to prevent defect formation in welds made by electroslag welding. To achieve a sound weld formation, a device signaling the surface-melting of the edges being welded is used at the start of the welding process, this ensuring transition from the stage of inducing a slag pool to the welding process proper. A device controlling the metal pool level is used to eliminate the shrinkage cavity, thus providing a sound weld formation at the final stage.

Keywords: *electroslag welding, weld formation, signaling device*

One-pass welding of structures of heat-resistant steel and alloys of large thickness is widely used in rocket and aviation engineering. The method of electroslag welding (ESW) distinguished by its broad metallurgical and technological possibilities is very promising for production of the mentioned products since rod bars of relevant rolled stock and high-fluoride fluxes, which decrease the burning loss of the active elements responsible for heat-resistant properties of the alloys, may be used as electrodes.

However, welded joints produced by the ESW method may have specific defects, such as poor fusing of edges, formation of undercuts in the transition zone and shrinkage cavities at the end site of the welds. In this case it is necessary to considerably increase the sizes of the run-on tubs and run-off tabs, which condition the presence of considerable heads at the beginning and the end of the weld. Such technological technique leads to the increased metal consumption and labor intensity of the subsequent machining. Because of this fact when producing billets of hard-to-treat heat-resistant alloys one often refuses from welding in favor of other methods of hot process stages, such as forging, forming, extrusion and rolling. Therefore, development of equipment and fixtures that allow excluding the above defects is the urgent task.

With the aim of removing the above defects the devices are developed for improving quality of the ESW weld formation (Figure 1).

For solution of the above problems it is in the first place necessary to provide quality fusion of the edges at the beginning of welding. For this purpose it is first necessary to fuse the faces of the billets since the non-fused edges do not connect with the weld metal and its solidification takes place in a sort of metallic mould. At this state of the ESW the decisive step is to determine the moment of transition from the process of inducing the slag pool to the welding. With this aim a device is developed for signaling the fusion of the edged being welded. The device consists of the forming water-cooled device and a unit for signaling the fusion of the weld edges (Figure 1). There is a hole in the lower part of the front cover plate of the device to which the water-cooled probe with the clamp of a collet type is installed (Figure 2). The probe in its initial position is in contact with the butt edge in the site of its initial fusion. After fusion of the edge the contact of the probe with the article is disturbed

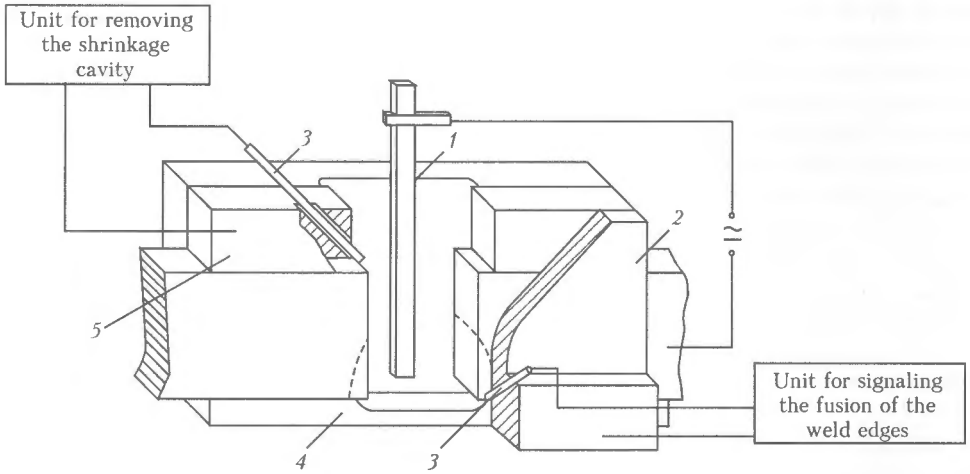

Figure 1. Diagram of the ESW welding complex with devices for weld formation: *1* — consumable electrode; *2* — front cover plate of the forming water-cooled device; *3* — probe; *4* — run-on tub; *5* — run-off tab

© E.N. ERYOMIN, 2005

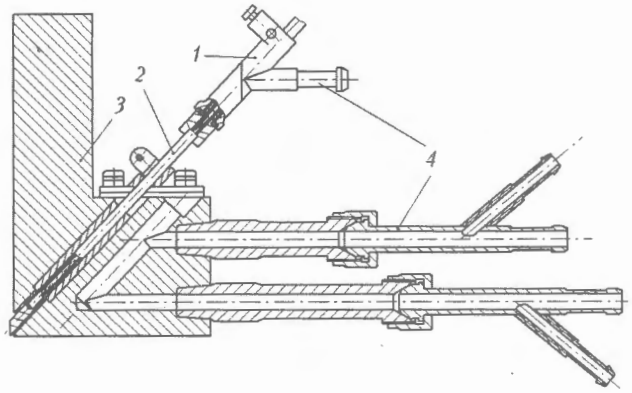

Figure 2. Diagram of front cover plate with edge fusion sensor: *1* — forming plate; *2* — probe; *3* — probe body; *4* — cooling system

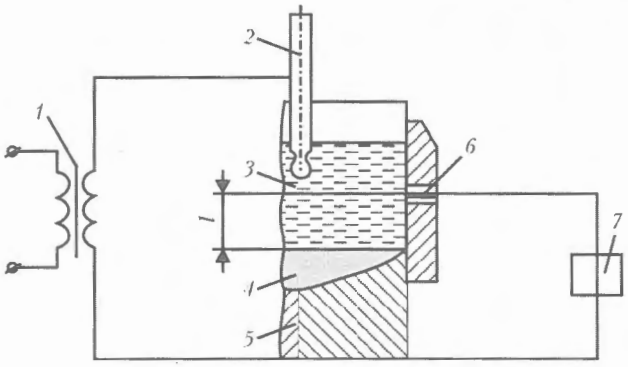

Figure 3. Diagram of device for removing shrinkage cavity: *1* — welding transformer; *2* — consumable electrode; *3, 4* — slag and weld pool, respectively; *5* — weld; *6* — probe; *7* — control

and at this moment a sharp increase of the potential from the welding current passing through the slag occurs. The appearance of the potential is confirmed by measuring the voltage on the probe (oscilligram). This potential is the control signal informing about the penetration of the edges being welded at the initial welding stage. The signal from the probe comes to the signaling unit and informs about the fusion of the weld edges and transition to the welding process. The device employs a tungsten probe, which is drawn inside the forming cover plate by a special mechanism to prevent the «freezing-on» of the probe.

To provide a quality weld formation under ESW it is necessary to perform control at the level of the weld pool. With this aim a device with the signaling sensor is created for removal of the shrinkage cavity (its diagram is presented in Figure 3). The device includes the tungsten probe, which is immersed into the slag pool. The design of this device is similar to the above-described device for signaling about the fusion of the edges being welded. It consists of the cooled run-off tab with a hole to where the probe with the clamp of the collet type is inserted. The process proceeds without cooling to prevent formation of the slag lining on the probe. A change of the potential at the probe–metal site from the welding current passing through the slag is a control signal for operation of the automation system. It was determined by means of the oscillograph that the potential changes depending on the distance from the probe to the molten metal. Input resistance of the control is one-fold higher than in the slag lining, which provides a reliable work of the device in case of abundant slaging.

This device allows controlling a level of the molten metal preventing the contact of the probe with it. After receiving a control signal the automation system of the welding apparatus starts gradual lifting the electrode from the weld pool, which provides the removal of the shrinkage cavity.

The production tests have shown that the use of ESW for production of critical billets of heat-resistant nickel alloys using the above-described devices provides a quality weld formation and a decrease of the head part down to 1.5–2.0 mm, which essentially increases the utilization factor of expensive alloys and decreases a labor intensity for producing articles from hard-to-treat materials.

CONCLUSIONS

1. To prevent lack of fusion of the edges and incomplete penetration it is proposed to use at the initial ESW stage in the transition zone the tungsten probe, which contacts with the butt edge and at the moment of its fusion registers the appearance of the potential from the welding current passing through the slag. This potential is a control signal on the fusion of the edges being welded and informs about the transition from the process of the inducing of the slag pool to the welding.

2. The tungsten probe immersed into the slag pool is used for registration of the potential at its emergence. This makes it possible to control a level of metal pool without its contact with the probe, thus providing a timely lift of the electrode from the slag pool and removal thereby of the shrinkage cavity.

3. It is advisable to employ the considered devices, which increase the quality of the weld formation in ESW, for manufacturing articles of the rocket and aviation industry.

MULTIFUNCTIONAL WELDING CURRENT SOURCE

V.A. LEBEDEV[1], **N.I. POSTOLATY**[2] and **A.V. MOTRY**[2]
[1]E.O. Paton Electric Welding Institute, NASU, Kiev, Ukraine
[2]Kakhovka Plant of Electric Welding Equipment, Kakhovka, Ukraine

A multifunctional source is described, which is manufactured by Kakhovka Plant of Electric Welding Equipment for application in different processes of welding, surfacing, cutting, including use of acrotrons.

Keywords: *welding technology, plasma-arc process, welding current source, purpose, reliability, multifunctionality, technical solutions*

New welding technologies have now being developed, using the effects inherent to arc processes. A plasma-arc process implemented in air using special devices (plasmatrons with special oxide cathodes) should be regarded as one of them [1]. This process is highly efficient for solving problems related to intensive heating, welding, etc. In a number of cases application of this process allows performing operations, which could not be done earlier, for instance welding of metals to carbon-graphite materials, when developing welding current conduits to graphite electrodes widely applied in electrometallurgy in electrode manufacturing [2]. In this case the open-air plasma-arc process has practically no alternative.

Performance of the above process requires a welding current source, providing a drooping volt-ampere characteristic. Requirements to its design are determined by the need to achieve high values of open-circuit voltage (more than 120 V) and working voltage (50–60 V). In addition, specifics of plasma arc excitation, as well as the need to extend the operating life of the above oxide cathode, and follow the safety rules in this case predetermine the method of controlling the operation of such a welding source.

Appearance of a multifunctional welding current source

Specialists of KPEWE and E.O. Paton Electric Welding Institute developed a welding power source KIU-701 (Figure), which after trials and retrofitting was manufactured for industrial application. Considering a number of engineering solutions implemented in KIU-701, it may be regarded as a multifunctional source. In addition to the above capabilities, a flat volt-ampere characteristic may be set in it, open-circuit voltage may be lowered to 75 V, and working voltage may be selected in a range required for implementation of mechanized and automated arc processes. Welding current source KIU-701 supports operation of various-purpose semi-automatic machines designed for welding, surfacing and cutting of metals with solid (in shielding gases and using flux) and self-shielded flux-cored electrode wires of the most widely used diameters, including more than 3 mm diameter.

KIU-701 power source was tested in a set with semi-automatic machines of modular design of PSh107V type. Highly efficient and sound processes of welding, surfacing and cutting of steels, cast irons and aluminium were performed. During the experiments it became obvious that a complete package of welding operations can be performed in a number of cases using a multifunctional welding current source of KIU-701 type, as well as arcotron and semi-automatic machines, for instance, in fabrication of current conduits (rigid structures of current-carrying buses, flexible current conductors, etc.) to graphite electrodes in electrometallurgy.

Basic engineering solutions, which allow using KIU-701 sources to implement a multitude of technologies, were developed proceeding from experience of application of batch-produced designs of welding current sources KIU-501 and KIU-1201 tried out in industry. This concerns the power components proper, as well as original development of an all-purpose electronic regulator, providing different types of volt-ampere characteristics, namely flat, drooping, fan-like (with the capability of selection of the slope). This is implemented by appropriate feedbacks by current or voltage. A high quality of the arc process is ensured by adding special correcting links into the regulator to form the required dynamic properties of the power source. In addition to the above, the electronic regu-

© V.A. LEBEDEV, N.I. POSTOLATY and A.V. MOTRY, 2005

lator also has a function of protection from short-circuiting supercurrents, namely bar characteristic, where the peak point is variable in a broad range.

An original engineering solution in the above source in a device embodied ensuring a programmed increment of welding current with adjustment of current levels and time of their setting. Program adjustment elements are mounted on the front panel of KIU-701 source. Addition of such a regulator to the source design primarily provides a reliable and safe operation of the arcotron oxide cathode in the plasma-arc process. This regulator can be used also for solving other engineering and technology problems related to surfacing and welding of steels and aluminium alloys.

KIU-701 welding current source is recommended for application in the plants of non-ferrous and ferrous metallurgy, as well as plants involved in production of carbon-graphite materials.

1. Lakomsky, V.I. (1997) *Oxide cathodes of electric arc*. Zaporozhie.
2. Lakomsky, V.I. (1995) Open arc welding of carbon materials to metals. *Avtomatich. Svarka*, **8**, 11–18.

INFORMATION RETRIEVAL SYSTEM «ELECTRODES FOR MANUAL ARC WELDING»*

Yu.A. SKOSNYAGIN and **A.B. LESNOJ**
E.O. Paton Electric Welding Institute, NASU, Kiev, Ukraine

Software allowing selection of covered electrodes for manual arc welding is presented. The information system contains the most comprehensive data on electrodes (more than 500 grades) manufactured in the CIS countries. In addition to the reference information, the software provides wide possibilities for multi-parametrical retrieval on the basis of criteria set by a user.

Keywords: *manual arc welding, covered electrodes, information system, software, multi-parametrical retrieval*

Analysis of the present and future of the welding industry shows that manual arc welding using covered metal electrodes is still one of the most common methods for producing permanent joints. The rational choice of electrodes providing the required quality of a weld is an important point in performing welding operations.

When selecting an electrode, it is necessary to allow not only for the application field, required chemical composition and mechanical properties of the deposited metal, but also for a number of other requirements to the parameters that determine welding conditions, such as spatial position, electrode diameter, kind, polarity and value of the welding current, arc voltage, welding speed and preheating temperature (the last two parameters are characteristic of welding of steels requiring the use of special techniques).

In addition to the above objective technological criteria, it is also necessary to allow for the purely subjective ones, such as a price factor and availability of the information on suppliers of a given electrode to the market, availability of appropriate certificates granted to an individual supplier, and their validity terms.

National and foreign manufacturers produce today a large amount of different electrode grades for manual arc welding, and it should be noted that one and the same technological process can be performed using different electrode grades. In this connection, selection of electrodes involves a complicated multi-parametrical retrieval, and handling of this problem can be substantially facilitated by application of the specialised software «Electrodes for Manual Arc Welding» developed by the E.O. Paton Electric Welding Institute of the NAS of Ukraine.

The information system contains data on electrodes manufactured by both CIS and some foreign countries. Functionally, the system is designed so that it is an electronic directory that provides the most comprehensive data on an electrode selected. In addition, it offers wide possibilities in terms of finding electrodes based on the set criteria.

The reference data on electrodes include the main purpose, field, technological peculiarities and additional data on application, type of electrode covering, kind and polarity of current, permissible spatial positions, recommended conditions and productivity of welding, consumption and yield coefficients, mechanical properties and chemical composition of deposited metal, as well as data on suppliers of a given electrode, designations, markings of electrodes according to the American (AWS), International (ISO), German (DIN) standards and GOST (CIS countries).

*The article is based on the presentation made at the Second International Conference «Mathematical Modelling and Information Technologies in Welding and Related Processes» (Katsiveli, Crimea, September 13–17, 2004). Kiev: PWI.

© Yu.A. SKOSNYAGIN and A.B. LESNOJ, 2005

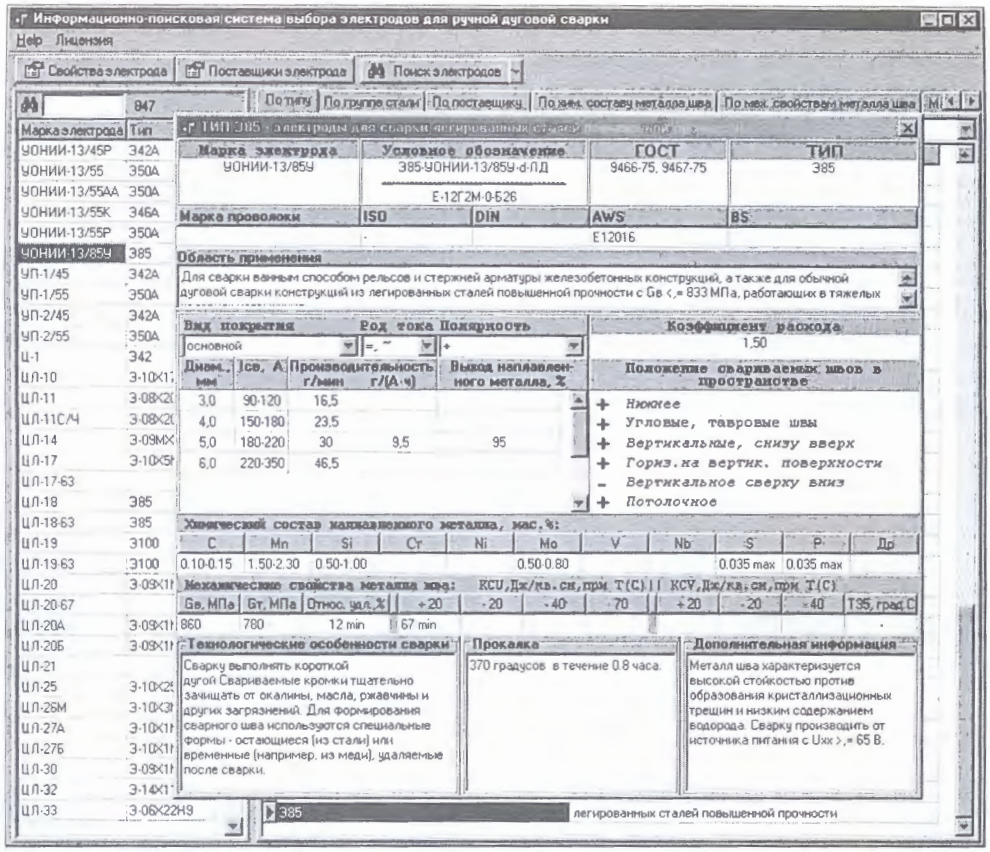

Figure 1. Reference information for electrode UONII-13/85U

Figure 1 shows the main window of the software with the list of electrodes given in its left part. Detailed data on a selected electrode (e.g. UONII-13/85U) are displayed in an additional information window, and data on a supplier are also displayed in a separate window (Figure 2).

For the retrieval purposes, the software offers a multi-parametrical incremental selection from the list of available electrodes. The simplest retrieval is the search based on a known electrode grade, where it is necessary to obtain only the reference data. In this case, it is enough just to enter the electrode grade in the text field located over the list of electrodes, and the current electrode list will always be limited according to the entered text mask.

In cases where the required electrode grade is not known beforehand, the software provides the possibilities for a multi-variant retrieval using two types of criteria. The first type includes the mutually exclusive citeria, such as type of electrode (67 grades), recommendations on weldability (14 groups of dissimilar materials), and electrode suppliers (102 names). The second type includes complementary criteria, such as chemical composition and mechanical

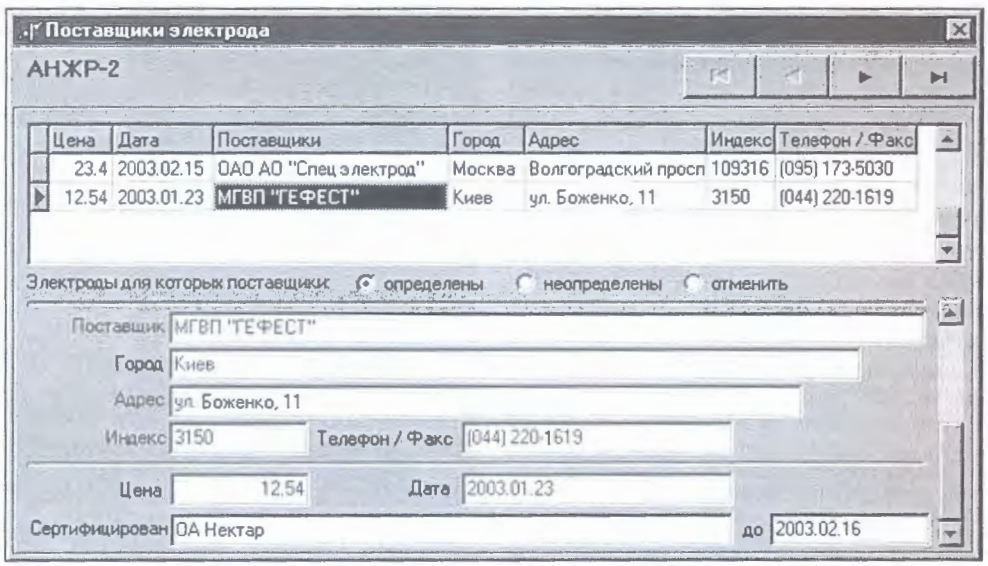

Figure 2. Information on suppliers of electrode ANZhR-2

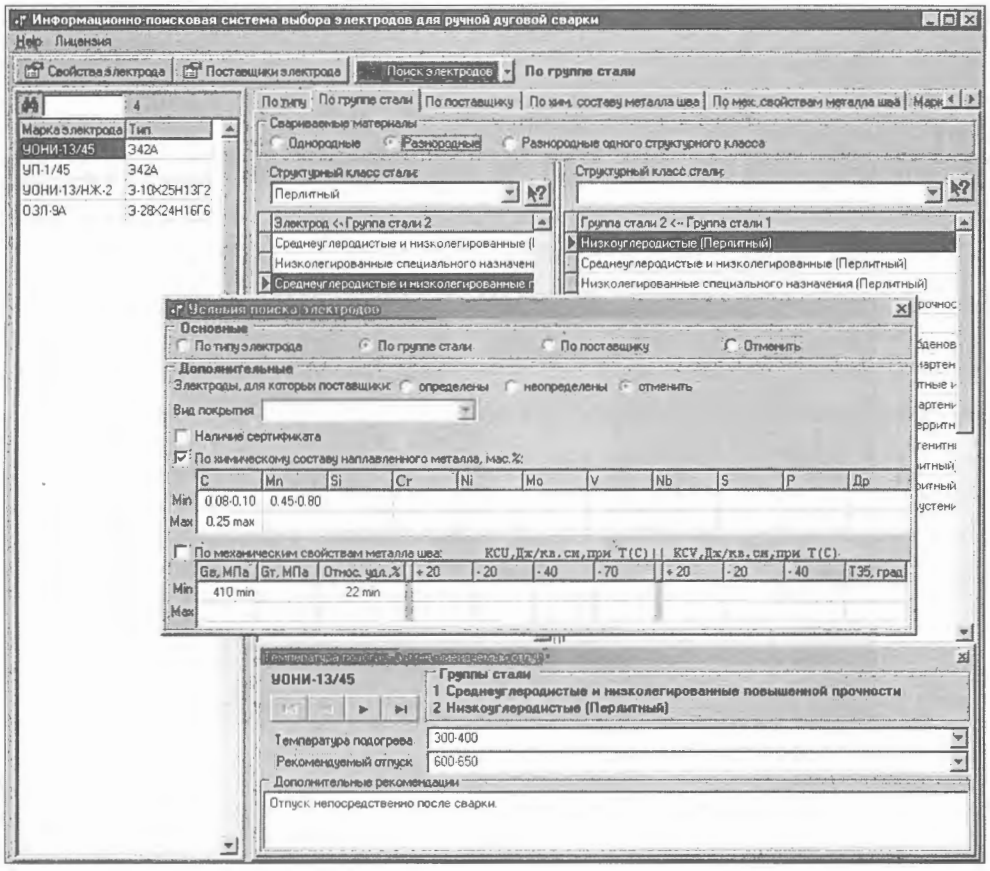

Figure 3. Tools for multi-parametrical retrieval of electrodes

properties of the weld metal (11 characteristics in each criterion), type of electrode covering (16 types), and data on suppliers.

With the first type of the retrieval criteria, first the required insert of the main window is selected (Figure 3), followed by selection of the corresponding sub-criterion, which limits the current list of electrodes. The case shown in Figure 3 demonstrates the sequence of selection of an electrode based on recommendations on weldability of dissimilar groups of steels. First a group of steels of the first material (low-carbon steels of the pearlitic grade) is indicated in the rightmost table, and the available variants for the selected group are displayed in the table shown more to the left. For the second group of steels (medium-carbon and low-alloy increased-strength steels of the pearlitic grade) the leftmost table will give a recommended list of electrodes for welding. Certain type of an electrode or supplier can be sampled in a similar way. Alternative variants for procurement of electrodes can be analysed by combining outputs of the «supplier–electrodes» and «electrode–suppliers» lists.

Consider the sequence of using retrieval criteria of the second type, which can be applied independently or as complementary parameters for the first-type retrieval criteria. Additional electrode retrieval criteria, e.g. limitations on chemical composition and mechanical properties of deposited metal, as well as data on a supplier, can also be set in a case shown in Figure 3.

It should be noted that the software automatically updates the current list of electrodes, meeting every new definition of the retrieval criterion. Therefore, a user can sequentially check the resulting data set. Specific feature of the software is openness of the retrieval criteria, which consists in the fact that corresponding inserts show the corresponding summary data, thus allowing orientation to an available range of values, avoiding the effect of «browsing in a dark room» in the information retrieval.

The information system is designed so that the functions of browser and editor of the data base are combined in one program, which allows the end user to maintain the relevance of data by adding a new information and correcting the existing one to meet his needs.

The software is intended for engineers and technicians of industrial and construction enterprises, design, development and research institutions, manufacturers, suppliers and distributors of electrodes.

The operating environment of the software is Windows 9x/Me/2000. The 6 MB disk space is required for installation. For detailed information please visit: http://www.paton.kiev.ua

3-GUN MACHINE KL-117 FOR ELECTRON BEAM WELDING OF DRILL BITS

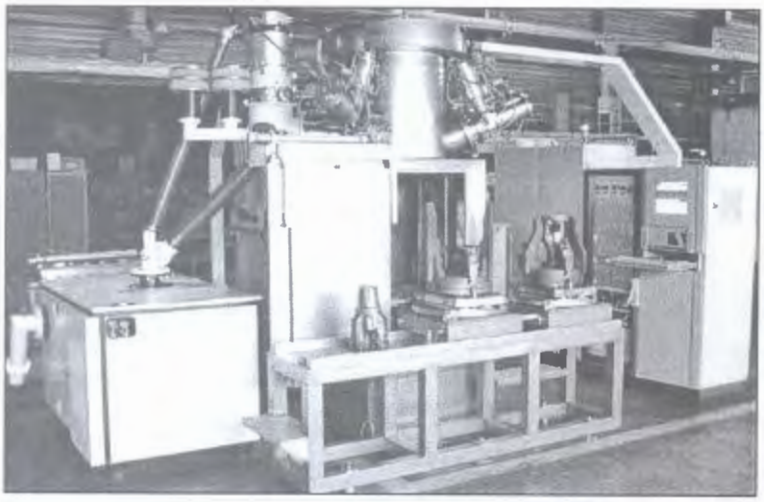

✔ Machine is intended for electron beam welding of drill bits up to 17.5" diameter with simultaneous performance of three welds, thus increasing both accuracy of drill bits dimensions and welding output.

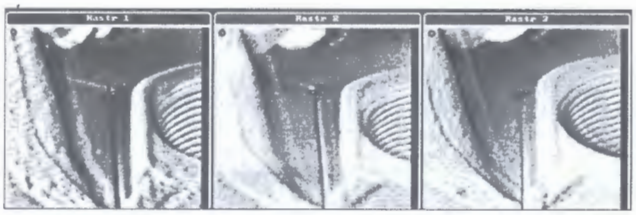

✔ Application of a powerful control electronic tube in the accelerating voltage source prevents the arc processes in the welding gun by a short interruption of accelerating voltage, which does not lead to weld formation defects.

✔ The RASTR system, functioning on the principles of raster electron microscope, enables following the welding process and automatic coquidance of each of three electron beams to the butts of groove faces in the real time. The clear picture of the welding process is displayed on the monitor screen and is not exposed to the welded metal vapors, which is characteristic for traditional optical observing systems.

✔ Machine is provided with the electron beam diagnostic system allowing an operator:

- to define the beam focusing plane position prior to welding;
- to periodically evaluate changes in space and energy beam parameters in order to define the necessity of the welding gun cathode replacement.

✔ Lanthanum hexaboride cathode as a tablet has service life of not less than 40 h in the welding mode at beam power of 20 kW, and the beam axis position does not change at changes in beam focusing.

✔ Control of all equipment subsystems by means of CNC + PLC.

✔ The computer system of electron beam scanning stabilizes the molten pool state and improves the quality of face and root surfaces formation of the weld.

E.O. Paton Electric Welding Institute of NASU
11, Bozhenko Str., 03680, Kiev, Ukraine; Tel./fax: (38044) 525 4319
E-mail: nazarenko@technobeam.com.ua www.nas.gov.ua/pwj/beam/index.html

ADVANCE BOOK INFORMATION

FORTHCOMING BOOK INFORMATION

Vladimir I. Makhnenko, Viktor E. Pochynok. STRENGTH CALCULATION OF WELDED JOINTS WITH CRACK-LIKE IMPERFECTIONS.
Approx. 300 pp., 165×235 mm, hardback. November 2005. US$ 90

In this manuscript, the idea of the fitness-for-purpose concept is used to improve strength calculations of welded joints with crack-like imperfections caused by structural or technological factors. These include welded joints with fillet, spot, slot and butt welds having sharp fissures brought by geometry of the elements welded and limited sizes of the weld sections. Such joints are widely encountered in modern general-purpose welded structures used in civil building, shipbuilding, automobile industries, etc.

The welded joints just mentioned do not usually cause problems for structures of relatively ductile materials with small-to-medium thicknesses of component sections, and operating under predominantly static loading. However, the use of new structural materials, especially high-strength steels and aluminum alloys, etc., large cross sections of structural elements, and loading with alternate loads, requires a certain caution to be taken. Nonetheless, the technological advantages that these joints produce attract an interest in their use, of course, when it does not cause any harm to the structure safety and its residual service life.

Performing strength calculations based on the fitness-for-purpose criterion for the joints encountered in general-purpose structures, allows ensuring the requirements concerning the service life-time. However, there is a difficulty of implementing such calculations in wide engineering practice. As shown by the authors, a successful implementation of the mentioned concept for general-purpose welded joints and for wide range of users is possible only when it is based on the use of corresponding computer systems with friendly user interface, which do not require a user to have a special knowledge in fracture mechanics, deformation mechanics, numerical methods, etc. Such systems are to be portable and efficient, i.e. calculations of appropriate section sizes or verification of strength of specific joints should be done promptly. In turn, it requires development of numerical procedures and creation of specialized databases that simplify and accelerate calculations.

Viktor Ya. Kononenko. TECHNOLOGIES OF UNDERWATER WET WELDING AND CUTTING.
Approx. 140 pp., 140×200 mm, softback. December 2005. US$ 40

The book deals with the features of arcing, metal transfer and joint formation in consumable-electrode wet underwater welding. Principles of development of coated electrodes and self-shielded flux-cored wires for underwater welding and cutting are established. Characteristics of welding consumables and mechanical properties of weld metal are given. Some types of joints, procedure of preparation and fit-up for welding, possible defects of the joints and methods to prevent their formation are described.

Information on characteristic damage to the underwater metal structures is generalized, and technological solutions are given, which have been implemented during restoration of their performance, using wet processes of underwater welding and cutting. The book gives the characteristics of the equipment for implementation of underwater arc welding process.

The main processes of thermal underwater cutting are presented, and characteristics of consumable materials and equipment for its implementation are described. Examples of work performance using underwater cutting are given.

The book is designed for scientific and engineering-technical personnel, qualified welders-divers involved in design, fabrication and repair of underwater constructions.

The book is written by a specialist, who is developing electrode materials and technologies and has a vast experience of practical work under the water.

ADVANCE BOOK INFORMATION

TITANIUM: Titanium and its alloys. Technologies. Equipment. Production. Electrometallurgy. Welding

Approx. 180 pp., 200×290 mm, softback. December 2005. US$ 50

The collection presents papers on electrometallurgy and welding of titanium and its alloys published between 2002 and 2005 in «Advances in Electrometallurgy» and «The Paton Welding Journal» journals. The authors of the papers are scientists and specialists in the field of titanium and its production, known in Ukraine and abroad. The collection is designed for a broad range of readers dealing with the problems of production, processing and use of titanium.

ORDER RORM

Please return to:

International Association «Welding»,
11, Bozhenko str., Kiev, 03680, Ukraine
Tel.: (38044) 287 6757, 287 6049, 529 2623
Fax: (38044) 287 4677
E-mail: journal@paton.kiev.ua; tomik@mac.relc.com

Please send me:

❑ Vladimir I. Makhnenko, Viktor E. Pochynok «Strength Calculation of Welded Joints with Crack-Like Imperfections». US$ 90, postage included

❑ Viktor Ya. Kononenko «Technologies of Underwater Wet Welding and Cutting». US$ 40, postage included

❑ «Titanium». Collection of Scientific Paper. US$ 50, postage included

How to Pay and Payment Details

❑ By bank transfer (or mail a cheque) into our account
№ 2600801283433
UKREXIMBANK, Kiev, Ukraine
S.W.I.F.T.: EXBSUAUX
CORR. ACC. #04-094-227
Bankers Trust Company,
New York, U.S.A.
S.W.I.F.T.: BKTR US 33

❑ Please Invoice

❑ Your Details
Name _____

Organization _____

Address _____

Signed _____ Date _____